Alexander Schossmann, BSc

Self Consistent Approach for Master-Equation-Based Nonequilibrium Cluster Perturbation Theory

MASTER'S THESIS

to achieve the university degree of

Diplom-Ingenieur

Master's degree programme: Technical Physics

submitted to

Graz University of Technology

Supervisor

Univ.-Prof. Dr. Enrico Arrigoni

Institute of Theoretical and Computational Physics

Graz, June 2019

AFFIDAVIT

I declare that I have authored this thesis independently, that I have not used other than the declared sources/resources, and that I have explicitly indicated all material which has been quoted either literally or by content from the sources used. The text document uploaded to TUGRAZonline is identical to the present master's thesis.

_____   _____

Date   Signature

Abstract

The development of new nanoscale electronic devices, based on molecular scale electronics, is of great interest in fundamental research. In recent experimental research there has been a tremendous progress towards the realization of such nanoscale structures [1, 2, 3, 4, 5]. A recently developed method to study electronic transport characteristics of nanoscale components out of equilibrium is *master equation based steady-state cluster perturbation theory* (ME-CPT) [6]. While it remarkably improves the results of steady-state cluster perturbation theory, this approach is limited to systems with comparably small correlated central regions. Thus, it is not suitable for studying complex molecular configurations or heterostructures. The motivation of this thesis is to extend this new method in order to make these large systems accessible within nonequilibrium physics. This extension consists of a new iterative self-consistent scheme, based upon a division of the central region into clusters. This division drastically reduces the memory requirements in the numerical implementation compared to ME-CPT. As a benchmark, we apply the new scheme to a system of two interacting double quantum dots and compare the results with those from ME-CPT computations. The first proposed iteration scheme, which we designate as *scheme A*, does not sufficiently reproduce the results from ME-CPT. It turns out that this scheme has an inconsistency in the self-consistent procedure. For this reason we further modify the method such that in each iterative step the physical situation is consistent. The obtained new scheme, which we designate as *scheme B*, provides transport characteristics that are in good concordance with those from ME-CPT. In order to show that this new iteration scheme requires the correlations beyond the extend of the chosen clusters to be small, we further apply scheme B to a serial quadruple quantum dot. We conclude that scheme B, as introduced in this thesis, provides reliable results for systems consisting of weakly interacting clusters.

Kurzfassung

Die Entwicklung neuer elektronischer Bauteile auf molekularer Ebene ist von großem Interesse in der Grundlagenforschung. Neueste experimentelle Forschungsergebnisse zeigen große Fortschritte im Hinblick auf die Realisierung solcher Bauelemente im Nanobereich [1, 2, 3, 4, 5]. Eine kürzlich entwickelte Methode um elektronische Transporteigenschaften von solchen Bauteilen im Nichtgleichgewicht zu erforschen ist *master equation based steady-state cluster perturbation theory* (ME-CPT) [6]. Wenngleich diese Methode die Ergebnisse von *steady-state cluster perturbation theory* nennenswert verbessert, so ist sie dennoch auf Systeme mit vergleichsweise kleinen korrelierten Zentralregionen beschränkt. Somit ist ME-CPT nicht in der Lage komplexe Anordnungen von Molekülen oder Heterostrukturen zu erfassen. Die Motivation dieser Arbeit liegt darin diese Methode zu erweitern, um auch solch große Systeme im Rahmen der Nichtgleichgewichtsphysik erfassen zu können. Diese Erweiterung besteht aus einem selbst-konsistentes Iterationsverfahren, welches auf einer Unterteilung der Zentralregion in Cluster basiert. Diese Unterteilung reduziert den Bedarf an Arbeitsspeicher für die numerische Implementierung, im Vergleich zu ME-CPT, drastisch. Als Vergleich ziehen wir zwei wechselwirkende Doppelquantenpunkte heran und stellen die Ergebnisse jenen von ME-CPT gegenüber. Das erste von uns vorgeschlagene Iterationsschema, welches wir als *scheme A* bezeichnen, reproduziert die Ergebnisse von ME-CPT jedoch nicht hinreichend. Es stellt sich heraus, dass dieses Schema eine Inkonsistenz innerhalb des Iterationsverfahrens aufweist. Aus diesem Grund modifizieren wir die Methode dahingehend, sodass in jedem Iterationsschritt die Situation physikalisch konsistent ist. Das erhaltene neue Verfahren, welches wir als *scheme B* bezeichnen, liefert Transportcharakteristiken welche mit den ME-CPT Ergebnissen gut übereinstimmen. Um zu zeigen, dass das neue Iterationsverfahren eine schwache Korrelation zwischen den gewählten Clustern voraussetzt, wenden wir es weiters auf einen Quadruple-Quantenpunkt an. Wir kommen zu dem Schluss, dass das in dieser Arbeit eingeführte *scheme B* für Systeme, zusammengesetzt aus schwach wechselwirkenden Clustern, zuverlässige Resultate liefert.

Acknowledgements

First of all, I want to thank Prof. *Enrico Arrigoni* for supervising me throughout my work on this thesis. His support and the fact that he was always available for answering my questions enabled me to complete this thesis.

I am grateful to *Delia Fugger*, *Max Sorantin* and *Irakli Titvinidze* for many practical hints and discussions.

I want to thank *Michael Rumetshofer* for a lot of very fruitful discussions. Further, I want to thank *Gerhard Dorn* for a lot of very enthusiastic and fruitful discussions.

I want to thank my dear friends *Michael Draxler*, *Ralf Meyer*, *Alexander Schiffmann*, *Leonhard Treiber*, *René Vötter*, *Roman Lucrezi*, *Paul Maierhofer*, *Markus Bainschab* and, again, *Michael Rumetshofer* for sustaining my motivation with humorous discussions and coffee. Further, I am grateful to my fellow bureau inmates *Andrei-Viorel Man* and *René Vötter* for the excellent work atmosphere.

I want to thank our system administrator *Andreas Hirczy* for his great work and support.

A big thank you goes to *Brigitte Schwarz* for always helping me out with the bureaucratic work.

In particular I thank my father for showing me that physics is far more than a Master's programme.

Further, I want to thank my grandparents for their generous support during my studies.

Finally, I want to thank *Lisa* for her particular patience and encouragement. Her loving nature has been substantial to me over the last years.

Contents

1. Introduction

The understanding of quantum mechanical systems out of equilibrium is of great interest in fundamental research. For the development of future nanoscale electronic devices it is essential to comprehend quantum mechanical effects inside an open system that is not in thermal equilibrium. Recent experiments show a tremendous progress in the realization of these kind of systems. The controlled assembly of covalently bound molecules into desired architectures on gold surfaces was achieved [1], which has possible future applications in sensing devices. Furthermore, measurements on molecular wire-node architectures have become accessible [4]. A tunable Kondo effect has recently been observed in quantum dots [7] and in single-molecule transistors [2]. Electron transport experiments have been conducted for serial double and serial triple quantum dots [8, 9] which have an important relevance for the realization of solid state quantum bits as proposed in [10].

These examples make it clear that it is of major importance to have a satisfactory theoretical description of such systems. The challenging task therein is to include the electron-electron interactions. Due to the fact that these interactions have a significant influence on transport properties in strongly correlated systems, it is not always appropriate to treat them by means of mean field theory. In modern physics the investigation of strong correlated open quantum systems out of equilibrium is an active field of research [11, 12, 13]. A new method within this field of research has been introduced with the so-called *master equation based cluster perturbation theory* (ME-CPT) [6]. It is particularly suitable for the description of small correlated systems that are contacted with large baths. It has been shown that with ME-CPT interaction-induced current blocking effects are correctly predicted which, for example, lead to negative differential conductance [6].

Within ME-CPT one needs to solve the Hamiltonian of the entire central region that lies between the baths. This limits the method to small systems since the matrix representation in many-body space grows exponentially with system size. Large and complex systems, such as large clusters of molecules or three dimensional structures of correlated layers, are not accessible within this method.

However, as mentioned above, the experimental characterization of such systems has become feasible in recent years. A theoretical description of them is therefore strongly required. The motivation of this work is to explore a new method, based on the ME-CPT approach, that makes these large systems accessible within nonequilibrium many-body quantum mechanics. In this thesis we develop an extension of ME-CPT by including a self-consistent iteration scheme.

This thesis is organized as follows: In the introductory chapter 2 we provide an overview of the physical methods used within this thesis. We discuss the concept of

Green's functions and their usage in many-body physics. We further explain the cluster perturbation theory (CPT) method and show that within CPT one obtains a Landauer-type current formula. Furthermore, we show that in the general formula for the current across an interacting region, the nonequilibrium distribution explicitly plays a role. In the end of chapter 2 we sketch the derivation of the Born-Markov-Secular master equation (BMS-ME) for open quantum systems and discuss the Hubbard model.

Chapters 3 and 4 constitute the main work carried out within this thesis. In particular, in chapter 3 we present ME-CPT, based on the work of [6]. Further we explain the numerical implementation of ME-CPT within this thesis.

In chapter 4 we present the results from ME-CPT calculations for a linear chain of interacting quantum dots between two semi-infinite baths. We model this with the help of a one dimensional Hubbard model, containing four sites in two different configurations:

- **Two double quantum dots connected in series**. In this case the hopping parameter in the middle of the system is significantly smaller than those between the other sites.

- **Serial quadruple quantum dot**. All hopping parameters inside the system are the same.

We discuss two possible self-consistent iterative schemes that can be applied. We present them in Chapter 5. We discuss the first one, 5.1, in section 5.1. We show the results for two double quantum dots connected in series and compare them with those from ME-CPT. Scheme A does not reproduce the ME-CPT results properly and it turns out that it has an inconsistency in the self-consistent procedure. Due to that, we modify it and present another iterative scheme, which we designate **scheme B**.

We present the results for two double quantum dots connected in series in comparison with ME-CPT in section 5.2. Further, we apply scheme B to the serial quadruple quantum dot and as well compare with the results from ME-CPT.

In the end of this thesis we summarize the main results in chapter 6.

2. Physical basics and formalism

In this chapter we provide an introduction to the theoretical approaches we use within this thesis. We mention that from here on atomic units are used with $\hbar = e = m_e = 1$.

2.1. Green's Functions

2.1.1. Classical Green's Functions

We discuss in this section the formalism of Green's functions within the framework of many-body physics. Thereby we mainly follow [14] as well as [16].
The method of Green's functions was first introduced by George Green in the 19th century and further developed by Sturm, Liouville, Dirichlet, Riemann, Neumann and others [17]. Nowadays Green's functions are a well known and powerful tool in mathematics to solve linear inhomogeneous differential equations with boundary conditions [15]. Within the framework of quantum mechanics, correlation functions of field operator are referred to as Green's functions. Here we first consider classical Green's functions and afterwards illustrate their definition in quantum mechanics and many-body theory. Suppose one has a general inhomogeneous linear differential equation:

$$\hat{L}[f(\vec{x},t)] \ = \ g(\vec{x},t) \tag{2.1}$$

$\hat{L}$ is the linear differential operator defined on a domain with specified initial or boundary conditions. $g(\vec{x},t)$ is a given inhomogeneity. $\hat{L}$ is referred to as linear if $f(\vec{x},t)$ and all its derivatives $\nabla_x f(\vec{x},t), \nabla_x^2 f(\vec{x},t), \dots, \frac{\partial f(\vec{x},t)}{\partial t}, \frac{\partial^2 f(\vec{x},t)}{\partial t^2}, \dots$ only appear linearly. The particular solution is then formally given by

$$f_p(\vec{x},t) \ = \ \iint G(\vec{x},t,\vec{x}',t')g(\vec{x}',t')d\vec{x}', dt' \tag{2.2}$$

with $G(\vec{x},t,\vec{x}',t')$ satisfying the relation

$$\hat{L}[G(\vec{x},t,\vec{x}',t')] \ = \ \delta(\vec{x}-\vec{x}')\delta(t-t')\,, \tag{2.3}$$

as well as the specified boundary or initial conditions. It can be interpreted such that a Green's function is the solution of a linear differential equation with a delta inhomogeneity [15] and defined boundary or initial conditions. This solution then serves as a building block to obtain the particular solution according to equation (2.2). The general solution is obtained by adding a solution of the homogeneous problem $\hat{L}[f(x)] = 0$ that fulfils the boundary conditions. Important examples for boundary value problems are

the Dirichlet or Neumann problem which have various applications in physics [18, 15].

2.1.2. Green's function in quantum mechanics

In the following we briefly sketch that one can relate the linear response of a system with a Green's function. The dynamics of a closed system in non relativistic quantum mechanics is given by the Schrödinger equation. The time dependent form reads

$$i\frac{\partial}{\partial t}\left|\Psi(t)\right\rangle \;=\; H\left|\Psi(t)\right\rangle \;=\; (H_0 + V(t))\left|\Psi(t)\right\rangle \tag{2.4}$$

with H the total Hamiltonian, H_0 the Hamiltonian describing the isolated system and $V(t)$ an external potential or field respectively. In this work we calculate expectation values of observables with the help of the density matrix. An expectation value of an observable A is therewith given by

$$\langle A \rangle \;=\; tr\left\{\rho A\right\}. \tag{2.5}$$

The dynamics of the density matrix are described by the so called Von-Neumann equation:

$$i\frac{\partial}{\partial t}\rho(t) \;=\; [H(t), \rho(t)]. \tag{2.6}$$

For the following considerations we switch to the Dirac-picture with respect to H_0 [14], which we indicate with the superscript ρ^D. To find a unique solution for the Von-Neumann equation one needs to imply a boundary condition for this first order linear differential equation. Here we regard the following initial boundary condition:

$$\lim_{t\to-\infty}\rho(t) \;=\; \rho_0. \tag{2.7}$$

From that we obtain as a formal solution for the Von-Neumann equation

$$\rho^D(t) \;=\; \rho_0 - i\int_{-\infty}^{t}\left[V^D(t'), \rho^D(t')\right]dt'. \tag{2.8}$$

In general it is not possible to solve this integral equation. For this reason we write it as a series expansion by integrating and formally reinserting it up to infinite order:

$$\begin{aligned}\rho^D(t) \;=\; \rho_0 + \sum_{n=1}^{\infty}(-i)^n\int_{-\infty}^{t}dt_1\int_{-\infty}^{t1}dt_2\cdots\int_{-\infty}^{t_{n-1}}dt_n \\ \cdot\left[V^D(t_1), \left[V^D(t_2), \left[\ldots, \left[V^D(t_n), \rho_0\right]\ldots\right]\right]\right].\end{aligned} \tag{2.9}$$

Within **linear response** one assumes the external field to be small enough such that it is justified to solely regard the linear terms of the series expansion [14]:

$$\rho^D(t) \approx \rho_0 - i \int_{-\infty}^{t} \left[V^D(t'), \rho_0 \right] dt' . \tag{2.10}$$

Using this relation one obtains after a short calculation for the expectation value of an observable within linear response [14]

$$tr\{\rho(t)A(t)\} = tr\{\rho_0 A(t)\} - i \int_{-\infty}^{t} dt' \left\{ \left[A^D(t), V^D(t') \right] \right\} . \tag{2.11}$$

Denoting the expectation value with $\rho(t)$ as $\langle\ldots\rangle_t$ and the expectation value of the undisturbed system with ρ_0 as $\langle\ldots\rangle_0$ gives then

$$\langle A \rangle_t - \langle A \rangle_0 = -i \int_{-\infty}^{t} dt' \left\langle \left[A^D(t), V^D(t') \right] \right\rangle_0 . \tag{2.12}$$

The left side of the above equation is often written as $\langle A \rangle_t - \langle A \rangle_0 = \Delta A_t$, which corresponds to the linear response of the system in terms of the observable A. The term on the right side under the integral is called *retarded* Green's function and is written as

$$G^{ret}(t,t') = -i\,\Theta(t-t') \left\langle \left[A^D(t), V^D(t') \right] \right\rangle_0 . \tag{2.13}$$

In many-body physics, which is the framework of this thesis, the term Green's function is generalized and referred to various types of correlation functions of creation and annihilation operators in second quantization. The retarded Green's function is then written as

$$G_{\alpha,\beta}^{ret}(t,t') = -i\,\Theta(t-t') \left\langle \left[\hat{c}_\alpha(t), \hat{c}_\beta^\dagger(t') \right] \right\rangle \tag{2.14}$$

whereby the expectation value is no necessarily calculated with a density matrix of the undisturbed system. One further defines the *greater*

$$G_{\alpha,\beta}^{>}(t,t') = -i\,\langle \hat{c}_\alpha(t)\hat{c}_\beta^\dagger(t') \rangle \tag{2.15}$$

and *lesser*

$$G_{\alpha,\beta}^{<}(t,t') = -i\,\eta\,\langle \hat{c}_\beta^\dagger(t')\hat{c}_\alpha(t) \rangle , \tag{2.16}$$

Green's function. The prefactor $(-i\eta)$ depends on the chosen convention, whereas it is convenient to choose $\eta = -1$ for fermions. This allows to write the retarded Green's function as

$$G_{\alpha,\beta}^{ret}(t,t') = \theta(t-t') \left(G_{\alpha,\beta}^{>}(t,t') - G_{\alpha,\beta}^{<}(t,t') \right) \tag{2.17}$$

If the ladder operators $\hat{c}_\alpha$ are defined in spatial domain, the lesser Green's function corresponds to the expectation value that a particle is hopping from place α at time t to place β at time t'. In physics it is often necessary to demand causality for the corresponding correlation functions. This is achieved with the time ordering operator $\hat{T}$, which is defined as

$$\hat{T}\ \hat{c}(t_1)\hat{c}(t_2) \;=\; \begin{cases} \hat{c}(t_1)\hat{c}(t_2) & \text{if } t_1 > t_2 \\ \eta\hat{c}(t_2)\hat{c}(t_1) & \text{if } t_2 > t_1 \end{cases} \tag{2.18}$$

and

$$\eta \;=\; \begin{cases} +1 & \text{for bosons and} \\ -1 & \text{for fermions.} \end{cases}$$

The single-particle *time ordered* Green's function is therewith defined as

$$G_{\alpha,\beta}(t,t') \;=\; \langle \hat{T}\ \hat{c}_\alpha(t)\ \hat{c}_\beta^\dagger(t') \rangle \;, \tag{2.19}$$

whereby we choose here the convention that time-ordered correlation functions do not have a prefactor $(-i)$. This Green's function plays an important role in perturbation theory which we will discuss in section 2.1.3 in more detail. Within this thesis the physical properties of interest are calculated using single particle Green's functions in the many-body picture. At this point we mention that if the corresponding Hamiltonian $\hat{H}$ does not have an implicit time dependence, meaning that $\frac{\partial}{\partial t}\hat{H} = 0$ holds, the Green's functions only depend on the time difference $t - t'$ [14]. The physical models that are studied within this thesis have a time-independent Hamiltonian and therefore we write all Green's functions with just one time argument $G_{\alpha,\beta}(t,t') \rightarrow G_{\alpha,\beta}(t)$.

For a more detailed analysis we introduce the so called *Lehmann representation* according to [19, 14]. It is the spectral representation of the Green's functions in terms of eigenstates $|n\rangle$ of the undisturbed Hamiltonian $\hat{H}$ in frequency domain. First we regard the Lehmann representation of the *greater* Green's function of equation (2.15):

$$\begin{aligned} G_{\alpha,\beta}^{>}(t) \;&=\; -i\ \langle \hat{c}_\alpha(t)\hat{c}_\beta^\dagger \rangle \\ &=\; -i\ tr\left\{ \hat{\rho}\ \hat{c}_\alpha(t)\hat{c}_\beta^\dagger \right\} \\ &=\; -i\ \sum_{abc} \langle a|\ \rho_{cb}\,|c\rangle\,\langle b|\, e^{i\hat{H}t}\hat{c}_\alpha e^{-i\hat{H}t}\hat{c}_\beta^\dagger\,|a\rangle \\ &=\; -i\ \sum_{nab} \rho_{ab}\,\langle b|\, e^{i\hat{H}t}\hat{c}_\alpha e^{-i\hat{H}t}\,|n\rangle\,\langle n|\,\hat{c}_\beta^\dagger\,|a\rangle \\ &=\; -i\ \sum_{nab} \rho_{ab} e^{i(\omega_b - \omega_n)t}\,\langle b|\,\hat{c}_\alpha\,|n\rangle\,\langle n|\,\hat{c}_\beta^\dagger\,|a\rangle \end{aligned} \tag{2.20}$$

6

with ρ the density matrix. In the fourth line the unity $\sum_n |n\rangle \langle n|$ has been inserted. Then we perform a Fourier transform defined by

$$\tilde{g}(\omega) = \int\limits_{-\infty}^{\infty} g(t)e^{i\omega t}dt \qquad (2.21)$$

whereat in the following we omit the tilde. Then we can write the greater Green's function as

$$G_{\alpha,\beta}^{>}(\omega) = -i \sum_{nab} \rho_{ab} \langle b| \hat{c}_\alpha |n\rangle \langle n| \hat{c}_\beta^\dagger |a\rangle \cdot 2\pi \, \delta(\omega - (\omega_n - \omega_b)). \qquad (2.22)$$

For the retarded Green's function we have to consider the Θ-function, which implies the causality and can be interpreted as a form of a boundary condition. Exploiting the residue theorem it follows that

$$\Theta(t) = \frac{i}{2\pi} \int d\omega \frac{e^{-i\omega t}}{\omega + i0^+} \qquad (2.23)$$

holds, with 0^+ an infinitesimally small positive real number. We use this in the Fourier transform of the retarded Green's function which gives

$$G_{\alpha,\beta}^{ret}(\omega) = \lim_{0^+ \to 0} \sum_{nab} \rho_{ab} \left(\frac{\langle b| \hat{c}_\alpha |n\rangle \langle n| \hat{c}_\beta^\dagger |a\rangle}{\omega + i0^+ - (\omega_n - \omega_b)} + \frac{\langle b| \hat{c}_\beta^\dagger |n\rangle \langle n| \hat{c}_\alpha |a\rangle}{\omega + i0^+ - (\omega_a - \omega_n)} \right). \qquad (2.24)$$

From that we identify important properties of the retarded Green's function:

- It is analytic in the upper half of the complex plane, as all of its poles lie underneath of the real axis.

- Its poles are at the many-body excitation energies of the system.

- For the case $\alpha = \beta$ one can show that

$$\text{Im}\left\{ G_{\alpha,\alpha}^{ret}(\omega) \right\} = -\pi S_{\alpha,\alpha}(\omega) \qquad (2.25)$$

  is valid with $S_{\alpha,\alpha}(\omega)$ the spectral density [20].

Thus it comes clear that Green's functions are an important and powerful tool in treating quantum mechanical many-body systems. A more detailed introduction to equilibrium Green's functions can be found in [14] and [15].

2.1.3. Perturbation Theory

In the last section it was necessary to diagonalize the full system Hamiltonian for calculating the Green's functions. This, however, is in general not possible. An example are

the physical situations that are investigated in this thesis. They consist of a small system that is connected to large baths. The Hamiltonian describing the whole situation is too big to be diagonalized. One possible way to solve this is to diagonalize the Hamiltonian of the small system and reintroduce perturbatively the influence of the large baths. The many degrees of freedom of the bath thereby have to be traced out. For that purpose one uses perturbation theory within the framework of Green's functions. In this chapter we give a brief introduction to perturbations theory. First we explain the concept of the S-Matrix and then its application within many-body physics. We further mention that from here on the hat upon operators is omitted.

Perturbation theory is performed within the so-called *interaction picture* in which Schrödinger's equation has the form

$$i\frac{\partial}{\partial t}\left|\Psi(t)\right\rangle_I \;=\; H_I\left|\Psi(t)\right\rangle_I \tag{2.26}$$

with

$$\left|\Psi(t)\right\rangle_I \;=\; e^{iH_0 t}\left|\Psi(t)\right\rangle \tag{2.27}$$

and

$$H_I \;=\; e^{iH_0 t}H_{int}e^{-iH_0 t}. \tag{2.28}$$

$H \;=\; H_0 + H_{int}$ is the Hamiltonian describing the whole situation, with H_0 the non-interacting part and H_{int} describing the interaction term. A formal solution of the above equation (2.26) is given by

$$\left|\Psi(t)\right\rangle_I \;=\; T_D e^{-i\int_{t_0}^{t} H_{int}(t')dt'}\left|\Psi(t_0)\right\rangle_I \;=\; S(t,t_0)\left|\Psi(t_0)\right\rangle_I, \tag{2.29}$$

with T_D the Dyson time ordering operator [14]. It is a generalization of the time ordering operator of equation (2.18) for an arbitrary number of operators. The sequence of operators is therewith ordered in ascending order such that operators with earliest times are to the left and latest times to the right. The solution in equation (2.29) is achieved with a series approach to equation (2.26) by formal integrating and reinserting iteratively [14]. $S(t,t_0)$ is the so called *S-matrix*, describing the unitary time evolution from state $\left|\Psi(t_0)\right\rangle_I$ to $\left|\Psi(t)\right\rangle_I$. It has the following two important properties:

- $S(t,t_0) \;=\; S(t_0,t)^{-1} \;=\; S(t_0,t)^{\dagger}$

- $S(t_0,t_0) \;=\; \mathbb{1}$

The time evolution of an Operator $O(t)$ is written as

$$\hat{O}(t) \;=\; \hat{S}(t_0,t)\hat{O}_I(t)\hat{S}(t,t_0). \tag{2.30}$$

We want to point out that O has an implicit time dependence coming from the interaction picture, which is given by $O_I(t) \;=\; e^{iH_0 t}Oe^{-iH_0 t}$. The S-matrix is the central object in perturbation theory and has a broad range of applications [21, 22].

Within the framework of this thesis we perform perturbation theory with Green's functions. To explain this in the following we assume that temperature $T \approx 0\,K$ and thus the non-interacting system stays in the ground state ψ_0. For finite temperatures one has to use the *Matsubara method* which will be briefly sketched later. Here we rewrite the time ordered Green's function in the ground state, using the above relation (2.30):

$$
\begin{aligned}
G_{\alpha,\beta}(t,t') &= \langle T_D \ c_\alpha(t) \ c_\beta^\dagger(t') \rangle_0 = \\
\dots &= \langle \psi_0 |_I \ T_D \ S(t_0,t) c_\alpha(t)_I S(t,t_0) \ S(t_0,t') c_\beta^\dagger(t')_I S(t',t_0) \ |\psi_0\rangle_I .
\end{aligned}
\tag{2.31}
$$

After exploiting the relations

$$
S(t,t_0) S(t_0,t') = S(t,t')
$$

and

$$
S(t_0,\infty) S(\infty,t_0) = \mathbb{1}
$$

as well as setting $t_0 = -\infty$ we get

$$
\begin{aligned}
G_{\alpha,\beta}(t,t') &= \langle \psi_0 |_I \ S(-\infty,\infty) S(\infty,-\infty) \ T_D \ S(-\infty,t) c_\alpha(t)_I S(t,-\infty) \cdot \dots \\
&\quad \dots S(-\infty,t') c_\beta^\dagger(t)_I S(t',-\infty) \ |\psi_0\rangle_I \\
&= \langle \psi_0 |_I \ S(-\infty,\infty) \ T_D \ c_\alpha(t)_I \ c_\beta^\dagger(t)_I \ S(\infty,-\infty) |\psi_0\rangle_I
\end{aligned}
\tag{2.32}
$$

In the third line it was exploited that on the right side of T_D one does not have to care about time ordering as the time-ordering operator already makes sure that it is fulfilled. The term on the left side of T_D, however, has to be treated separately. Basically it is the state that has evolved from $t = -\infty$ to $t = \infty$

$$
\langle \psi_0 |_I \ S(-\infty,\infty)
\tag{2.33}
$$

which in general is unknown. Therefore, one makes the further assumption that the interaction is turned on and off adiabatically. This is done by writing the Hamiltonian as

$$
H = H_0 + H_{int} \cdot e^{-\epsilon|t|}
\tag{2.34}
$$

with ϵ a very small positive number. Now it is possible to exploit *Gell-Man-Low's* theorem: It states that if $\langle \psi_0 |_I$ at $t = -\infty$ is an eigenstate of H_0 and H_{int} is switched on adiabatically, the state at $t = \infty$ differs from the initial state solely by a phase-factor. Additionally we have to assume that there is no level crossing which is true in most cases. A detailed discussion thereof can be found in [14]. Using Gell-Man-Low's theorem we get for the wave function the relation

$$
\langle \psi_0 |_I S(-\infty,\infty) = \langle \psi_0 |_I \cdot e^{i\varphi},
\tag{2.35}
$$

with the phase-factor given by

$$e^{i\varphi} = \langle\psi_0|_I S(-\infty,\infty) |\psi_0\rangle_I .\qquad(2.36)$$

We use this in equation (2.32) and write the phase factor out in front of the terms:

$$G_{\alpha,\beta}(t,t') = e^{i\varphi} \langle\psi_0|_I T_D c_\alpha(t)_I c_\beta^\dagger(t)_I S(\infty,-\infty)|\psi_0\rangle_I \qquad(2.37)$$

$$= \frac{\langle\psi_0|_I T_D c_\alpha(t)_I c_\beta^\dagger(t')_I S(\infty,-\infty)|\psi_0\rangle_I}{(e^{i\varphi})^\dagger}\qquad(2.38)$$

$$= \frac{\langle\psi_0|_I T_D c_\alpha(t)_I c_\beta^\dagger(t')_I S(\infty,-\infty)|\psi_0\rangle_I}{\langle\psi_0|_I S(\infty,-\infty)|\psi_0\rangle_I}\qquad(2.39)$$

The last line is an important result since it is possible to expand both numerator and denominator separately in terms of a series expansion. In the following we discuss this in more detail and show how to obtain Dyson's equation for Green's functions. Thereby we mainly follow the argumentation of [14] as well as [16].
First we considered the denominator of equation (2.39) and write out the integral explicitly:

$$\langle\psi_0|_I S(\infty,-\infty)|\psi_0\rangle_I = \sum_{n=0}^{\infty}\frac{(-i)^n}{n!}\int_{-\infty}^{\infty}\cdots\int dt_1\ldots dt_n e^{-\epsilon(|t_1|+\cdots+|t_n|)}\ldots$$

$$\ldots\langle\psi_0|_I T H(t_1)_{int}\ldots H(t_n)_{int}|\psi_0\rangle_I .\qquad(2.40)$$

This is often referred to as the vacuum amplitude. The numerator of the causal single particle Green's function from equation (2.39) becomes

$$\langle\psi_0|_I T_D c_\alpha(t)_I c_\beta^\dagger(t')_I S(\infty,-\infty)|\psi_0\rangle_I = \sum_{n=0}^{\infty}\frac{(-i)^n}{n!}\int_{-\infty}^{\infty}\cdots\int dt_1\ldots dt_n\ldots$$

$$\ldots\cdot e^{-\epsilon(|t_1|+\cdots+|t_n|)}\langle\psi_0|_I T H(t_1)_{int}\ldots H(t_n)_{int} c_\alpha(t)_I c_\beta^\dagger(t')_I|\psi_0\rangle_I ,\qquad(2.41)$$

The integrals in equations (2.40) and (2.41) are now suitable for using perturbation theory in terms of Feynman diagrams. In the following we provide an overview of the steps, that lead to a consistent diagrammatic perturbation theory for Green's functions. For a more detailed derivation the reader is referred to [14]. We want to find a translation of the integrals of every order (n) in equation (2.40) and (2.41) into Feynman diagrams. Therefore we consider three important concepts:

i) **Normal Product**

ii) **Wick-contraction**

iii) **Wick's theorem**

i) For a given product of annihilation and creation operators the **normal product** $N(...)$ is defined as the arrangement when all the creation operators are to the left of all annihilation operators. The initial order among creators and annihilators is thereby not changed. Here we solely consider systems with fermionic operators. In this case we have to consider in principle the factor (-1) when commuting two operators. For the following considerations, however, we need the expectation value of the sequence of operators in the ground state $\langle \ldots \rangle_0$, which provides

$$\langle N(\ldots a_k^\dagger \ldots a_j) \rangle_0 \;=\; \langle \psi_0 | \, N(\ldots a_k^\dagger \ldots a_j) \, | \psi_0 \rangle \;=\; 0 \tag{2.42}$$

due to the fact that $a_j \, |\psi_0\rangle = 0$.

ii) We use this result to rewrite expectation values of two T_D-ordered creation and annihilation operators by defining the so-called **Wick-contraction**:

$$\overparen{A(t)B(t')} := T_D(A(t)B(t')) - N(A(t)B(t')) , \tag{2.43}$$

with $A(t)$ and $B(t')$ being arbitrary fermionic creation or annihilation operators and their time dependence given by the quadratic free Hamiltonian:

$$A(t) \;=\; e^{-iH_0 t} A e^{-iH_0 t} . \tag{2.44}$$

For the expectation value of a Wick-Contraction in the ground state, using equation (2.42), we obtain

$$\langle \overparen{A(t)B(t')} \rangle_0 = \langle T_D(A(t)B(t')) \rangle_0 . \tag{2.45}$$

Using this we can identify the following relations for contractions of creation and annihilation operators:

$$\overparen{a_k(t)a_k^\dagger(t')} \;=\; iG_{k,k}^0(t-t') . \tag{2.46}$$

G^0 is a free, time-ordered Green's functions. A more detailed discussion thereof can be found in [14]. This is an important result for the further diagrammatic consideration of time-ordered Green's functions. In order to apply this result to equations (2.40) and (2.41) we have to generalize it for expectation values of a product of an arbitrary even number of operators.

iii) For that purpose we need **Wick's theorem**. It states that the time-ordered product of an *even number* of operators can be rewritten as sums of normal products plus

the total pairing of all the operators [14]. We write it schematically as

$$
\begin{aligned}
T(AB \ldots X \ldots) \;=\; & N(ABC \ldots X \ldots) + \ldots \\
& + N(\overset{\frown}{A}B\overset{\frown}{C} \ldots X \ldots) + \ldots N(\overset{\frown}{A}BC \ldots \overset{\frown}{X} \ldots) \\
& + (N(\ldots) \text{ with one contraction}) + \ldots \\
& + N(\overset{\frown}{AB\overset{\frown}{C}} \ldots X \ldots) + \ldots \\
& + (N(\ldots) \text{ with two contraction}) + \ldots \\
& \qquad\qquad \vdots \\
& + \{\text{total pairing}\} \;.
\end{aligned}
\tag{2.47}
$$

The Wick-contractions inside the normal products are numbers, which in principle could be drawn out in front. The important result is, that for the ground-state expectation value, using equation (2.42), only the last term in (2.47) is not equal to zero:

$$
\langle T(AB \ldots XY \ldots)\rangle_0 \;=\; \langle \{\text{total pairing}\}\rangle_0 \;.
\tag{2.48}
$$

Total pairing is the sum of all possible complete decompositions of the product of operators into contractions of pairs, schematically written as

$$
\begin{aligned}
\{\text{total pairing}\} \;=\; & \overset{\frown}{AB} \cdot \overset{\frown}{CD} \cdot \ldots \cdot \overset{\frown}{XY} \\
& - \overset{\frown}{AC} \cdot \overset{\frown}{BD} \cdot \ldots \cdot \overset{\frown}{XY} \\
& + \ldots .
\end{aligned}
\tag{2.49}
$$

In doing so it is of course important to consider the anti-commutator relations for the fermionic operators, which we indicated with the minus sign in the second line. As a result, Wick's theorem allows to rewrite the ground state expectation value of a T_D-ordered product of operators as a sum of products of all possible pair-wise contractions. This is especially useful for the numerator and denominator of the time-ordered Green's function in equations (2.40) and (2.41).

Using the results of (i),(ii) and (iii), we are now able to translate the terms in the series expansion of the time-ordered Green's function of (2.40) and (2.41) into Feynman diagrams. In the following we will do that exemplarily for the first order term in equation (2.41) (n=1). For that purpose we write out explicitly the first order numerator:

$$
(\text{numerator})^{(1)} \;=\; (-i) \int\limits_{-\infty}^{\infty} dt_1 \cdot e^{-\epsilon(|t_1|)} \, \langle \psi_0|_I \, T H(t_1)_{int} \, c_\alpha(t)_I \, c_\beta^\dagger(t')_I \, |\psi_0\rangle_I \;.
\tag{2.50}
$$

We assume that H_{int} describes a pair interaction of the form

$$H(t_1)_{int} = V_{kl,mn} \int_{-\infty}^{\infty} dt_1' \delta(t_1 - t_1') c_k^\dagger(t_1')_I c_l^\dagger(t_1)_I c_m(t_1')_I c_n(t_1)_I, \qquad (2.51)$$

where the Kronecker-Delta indicates that it is an instantaneous interaction. Putting this into equation (2.50) provides

$$(\text{numerator})^{(1)} = (-i) \iint_{-\infty}^{\infty} dt_1 dt_1' \delta(t_1 - t_1') e^{-\epsilon(|t_1|)} \cdot \ldots$$

$$\ldots \langle \psi_0|_I \, T V_{kl,mn} c_k^\dagger(t_1')_I c_l^\dagger(t_1)_I c_m(t_1)_I c_n(t_1')_I \, c_\alpha(t)_I \, c_\beta^\dagger(t')_I \, |\psi_0\rangle_I \, . \qquad (2.52)$$

For the ground-state expectation value of the product of ladder operators we use Wick's theorem as explained above. The result is a sum over all possible products of pairings. We translate this into Feynman diagrams using the following rules:

- **Vertex:** The interaction is represented by a dashed line between two points.

- **Line:** A free Green's functions is represented by a continuous line, connecting vertex-points.

For the term in equation (2.52) we obtain from Wick's theorem six different summands. In the following we will not study all of them in detail but exemplarily regard two of them:

a) $\ T V_{kl,mn} c_k^\dagger(t_1') c_l^\dagger(t_1) c_m(t_1) c_n(t_1') c_\alpha(t) c_\beta^\dagger(t')$

b) $\ T V_{kl,mn} c_k^\dagger(t_1') c_l^\dagger(t_1) c_m(t_1) c_n(t_1') c_\alpha(t) c_\beta^\dagger(t')$

For better readability we omitted the subscript I in the above terms. Using the above rules we drew the corresponding Feynman diagrams in figure 2.1. Each Feynman diagram corresponds to a summand in the series expansion of the numerator of the Green's function from equation (2.41). This summand is calculated from the graphical representation using the following rules:

- Integrate over all intern variables. (In the current example t_1 and t_1'.)

- Sum over all intern indices. (In the current example k, l, m, n.)

- Do *not* integrate or sum over external variables. (In the current example α, β, t, t'.)

To obtain a complete series expansion of the numerator of the time ordered Green's function we have to draw each Feynman diagram for all possible pair-wise contractions. Especially for higher order terms this would be too expensive. However, it turns out that
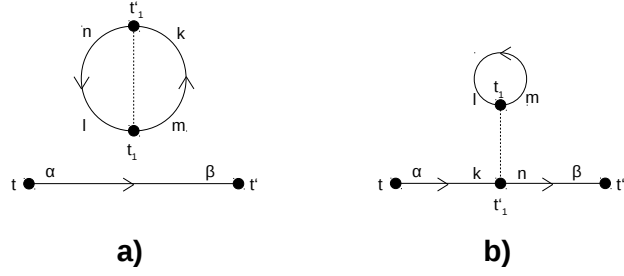
Figure 2.1.: Example of two Feynam diagrams according to a) and b).

for the series expansion of the full time-ordered Green's function we do not have to draw out all possible diagrams. To explain this we have to distinguish between connected and unconnected diagrams: Every Feynman graph that can be divided without cutting through a line is called unconnected. All other graphs are connected. In figure 2.1, diagram (a) is an unconnected graph and diagram (b) is a connected one. Further we have to distinguish between open and closed diagrams: An open diagram is connected with the external variables, a closed one not. It is possible to show that all unconnected diagrams can be written as a product of open and closed diagrams [14]. Again we have an example thereof in figure 2.1 (a). Further it turns out that we obtain all possible diagrams of the numerator if we multiply each combination of open and connected diagrams with all possible closed diagrams [14]. At this point we are now able to exploit the **linked-cluster-theorem**. It states that the diagrammatic expansion of the denominator, or the vacuum amplitude respectively, can be written as a product of solely closed and connected diagrams [14]. This allows to cancel out the denominator of the time-ordered Green's function with the corresponding factor in the numerator. As a result only the open and connected Feynman diagrams have to be considered in the series expansion. A more detailed discussion thereof can be found in [14]. Performing a series expansion in terms of Feynman diagrams using the relations derived so far, we see that in every order of perturbation theory we get topologically equivalent graphs. All these have the same contribution in the series expansion and therefore have to be considered only once, regarding the corresponding pre-factor. From this we finally obtain the following rules for Feynman diagrams for Green's functions:

- Draw all topological different diagrams from the numerator of the Green's function.

- Only those who are open and connected have to be considered.

- Sum over all intern indices and integrate over all intern variables.

- Multiply every term with the factor $i^n(-1)^f$, where n is the order of perturbation theory and f is the number of closed loops.

14

We point out that this section serves as an overview of how to formulate Feynman diagrams within the framework of Green's functions in many-body physics. For a more detailed explanation the reader is referred to [14], [23] and [16].

2.1.4. Dyson Equation

In the previous section we have shown how to perform perturbation theory for Green's functions within the framework Feynman diagrams. It formerly has been necessary to treat every order in perturbation theory separately. Thus, for receiving a complete series expansion we are restricted to situations when the series expansion converges and allows to be truncated at some point. If this is not the case we have to find a way to formally sum up the terms up to infinite order. One possibility to do that is with the help of **Dyson's equation**. In this section we briefly explained how Dyson's equation is obtained, using Feynman diagrams. Thereby we mainly follow the argumentations of [14] and [16]. As an explanatory example we use the time-ordered Green's function for fermions with pairwise interactions, which we already treated in the previous section.
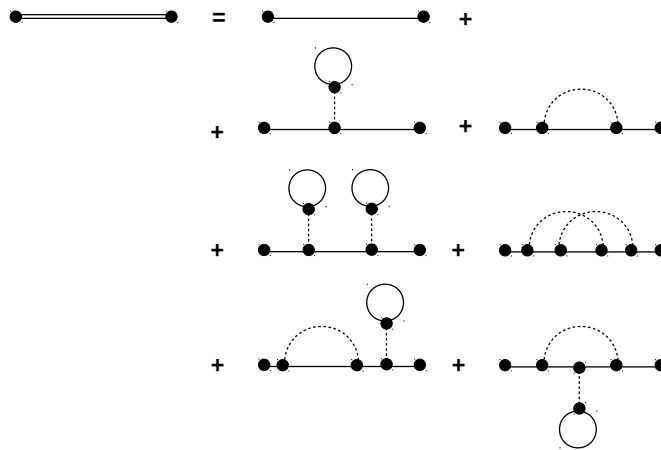
Figure 2.2.: Examples of connected Feynman diagrams of the time ordered Green's function for fermions with pair-wise interactions. The full Green's function is drawn as a double line.

In figure 2.2 we schematically sketch its diagrammatic expansion up to terms of second order, whereby we did not draw all diagrams. The ambition is to introduce the so called **self-energy**. It is defined as the part of a diagram that is left if one omits the external lines or external Green's functions respectively. This is shown in figure 2.3, where we highlighted the self energy terms of the series expansion in red. We further define the so called **irreducible self-energy** as the self-energy which can *not* be divided into two by cutting through a solid line or Green's function respectively. The self energy of the

15

first summand in the second line of figure 2.3, for example, is irreducible whereas the first summand in the third line is reducible.
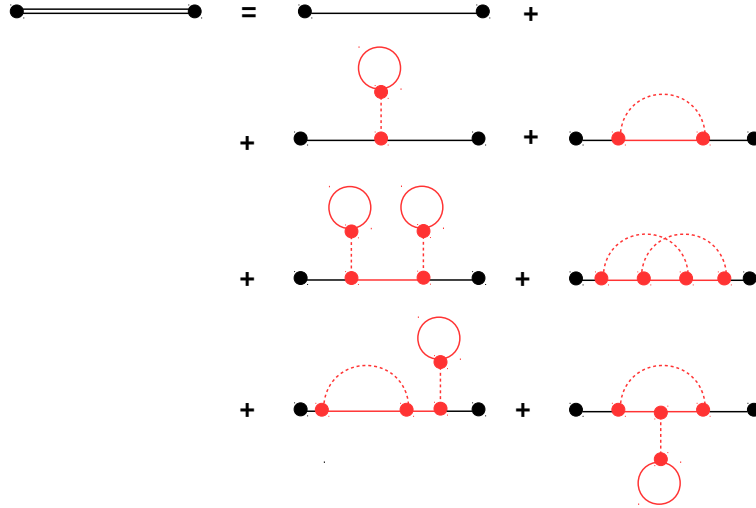
Figure 2.3.: Same example of Feynman diagrams as in figure 2.2, whereby the self energy terms have been highlighted in red.

We re-reorder the diagrammatic expansion in figure 2.4 and obviously each irreducible self-energy is connected to a complete series expansion of the full Green's function. Using this, we again obtain a complete series expansion by summing up all irreducible self-energy terms that are connected to full Green's functions. If we formally summarize all irreducible self-energy terms and write them as $\boldsymbol{\Sigma}$ we finally obtain Dyson's equation. We schematically sketched this in figure 2.5 a) in terms of Feynman diagrams. The diagrammatic expansion of the full self-energy can further be simplified. As sketched in figure 2.5 b) and c), also beneath the vertices a full series expansion of the Green's function occurs. Hence, the solid lines in the series expansion of the self-energy can be replace by double lines, which means replacing the unperturbed Green's functions by full ones. The results are called **Skeleton Diagrams**, which drastically reduce the variety of Feynman diagrams in the series expansion of the self-energy. Figure 2.5 a) is the diagrammatic representation of Dyson's equation which has the form

$$G_{1,2}(t_1, t_2) = g_{1,2}(t_1, t_2) + \sum_{3,4} \iint dt_3 dt_4 \ g_{1,3}(t_1, t_3) \, \Sigma_{3,4}(t_3, t_4) \, G_{4,2}(t_4, t_2), \qquad (2.53)$$

where the indices stand for internal, (3,4), respectively external, (1,2), variables. The small g_{jk} is the unperturbed free Green's function and G_{jk} the full Green's function. With this we formally have a solution for the perturbative series expansion up to infinite
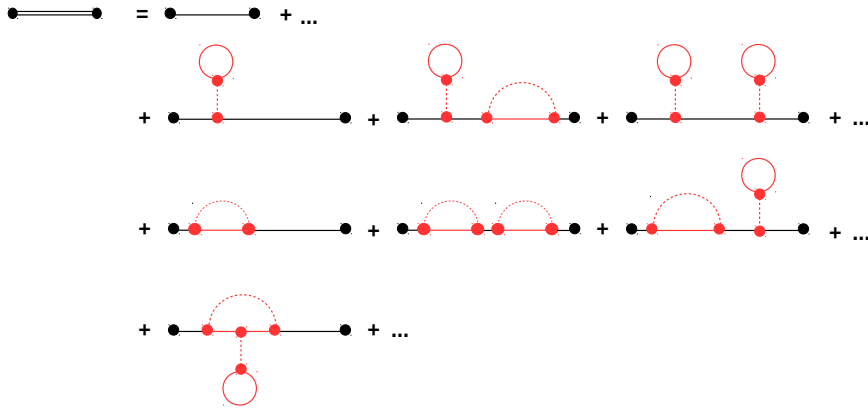
Figure 2.4.: Diagrammatic series expansion of time ordered Green's function. The terms have been re-ordered to explain how Dyson's equation is obtained.
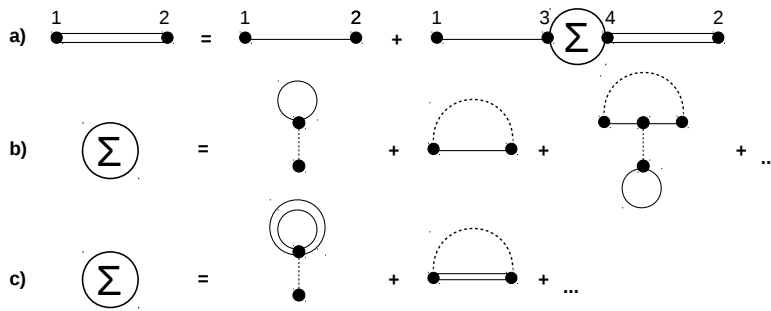
Figure 2.5.: a): Dyson's Equation written in Feynman diagrams. The points have been labelled to indicate the external and internal variables.
b): Sum over all irreducible self energies.
c): Skeleton diagrams of the self energy.

order. The challenging part therein is to obtain the self-energy, which in general is a non-linear complex functional of the internal variables as well as of the full Green's function. In most cases it is unknown. Nevertheless, we mention that the self energy diagrams are of simpler form than those of the full Green's function. In the end of this section we present the formulation of Dyson's equation in frequency space. In many cases this turns out to be very useful, especially if the Hamiltonian is not implicitly time-dependent. As we already mentioned in the previous section, in this case the Green's function only depends on the the time difference $(t_2 - t_1)$. The integrals in equation 2.53 then correspond to convolutions, which, after a Fourier transform to frequency space,

become products. We use this to write Dyson's equation (2.53) as

$$G_{1,2}(\omega) \;=\; g_{1,2}(\omega) \;+\; \sum_{3,4} g_{1,3}(\omega)\Sigma_{3,4}(\omega)\, G_{4,1}(\omega) \tag{2.54}$$

with $G(\omega) \;=\; \int \mathrm{G}(t)e^{i\omega t}dt$. Further, the sum over indices can be written in matrix form and we obtain a very compact form of Dyson's equation:

$$\mathbf{G}(\omega) \;=\; \mathbf{g}(\omega) \;+\; \mathbf{g}(\omega)\,\boldsymbol{\Sigma}(\omega)\,\mathbf{G}(\omega) \tag{2.55}$$

2.1.5. Matsubara Green's functions

In this section we discuss the Matsubara method, which allows to perform perturbation theory with Green's functions at finite temperatures $(\mathrm{T} > 0\,K)$. We thereby follow [14] and [16].

In the previous chapter we have introduced perturbation theory for correlation functions in the ground state of the system. However, at finite temperatures and in thermal equilibrium, expectation values are calculated within a grand canonical ensemble. In that case the perturbation theory from the previous section can not be applied straight forwardly. In particular, Wick's theorem has to be generalized. In quantum mechanics the grand canonical ensemble is described by a density matrix of the form

$$\rho = \frac{e^{-\beta(H-\mu)}}{Z} \;, \tag{2.56}$$

with $Z = tr\left\{e^{-\beta(H-\mu)}\right\}$ the grand canonical partition function. The idea of Matsubara was to introduce a generalization of the time-ordered Green's functions that allows for a treatment with perturbation theory at finite temperatures [24]. To explaining this we introduce the Matsubara Green's function

$$G_{jk}^{M}(\tau,\tau') \;=\; -tr\left\{e^{-\beta(H-\mu)}T_{\tau}\left(c_{j}(\tau)c_{k}^{\dagger}(\tau')\right)\right\}\cdot\frac{1}{Z} \tag{2.57}$$

with the imaginary time argument $\tau = it$ and an ordering operator along the imaginary time axis defined as

$$T_{\tau}\;A(\tau)B(\tau') \;=\; \begin{cases} A(\tau)B(\tau') & \text{for } \tau > \tau' \\ \epsilon^{p}\,B(\tau')A(\tau) & \text{for } \tau < \tau' \end{cases}. \tag{2.58}$$

Thereby p is the number of permutations of fermionic operators that is necessary to exchange A and B. $\epsilon \;=\; -1$ for fermions and $\epsilon \;=\; +1$ for bosons. If the Hamiltonian does not have an implicit time dependence the Matsubara functions only depend on the difference of the complex time arguments: $G_{jk}^{M}(\tau,\tau') \;=\; G_{jk}^{M}(\tau-\tau')$. In the following we will assume that this is the case and therefore set $(\tau - \tau') \to \tau$. An important property

of Matsubara Green's functions is

$$G_{jk}^M(\tau + \beta) \;=\; \epsilon\, G_{jk}^M(\tau),\qquad\qquad(2.59)$$

with $\epsilon = +1$ for bosons and $\epsilon = -1$ for fermions. This means that they have a cyclic periodicity along the imaginary time axis. A detailed derivation of that is given in [14]. Thus, Matsubara Green's functions are completely defined on the interval

$$-\beta < \tau < \beta \;.$$

The periodicity is used to express Matsubara Green's functions in terms of a Fourier series as follows:

$$G^M(\tau) \;=\; \frac{1}{\beta} \sum_n e^{-i\omega_n \tau} G^M(i\omega_n) \qquad\qquad(2.60)$$

with ω_n the Matsubara frequencies given by

$$\omega_n \;=\; \begin{cases} \frac{2(n-1)\pi}{\beta} & \text{for fermions} \\ \frac{2n\pi}{\beta} & \text{for bosons .} \end{cases}$$

The Fourier coefficients are given by

$$G^M(i\omega_n) \;=\; \int\limits_0^\beta d\tau\, e^{i\omega_n \tau} G^M(\tau) \;. \qquad\qquad(2.61)$$

A detailed discussion thereof is given in [14]. Within Matsubara formalism it is possible to define an interaction-picture with a time evolution operator that satisfies

$$-\frac{\partial}{\partial t} U_D(\tau, \tau') \;=\; H_I(\tau) U_D(\tau, \tau') \qquad\qquad(2.62)$$

and H_I the perturbation Hamiltonian in Dirac picture. The S-matrix, similar to that in the previous section, is written as

$$S(\tau, \tau') \;=\; T_\tau\, e^{-\int\limits_{\tau'}^{\tau} H_I(\tau'')d\tau''} \;. \qquad\qquad(2.63)$$

To perform perturbation theory, Wick's theorem is generalized. We do not discuss this here in detail and refer the reader to [14]. The important result is that one finds a diagrammatic perturbation theory in terms of Feynman diagrams, similar to the case of ground-state Green's functions. Further, it is possible to formulate a Dyson equation of the form

$$\mathbf{G^M}(i\omega_n) \;=\; \mathbf{g^M}(i\omega_n) \;+\; \mathbf{g^M}(i\omega_n)\,\mathbf{\Sigma^M}(i\omega_n)\,\mathbf{G^M}(i\omega_n) \qquad\qquad(2.64)$$

with $\mathbf{\Sigma^M}$ the Matsubara self-energy. We point out that these are very important results, since with them it is possible to perform diagrammatic perturbation theory at finite

temperatures. From the obtained Matsubara Green's functions we can calculate the retarded Green's function by analytic continuation from the imaginary to the real ω-axis:

$$\mathbf{G}^{ret}(z = i\omega_n) = \mathbf{G^M}(i\omega_n). \tag{2.65}$$

We conclude that the Matsubara method is a powerful tool in statistical many body physics that allows to perform perturbation theory at finite temperatures. It further is the basis for the formalism of nonequilibrium Green's functions which we discuss in the subsequent section.

2.1.6. Nonequilibrium Green's functions

In this section we provide a brief introduction to nonequilibrium Green's functions and the Keldysh formalism. For more detailed derivations we refer the reader to [25] and [16]. In the following we mainly follow the argumentation of [25].
WE first have to define how a nonequilibrium situation is achieved: A standard way is to consider a system that is at thermal equilibrium up to a certain time t_0. Then a disturbance, described by a contribution H' to the Hamiltonian, is turned on which induces a nonequilibrium situation. The whole Hamiltonian then has the form

$$H = H_0 + H_I + \Theta(t - t_0)H' . \tag{2.66}$$

with H_0 the non-interacting part, H_I the interaction term and H' the contribution that indices the nonequilibrium situation. In the previous chapter we have shown how to perform perturbation theory at finite temperatures. This procedure, however, does not work in the present case, since the S-matrix of equation 2.63 only considers the perturbation due to H_I. The remaining Hamiltonian, $H_0 + \Theta(t - t_0)H'$, is not necessarily quadratic in creation and annihilation operators. Therefore, the modified Wick's theorem used in the Matsubara formalism does not apply straightforwardly. We again regard the situation described by equation (2.66). At $t \leq t_0$ we still are in thermal equilibrium and we have the following relation

$$e^{-\beta H} = e^{-\beta H_0} U_D^I(t_0 - i\beta, t_0) , \tag{2.67}$$

with a complex time argument. This follows directly from Matsubaras formalism [14]. $U_D^I(t_0 - i\beta, t_0)$ is the time evolution operator along the complex time-axis, which we further write as

$$U_D^I(t_0 - i\beta, t_0) = T_\tau e^{-i \int_{t_0}^{t_0 - i\beta} H_I(t')dt'} \tag{2.68}$$
$$= S_I(t_0 - i\beta, t_0) ,$$

with S_I the S-matrix from the Matsubara method. This corresponds to an integration along the imaginary time-axis from 0 to $-i\beta$, with the real part equal t_0. We provide a sketch thereof in figure 2.6 a). In this chapter we want to perform perturbation theory

with Green's functions of the form

$$G_{jk}(t,t') = -i \, tr \left\{ e^{-\beta(H-\mu)} \, c_j(t) \, c_k^\dagger(t') \right\} \frac{1}{Z} \, . \tag{2.69}$$

The time dependence of ladder operators is given in the Heisenberg picture with $c_j(t) = e^{-iHt} c_j e^{-iHt}$. In order to be able to perform perturbation theory, we have to switch to the interaction picture with respect to H_0. In the nonequilibrium case, however, we have in principle two perturbation Hamiltonians: H_I and H'. Hence, we have to find a way to take into account both S-matrices, one according to H' and one according to H_I. We first write down the S-matrix regarding H'

$$S_{H'}(t,t_0) = T_D \, e^{-i \int_{t_0}^{t} H'_D(t') dt'} \tag{2.70}$$

which provides for the time evolution

$$c_j(t) = S_{H'}^\dagger(t,t_0) c_{j,(H_0+H_I)}(t) S_{H'}(t,t_0) \, . \tag{2.71}$$

H'_D denotes the operator H' in the Dirac or interaction picture with respect to (H_0+H_I). With this we are still not able to perform perturbation theory since $(H_0 + H_I)$ is not necessarily quadratic in terms of ladder operators. We additionally have to take into account the S-matrix regarding H_I. For this purpose we rewrite equation 2.71 as

$$c_j(t) = T_c \, e^{-i \int_c H'_D(t') dt'} \, c_{j,H'}(t) = S_{c,H'} \, c_{j,H'}(t) \, . \tag{2.72}$$

Thereby we combined the integrals in (2.71) to one integral along the contour as sketched in figure 2.6, b). The correct order of operators is ensured by replacing the time-ordering
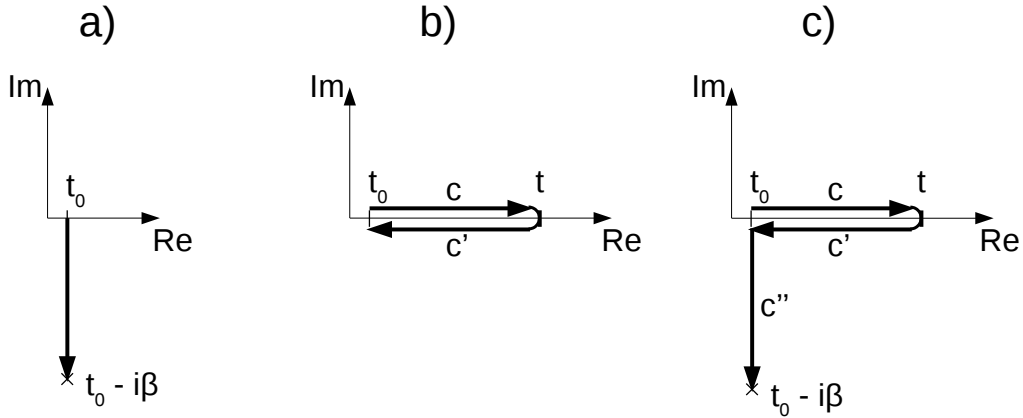
Figure 2.6.: Sketch of integration contours needed for the Keldysh formalism.

operator T_D by a contour-ordering operator T_c which orders time arguments along a specific contour. To explain this in more detail we provide a short example for the contour b) from figure 2.6: The idea is to additionally specify on which side of the contour the operators lay. The path of integration goes along the contours as indicated by the arrows in figure 2.6 b). From this we obtain the following ordering:

$$T_c \left(A(t, c_A) \, B(t', c_B) \right) \;=\; \begin{cases} A(t, c_A) \, B(t', c_B) & \text{if} \quad c_A = c \,,\; c_B = c' \\ \epsilon^p B(t', c_B) \, A(t, c_A) & \text{if} \quad c_A = c' \,,\; c_B = c \end{cases} \qquad (2.73)$$

$$T_c \left(A(t, c) \, B(t', c) \right) \;=\; \begin{cases} A(t, c) \, B(t', c) & \text{if} \quad t > t' \\ \epsilon^p B(t', c) \, A(t, c) & \text{if} \quad t < t' \end{cases} \qquad (2.74)$$

$$T_c \left(A(t, c') \, B(t', c') \right) \;=\; \begin{cases} A(t, c') \, B(t', c') & \text{if} \quad t < t' \\ \epsilon^p B(t', c') \, A(t, c') & \text{if} \quad t > t' \end{cases} \qquad (2.75)$$

with $\epsilon = -1$ for fermions, $\epsilon = +1$ for bosons and p the number of permutations that is necessary to exchange A and B. In the present case the contour goes from t_0 to t and then back to t_0. In principle we could arbitrarily deform it as long as we reach t. We use this to rewrite the Green's function from 2.69 as

$$G_{jk}^c(t, t') \;=\; -i \frac{tr \left\{ e^{-\beta(H-\mu)} \, T_c \left(S_{c,H'} \, c_{j,H'}(t) \, c_{k,H'}^\dagger(t') \right) \right\}}{tr \left\{ e^{-\beta(H-\mu)} T_c \, S_{c,H'} \right\}} \,. \qquad (2.76)$$

with the subscript c indicating the contour ordering. In this form it is still in the interaction picture with respect to $(H_0 + H_I)$. Thus, we exploit the relations 2.67 and 2.68, which allow us to transform into the interaction picture with respect to H_0:

$$G_{jk}^c(t, t') \;=\; -i \frac{tr \left\{ e^{-\beta(H_0-\mu)} \, T_c \left(S_{c,I} \, S_{c,H'} \, c_{j,H_0}(t) \, c_{k,H_0}^\dagger(t') \right) \right\}}{tr \left\{ e^{-\beta(H_0-\mu)} T_c S_{c,I} \, S_{c,H'} \right\}} \,. \qquad (2.77)$$

For this purpose we choose the contour as depicted in sketch c) of figure 2.6. Now we are able to apply Wick's theorem and perform perturbation theory analogous to the equilibrium case. The perturbative series expansion of the Green's function is then similarly mapped onto Feynman diagrams [25]. From that we can formulate Dyson's equation in the nonequilibrium case for the contour ordered Green's function:

$$G_{1,2}^c(t_1, t_2) = g_{1,2}^c(t_1, t_2) + \sum_{3,4} \iint_c dt_3 dt_4 \; g_{1,3}^c(t_1, t_3) \, \Sigma_{3,4}^c(t_3, t_4) \, G_{4,2}^c(t_4, t_2) \,. \qquad (2.78)$$

The important difference is that all integrals have to be evaluated along the corresponding contour. In Keldyshs formalism the contour is chosen from $-\infty$ to ∞ and back to $-\infty$, whereby the contour c" of sketch c) in figure 2.6 is neglected. It was shown that this corresponds to neglecting initial correlations [25, 26]. In this work we are interested in steady-state correlation functions which justify to set $t_0 \to -\infty$. The Keldysh contour

is then particularly suitable. In figure 2.7 we show a sketch of it.
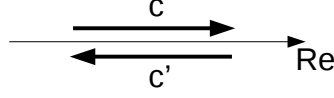
The benefit of Keldyshs formalism is that the contour ordering can be mapped onto 2x2 matrices of the form

$$\tilde{G} \;=\; \begin{pmatrix} G^t & G^< \\ G^> & G^{\tilde{t}} \end{pmatrix} , \tag{2.79}$$

with

$$G^t \;=\; -\,i\,\langle T\,c(t)c^\dagger(t')\rangle \tag{2.80}$$

$$G^{\tilde{t}} \;=\; -\,i\,\langle \bar{T}\,c(t)c^\dagger(t')\rangle \tag{2.81}$$

$$G^> \;=\; -\,i\,\langle c(t)c^\dagger(t')\rangle \tag{2.82}$$

$$G^< \;=\; -\,i\,\epsilon\,\langle c^\dagger(t')c(t)\rangle . \tag{2.83}$$

Again $\epsilon = -1$ for fermions and $\epsilon = +1$ for bosons. $G^<$ and $G^>$ are the lesser and greater Green's functions, G^t and $G^{\tilde{t}}$ are the time- and anti-time-ordered Green's functions. These four Green's functions are not linearly independent due to the following equation:

$$G^t + G^{\tilde{t}} \;=\; G^> + G^< . \tag{2.84}$$

We switch to a different representation, by introducing a transformation for the 2x2 matrix with

$$\underline{G} \;=\; L\sigma_3\tilde{G}L^\dagger \tag{2.85}$$

where $L = \frac{1}{\sqrt{2}}(\sigma_0 - i\sigma_2)$ and σ_j are the 2D Pauli matrices. From that we receive what is referred to as Keldysh space for Green's functions,

$$\underline{G} \;=\; \begin{pmatrix} G^{ret} & G^{kel} \\ 0 & G^{adv} \end{pmatrix} , \tag{2.86}$$

which we indicated by an underline "_". The Keldysh Green's function, G^{kel}, is given by

$$G^{kel} \;=\; G^t + G^{\tilde{t}} \;=\; G^> + G^< . \tag{2.87}$$

G^{ret} and G^{adv} are the well-known retarded and advanced Green's functions. The important advantage of Keldysh space is that it allows to write convolutions over internal

times as

$$\underline{C}(t) \;=\; \int\limits_{-\infty}^{\infty} \underline{A}(\tau)\underline{B}(t-\tau)d\tau \,. \tag{2.88}$$

One does not need any additional transformation [25]. This is especially helpful for the Fourier transform of Green's functions. At the end of this chapter we transform the nonequilibrium Dyson equation (2.78) into ω-space. Using relation (2.88) we obtain the compact form

$$\underline{G}(\omega) \;=\; \underline{g}(\omega) \;+\; \underline{g}(\omega)\,\underline{\Sigma}(\omega)\,\underline{G}(\omega)\,. \tag{2.89}$$

in Keldysh space. The important difference to the equilibrium situation as in equation (2.55) is that the here all Green's functions are 2x2 matrices in Keldysh space in addition to momentum, spin etc. indices. We further point out that in the nonequilibrium case the Keldysh Green's function can not be straight forwardly calculated from the retarded Green's function. This origins in the fact that we can not define a distinct temperature inside a system that is not in thermal equilibrium and therefore we do not have a thermal distribution.

2.2. Cluster Perturbation Theory (CPT)

In this section we provide a short introduction to cluster perturbation theory, following [27, 28, 29] as well as [30].
Cluster perturbation theory (CPT) was developed for treating Hubbard-type models with strongly correlated electrons [27]. Within CPT it is assumed that expectation values can be calculated in the ground-state of the system, which means requiring the temperature to be close to zero Kelvin and the situation to be in equilibrium. In principle, observables then could be calculated by computing the Green's functions of the whole system, as we explained in the previous section 2.1. However, the computation of ground-state Green's functions, based on exact diagonalization methods for example, is limited to small systems since memory requirement grows exponentially with system size. CPT provides an approximation for the ground-state Green's functions of the whole system by exactly diagonalising small parts of the system and reconnecting them with strong-coupling perturbation theory [27]. According to the work in [27], this is done in three steps:

(i) Divide the whole system into clusters and treat them as isolated systems.

(ii) Solve the isolated, decoupled clusters by calculating their ground-state Green's functions with exact diagonalization methods.

(iii) Introduce the interaction between the clusters according to Dyson's equation (2.55).

In the first step, the system Hamiltonian, after dividing into clusters, can be written as follows:

$$\boldsymbol{H} \;=\; \boldsymbol{H}_0^{Cl} \;+\; \boldsymbol{H}_1^{Cl} \;+\; \boldsymbol{H}^{InterCl} \tag{2.90}$$

24

H_0^{Cl} is the non interacting part and H_1^{Cl} describes the interaction within the isolated clusters. $H^{InterCl}$ denotes the instantaneous inter-cluster scattering. We point out that it is important to restrict the inter-cluster term to contain solely single particle hopping terms [28]. We abbreviate it here with V and write the Hamiltonian as

$$H \;=\; H_0^{Cl} \;+\; H_1^{Cl} \;+\; V\,. \tag{2.91}$$

In the following we show two examples of possible applications of CPT: In figure 2.8 the two dimensional grid is divided into four-times-four clusters. In figure 2.9 a one dimensional linear system is divided into a central region, containing one cluster, and two baths.
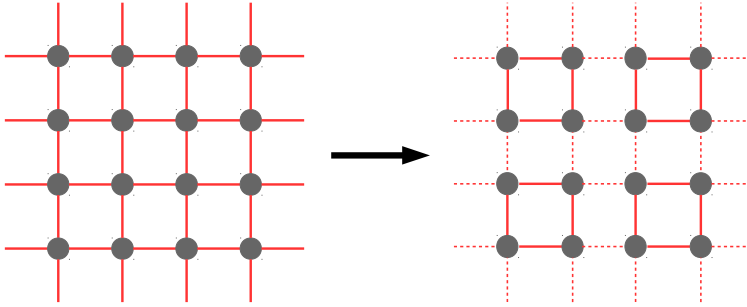
Figure 2.8.: Dividing a two dimensional lattice into clusters
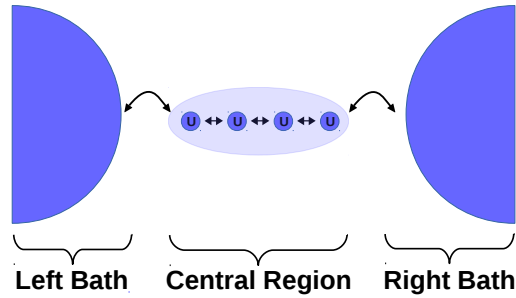
Figure 2.9.: One dimensional linear chain out of equilibrium: Four Hubbard places connected to two leads modelled by a flat DOS with different chemical potentials. The central region is treated as a cluster.

In the second step the exact Green's functions of the isolated clusters, described by $H_0^{Cl} + H_1^{Cl}$, are computed. This is formally the same as if one does a renormalization of the non-interacting cluster Green's functions due to the interacting term H_1^{Cl}. In terms

of Dyson's equation this is written as

$$G^{Cl} = G_0^{Cl} + G_0^{Cl} \cdot \Sigma_{H_1^{Cl}} \left[G_0^{Cl} \right] \cdot G^{Cl}. \qquad (2.92)$$

However, the functional $\Sigma_{H_1^{Cl}} \left[G^{Cl}{}_0 \right]$ is very complicated and generally unknown. This is bypassed by calculating G^{Cl} in many-body space, which for small clusters requires moderate numerical effort.

In the third step, a renormalization due to the inter-cluster scattering V is introduced:

$$G^{CPT} = G^{Cl} + G^{Cl} \cdot \Sigma_V \left[G^{Cl} \right] \cdot G^{CPT}. \qquad (2.93)$$

The self energy of the instantaneous inter-cluster scattering is simply given by the representation of V in Wannier space and we obtain the well known expression of CPT with Dyson's equation:

$$\boxed{G^{CPT} = G^{Cl} + G^{Cl} \cdot V \cdot G^{CPT}.} \qquad (2.94)$$

The exact self-energy could have been formally obtained by first renormalizing due to the inter-cluster scattering V,

$$G_0' = G_0 + G_0 \cdot V \cdot G_0', \qquad (2.95)$$

followed by the renormalization due to the interaction term H_1^{Cl},

$$G' = G_0' + G_0' \cdot \Sigma_{H_1^{Cl}} \left[G_0' \right] \cdot G'. \qquad (2.96)$$

Combining equations 2.95 and 2.96 provides

$$\left(G' \right)^{-1} = (G_0)^{-1} - V - \Sigma_{H_1^{Cl}}[((G_0)^{-1} - V)^{-1}]. \qquad (2.97)$$

From CPT, combining equations 2.92 and 2.94, one gets

$$\left(G^{CPT} \right)^{-1} = \left(G_0^{Cl} \right)^{-1} - \Sigma_{H_1^{Cl}}[G_0^{Cl}] - V. \qquad (2.98)$$

Comparing equation 2.97 and 2.98 shows that CPT neglects the inter-cluster scattering in the renormalization due to H_1^{Cl}. Simply put, this means that CPT approximates the full self-energy by that of the finite clusters. The main result of this section is equation 2.94. It provides a recipe for calculating single-particle Green's functions with appropriate numerical methods and requires only moderate computational effort [28]. It can be systematically improved by increasing the cluster size and is exact for $H_1^{Cl} = 0$ as well as for the case of decoupled clusters with $V = 0$.

2.3. Observables within CPT

In this section we discuss the evaluation of observables within the CPT approach. We point out that all the results of this section apply as well to the master equation based CPT (ME-CPT), which we explain later in chapter 3.

In this thesis we want to compute the current and local densities in a quantum mechanical system as shown in figure 2.9. These observables can be calculated directly from non-equilibrium Green's functions. For that purpose we use the following useful relation:

$$\tilde{G}_{a,b}^{kel}(t=0) = 2i \langle c_b^\dagger c_a \rangle - i\delta_{a,b}. \tag{2.99}$$

It follows from the definition of the Keldysh Green's function 2.87 for fermionic systems. The subscript a, or b respectively, stands for a site or an orbital as well as the corresponding spin index. It can be recast as follows

$$\langle c_b^\dagger c_a \rangle = -\frac{i}{2} \int \frac{d\omega}{2\pi} G_{a,b}^{kel}(\omega) + \frac{1}{2}\delta_{a,b}. \tag{2.100}$$

The occupation n at a distinct site, or orbital respectively, can be calculated directly from (2.100) with $\langle c_a^\dagger c_a \rangle = n_a$. For the current we have

$$I_{ab} = -e \operatorname{Re} \left\{ \int \frac{d\omega}{2\pi} G_{b,a}^{kel}(\omega) V_{a,b}. \right\} \tag{2.101}$$

In this work we want to calculate the current across a central region for a situation as depicted in figure 2.9. For the current from a certain bath μ with indices b into a central region with indices s we have

$$I^\mu = -e \operatorname{Re} \left\{ \int \frac{d\omega}{2\pi} \sum_{b,s} G_{s,b}^{kel}(\omega) V_{b,s}^\mu \right\} \tag{2.102}$$

$$= -e \operatorname{Re} \left\{ \int \frac{d\omega}{2\pi} tr \left(\mathbf{G}^{kel}(\omega) \mathbf{V}^\mu \right) \right\} \tag{2.103}$$

with $V_{s,b}^\mu$ the hopping terms between system orbitals s and the orbitals b of bath μ. Matrices are written in bold.

2.4. Current formula within CPT

In the following we show that within CPT the formula for the current across a central region (2.102) can be brought into a Landauer-type form. In [31] it was further shown that in the linear response scheme the Landauer formula generally holds, also in the interacting case. For the following derivations we consider Green's functions calculated within CPT.

As explained in section 2.2, from CPT we obtain approximations for the Green's functions *inside* the central region. For obtaining the Green's functions between an orbital s in the system and an orbital b in the bath we have to use Dyson's equation in Keldysh space

$$\underline{G}_{s,b} = \underline{G}_{s,s} \underline{V}_{b,s} \underline{g}_{b,b}, \tag{2.104}$$

which for the Keldysh component gives

$$G_{s,b}^{kel} = G_{s,s}^{ret} V_{b,s} g_{b,b}^{kel} + G_{s,s}^{kel} V_{b,s} g_{b,b}^{adv}. \tag{2.105}$$

In this section we denote the bath Green's functions with a small g. Putting this into equation (2.102) gives

$$I^\mu = -e \operatorname{Re} \left\{ tr \int \frac{d\omega}{2\pi} \left(\mathbf{G}^{ret}(\omega) \mathbf{V}^\dagger \mathbf{g}^{kel}(\omega) + \mathbf{G}^{kel}(\omega) \mathbf{V}^\dagger \mathbf{g}^{adv}(\omega) \right) \mathbf{V}^\mu \right\}, \tag{2.106}$$

whereby the superscript μ denotes the corresponding bath or lead. In the one dimensional case, as for example in figure 2.9, this μ denotes the left or the right bath. This formula (2.106) could already be used to put in straight forwardly the corresponding Green's functions from CPT to compute the current. However, as mentioned before, in this chapter we want to show that within the CPT approach and its approximations, formula (2.106) can be brought into the form of a Landauer formula. For that purpose we use

$$I^\mu = \int j^\mu(\omega) \frac{d\omega}{2\pi} \tag{2.107}$$

and introduce

$$\mathbf{V}^\dagger \mathbf{g}^{ret} \mathbf{V}^\nu = \mathbf{A}^\nu - i\mathbf{\Gamma}^\nu \tag{2.108}$$

with the bath retarded Green's function $\mathbf{g}^{ret}$ and the hermitian matrices $\mathbf{A}$ and $\mathbf{\Gamma}$. From here on we do not write out explicitly the ω-dependency and note that it is implicitly assumed for the corresponding matrices. For a bath in equilibrium we have

$$g^{kel} = (g^{ret} - g^{adv}) s(\omega), \tag{2.109}$$

with

$$s(\omega) = 1 - 2f_{FD}(\omega) \tag{2.110}$$

and $f_{FD}(\omega)$ the Fermi-Dirac distribution function. Combining (2.108) and (2.109) we get for the Keldysh part

$$\mathbf{V}^\dagger \mathbf{g}^{kel} \mathbf{V}^\nu = -2i\mathbf{\Gamma}^\nu s(\omega). \tag{2.111}$$

From the current formula (2.106), using (2.108) and (2.111) we obtain for the current

$$j^\mu = -e \operatorname{Re} \left\{ tr \left(-2i\mathbf{G}^{ret} \mathbf{\Gamma}^\mu s^\mu + \mathbf{G}^{kel} [\mathbf{A}^\mu + i\mathbf{\Gamma}^\mu] \right) \right\}. \tag{2.112}$$

The crucial point in the ensuing considerations is, that within CPT we have for the central region

$$\mathbf{G}^{-1} = \mathbf{g}_{cl}^{-1} - \mathbf{V}^{\dagger}\mathbf{g}\mathbf{V}, \qquad (2.113)$$

with $\mathbf{g}_{cl}$ the isolated cluster Green's function. This is the central equation in the CPT method, as we explained in section 2.2. Here we use it to rewrite the Keldysh Green's function. Furthermore, we use the relation

$$\mathbf{G}^{kel} = -\mathbf{G}^{ret}(\mathbf{G}^{-1})^{kel}\mathbf{G}^{adv} \qquad (2.114)$$

which holds in Keldysh space. From these two equations, (2.113) and (2.114), we obtain for the current formula

$$
\begin{aligned}
j^{\mu} &= e\operatorname{Re}\Big\{ tr\Big[-2i\mathbf{G}^{ret}\mathbf{\Gamma}^{\mu}s^{\mu} + \dots \\
&\quad \dots - \mathbf{G}^{ret}\Big((\mathbf{g}_{cl}^{-1})^{kel} + \sum_{\nu} 2i\mathbf{\Gamma}^{\nu}s^{\nu} \Big)\mathbf{G}^{adv}[\mathbf{A}^{\mu} + i\mathbf{\Gamma}^{\mu}] \Big] \Big\}.
\end{aligned}
\qquad (2.115)
$$

The term $(\mathbf{g}_{cl}^{-1})^{kel}$ therein is of the order 0^{+} and therefore can be neglected if there are no bound states which is fulfilled for example in the wide band limit. We explain this in A. The term

$$\mathbf{G}^{ret}\sum_{\nu} 2i\mathbf{\Gamma}^{\nu}s^{\nu}\mathbf{G}^{adv}\mathbf{A}^{\mu} \qquad (2.116)$$

in equation (2.115) does not contribute in the current formula as well. We show this in the following:

$$
\begin{aligned}
\operatorname{Re}\Big[tr\Big(i\mathbf{G}\mathbf{\Gamma}\mathbf{G}^{\dagger}\mathbf{A} \Big) \Big] &= \operatorname{Re}\Big[tr\Big(i\mathbf{G}\mathbf{\Gamma}\mathbf{G}^{\dagger}\mathbf{A} \Big) \Big]^{*} \\
&= \operatorname{Re}\Big[tr\Big(-i\mathbf{A}^{\dagger}\mathbf{G}\mathbf{\Gamma}^{\dagger}\mathbf{G}^{\dagger} \Big) \Big] \\
&= \operatorname{Re}\Big[tr\Big(-i\mathbf{A}\mathbf{G}\mathbf{\Gamma}\mathbf{G}^{\dagger} \Big) \Big] \\
&= -\operatorname{Re}\Big[tr\Big(i\mathbf{G}\mathbf{\Gamma}\mathbf{G}^{\dagger}\mathbf{A} \Big) \Big] \\
&= 0
\end{aligned}
\qquad (2.117)
$$

Thereby we used that $\mathbf{A}$ and $\mathbf{\Gamma}$ are hermitian and that the trace is invariant under cyclic permutation. Putting this result, as well as (??), into equation (2.115), yields

$$
\begin{aligned}
j^{\mu} &= -e\operatorname{Re}\Big\{ tr\Big[2i\mathbf{G}^{ret}\mathbf{\Gamma}^{\mu}s^{\mu} + \mathbf{G}^{ret}\sum_{\nu} 2i\mathbf{\Gamma}^{\nu}s^{\nu}\mathbf{G}^{adv}i\mathbf{\Gamma}^{\mu} \Big] \Big\} \\
&= 2e\operatorname{Im}\Big\{ tr\Big[\mathbf{G}^{ret}\mathbf{\Gamma}^{\mu}s^{\mu} + \mathbf{G}^{ret}\sum_{\nu} \mathbf{\Gamma}^{\nu}s^{\nu}\mathbf{G}^{adv}i\mathbf{\Gamma}^{\mu} \Big] \Big\}.
\end{aligned}
\qquad (2.118)
$$

For the subsequent considerations we have to write the retarded Green's function with Dyson's equation as

$$(\mathbf{G}^{ret})^{-1} = \sum_\nu \left[(\mathbf{g}_{cl}^{ret})^{-1} - \mathbf{A}^\nu + i\mathbf{\Gamma}^\nu \right] \qquad (2.119)$$

$$= \sum_\nu \left[\mathbf{X} + i\mathbf{\Gamma}^\nu \right] , \qquad (2.120)$$

again using (2.114). $\mathbf{X}$ thereby is a hermitian matrix due to the same considerations as used for the Keldysh Green's function in (**??**) and (**??**). Then we obtain for the imaginary part:

$$
\begin{aligned}
2i\mathrm{Im}\mathbf{G}^{ret} &= \mathbf{G}^{ret} - \mathbf{G}^{adv} \\
&= (\mathbf{X} + i\mathbf{\Gamma})^{-1} - (\mathbf{X} - i\mathbf{\Gamma})^{-1} \\
&= (\mathbf{X} + i\mathbf{\Gamma})^{-1} \left[-\mathbf{X} - i\mathbf{\Gamma} + \mathbf{X} - i\mathbf{\Gamma} \right] (\mathbf{X} - i\mathbf{\Gamma})^{-1} \\
&= \mathbf{G}^{ret}(-2i\mathbf{\Gamma})\mathbf{G}^{adv} .
\end{aligned}
\qquad (2.121)
$$

Therein we omitted the superscript $^\nu$. For the first term in equation (2.118) we use the relation that for a hermitian matrix $\mathbf{\Gamma}$ one has

$$
\begin{aligned}
i\,\mathrm{Im}\left[\,\mathrm{tr}\,(\mathbf{G}\mathbf{\Gamma})\right] &= \frac{1}{2}\mathrm{tr}\left(\mathbf{G}\mathbf{\Gamma} - \mathbf{\Gamma}^\dagger \mathbf{G}^\dagger \right) \\
&= \frac{1}{2}\mathrm{tr}\left(\mathbf{G}\mathbf{\Gamma} - \mathbf{G}^\dagger \mathbf{\Gamma}^\dagger \right) \\
&= i\,\mathrm{tr}\left(\mathrm{Im}\left[\mathbf{G}\right]\mathbf{\Gamma} \right) .
\end{aligned}
\qquad (2.122)
$$

Putting the above relations (**??**) and (2.122) into equation (2.118) provides

$$\mathrm{j}^\mu = 2e \cdot tr \left[-\mathbf{G}^{ret}\sum_\nu \mathbf{\Gamma}^\nu \mathbf{G}^{adv}\mathbf{\Gamma}^\mu s^\mu + \mathbf{G}^{ret}\sum_\nu \mathbf{\Gamma}^\nu s^\nu \mathbf{G}^{adv}\mathbf{\Gamma}^\mu \right] . \qquad (2.123)$$

For the second summand in (2.118) again relation (2.117) was used, which provides

$$\mathrm{Im}\left\{ tr\left[\mathbf{G}^{ret}\mathbf{\Gamma}^\nu \mathbf{G}^{adv}\mathbf{\Gamma}^\mu \right] \right\} = 0 . \qquad (2.124)$$

Thus we can write

$$
\begin{aligned}
\mathrm{Im}\left\{ tr\left[\mathbf{G}^{ret}\mathbf{\Gamma}^\nu \mathbf{G}^{adv}i\mathbf{\Gamma}^\mu \right] \right\} &= \mathrm{Re}\left\{ tr\left[\mathbf{G}^{ret}\mathbf{\Gamma}^\nu \mathbf{G}^{adv}\mathbf{\Gamma}^\mu \right] \right\} \\
&= tr\left[\mathbf{G}^{ret}\mathbf{\Gamma}^\nu \mathbf{G}^{adv}\mathbf{\Gamma}^\mu \right] ,
\end{aligned}
\qquad (2.125)
$$

which finally leads to the result in (2.123). We rewrite equation (2.123) in the compact form

$$\mathrm{j}^\mu = 2e \cdot tr \sum_\nu \left[(s^\nu - s^\mu)\mathbf{G}^{ret}\mathbf{\Gamma}^\nu \mathbf{G}^{adv}\mathbf{\Gamma}^\mu \right] \qquad (2.126)$$

which after exploiting equation (2.110) for the distribution function s^ν, leads to the current formula

$$\mathrm{j}^\mu = 4e \cdot tr \sum_{\nu \neq \mu} \left[(f_{FD}^\mu - f_{FD}^\nu) \mathbf{G}^{ret} \mathbf{\Gamma}^\nu \mathbf{G}^{adv} \mathbf{\Gamma}^\mu \right] \; , \qquad (2.127)$$

which is of Landauer type [31]. This is a very important result for CPT and its improvement, ME-CPT. It allows to calculate the current through an *interacting* region using the Landauer formula [31], that originally was derived for non-interacting systems [32].

2.5. Nonequilibrium distribution in general current formula

In the following we show that the non-equilibrium distribution inside the cluster plays an important role for the calculation of transport properties. This is of particular importance for discussing the applicability of CPT to situations far from equilibrium. Again we consider the general current formula from equations (2.106) as well as (2.112). We emphasize that in the following considerations we do not use the approximations from the CPT formalism.

For that purpose we start with equation (2.112) and exploit the following two relations:

(i) With $\mathbf{A}^\mu$ being hermitian and $\mathbf{G}^{kel}$ anti-hermitian, we have

$$\mathrm{Re}\left\{ tr \left(\mathbf{G}^{kel} \mathbf{A}^\mu \right) \right\} = 0 \qquad (2.128)$$

for all leads μ.

(ii) We further use that

$$\begin{aligned}
\mathrm{Re}\left\{ tr \left(i\mathbf{G}^{ret}\mathbf{\Gamma} \right) \right\} &= \mathrm{Re}\left\{ tr \left(i\mathbf{G}^{ret}\mathbf{\Gamma} \right) \right\}^* \\
&= \mathrm{Re}\left\{ tr \left(-i\mathbf{\Gamma}\mathbf{G}^{adv} \right) \right\} \\
&= \mathrm{Re}\left\{ tr \left(-i\mathbf{G}^{adv}\mathbf{\Gamma} \right) \right\}
\end{aligned} \qquad (2.129)$$

holds, which allows us to write

$$\mathrm{Re}\left\{ tr \left(i \left(\mathbf{G}^{ret} - \mathbf{G}^{adv} \right) \mathbf{\Gamma} \right) \right\} = 2\mathrm{Re}\left\{ tr \left(i\mathbf{G}^{ret}\mathbf{\Gamma} \right) \right\} \; . \qquad (2.130)$$

Inserting these relations (i and ii) into equation (2.112) gives

$$\mathrm{j}^\mu = -e \, \mathrm{Re}\left\{ tr \left(-i \left(\mathbf{G}^{ret} - \mathbf{G}^{adv} \right) \mathbf{\Gamma}^\mu s^\mu + i\mathbf{G}^{kel}\mathbf{\Gamma}^\mu \right) \right\} \; . \qquad (2.131)$$

Analogous to the equilibrium situation as in (2.109), we formally write the non-equilibrium Keldysh Green's function as

$$\mathbf{G}^{kel} = \left(\mathbf{G}^{ret} - \mathbf{G}^{adv} \right) \mathbf{S}(\omega) \qquad (2.132)$$

with $\mathbf{S}(\omega)$ a real function. The diagonal entries, $S_{aa}(\omega)$, describe the equivalent of $s(\omega)$ in the nonequilibrium case. Therefore, $S_{aa}(\omega)$ can be interpreted as a nonequilibrium distribution within the central region. With relation (2.132) we obtain for the current

$$j^{\mu} = -e \operatorname{Re} \left\{ tr \left(\left(\mathbf{G}^{ret} - \mathbf{G}^{adv} \right) \left(\mathbf{S} - s^{\mu} \right) \mathbf{\Gamma}^{\mu} \right) \right\} . \qquad (2.133)$$

Again, the ω-dependency of the matrices therein is given implicitly. Relation 2.133 shows that the non-equilibrium distribution in the central region explicitly occurs in the current formula in the diagonal elements of $\mathbf{S}$. We again point out that, when deriving relation (2.133), we did not exploit the approximations that are made within CPT. The CPT approximations provide us with a Landauer-type current formula, as we showed in the previous section 2.4 in equation (2.127). The non-equilibrium distribution does not occur therein, which indicates that CPT is not expected to provide reliable results for the current for systems far from equilibrium even in the parameter regime where $|\mathbf{\Gamma}|$ small.

2.6. Born-Markov-Secular Master Equation (BMS-ME)

In this section we show how to derive a master equation for open quantum systems. Further, we discuss the required approximations for obtaining the Born-Markov-Secular master equation (BMS-ME). We thereby follow the argumentation of [33, 6] as well as [34].
In general a master equation is a first order differential equation that describes the time evolution of probabilities in a system. An example of a situation with discrete events would be

$$\frac{dP_k}{dt} = \sum_l \left[T_{kl} P_l - T_{lk} P_k \right] . \qquad (2.134)$$

Here T_{kl} are transition rates between states l and k and P_l are the probabilities for events l [33]. One sees that the derivative only depends on the current situation and thus there are no memory effects. Therefore, the master equation is of markovian form. In quantum mechanics the probabilities of a system are described by the density matrix

$$\rho = \sum_k p_k \left| \psi_k \right\rangle \left\langle \psi_k \right| \qquad (2.135)$$

with p_k the probability to be in state $\left| \psi_k \right\rangle$. The states $\left| \psi_k \right\rangle \left\langle \psi_k \right|$ do not have to be orthogonal but they have to be complete [33]. Within this picture, the dynamic evolution in a closed quantum system is described by the von Neumann equation:

$$\frac{\partial \rho}{\partial t} = -i \left[H(t), \rho(t) \right] \qquad (2.136)$$

However, this is not yet the most general evolution of a density matrix. As stated in Schallers lecture notes: *"Formally, any matrix fulfilling the properties*

- *self-adjointness:* $\rho^\dagger = \rho$

- *normalization:* $Tr\{\rho\} = 1$

- *positivity:* $\langle\psi|\,\rho\,|\psi\rangle \geq 0$ *for all vectors* ψ

can be interpreted as a valid density matrix." [33] The most general evolution of a matrix that preserves these quantities is described by a Lindblad master equation of the form

$$\frac{\partial\rho}{\partial t} \;=\; -i\left[H'(t),\rho(t)\right] + \sum_{\alpha,\beta}\gamma_{\alpha,\beta}\left(A_\alpha\rho(t)A_\beta^\dagger - \frac{1}{2}\left\{A_\beta^\dagger A_\alpha,\rho(t)\right\}\right). \qquad (2.137)$$

$H'(t)$ is an effective Hamiltonian and $\gamma_{\alpha,\beta}$ a positive semidefinite matrix. It is of markovian form since the time-derivative of ρ does not depend on ρ at previous times. This Lindblad master equation is suitable for an accurate description of open quantum systems. In some cases it is possible to derive a Lindblad master equation phenomenologically. Examples thereof are given in [33]. In this work we consider a rigorous derivation within the weak coupling limit. Thereby we mainly follow [33] and [34].

We consider a situation as depicted in figure 2.10, consisting of a small interacting system that is connected to a large bath. A concrete example of such a situation in the one dimensional case is a linear chain connected to two baths, as shown in figure 2.11. This will be the system that we use to study the new iterative schemata in chapters 5.1 and 5.2. In principle the union of bath and system, or central region, as depicted in figures
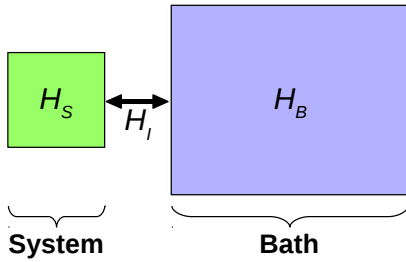
Figure 2.10.: Sketch of an open quantum system, consisting of a small system connected to a large bath.
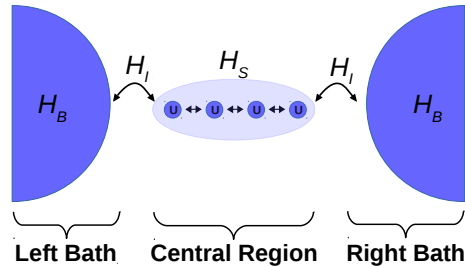
Figure 2.11.: 1D open quantum system as studied in this thesis.

2.10 and 2.11, is a closed quantum system described by a "universe" Hamiltonian H_U. This Hamiltonian, however, is too large to be treated exactly. To simplify this problem, one traces out the many degrees of freedom in the bath and regards the small system as an open quantum system that interacts with the large bath. The Hamiltonian describing this general situation of figure 2.10 is of the form

$$H \;=\; H_S \otimes \mathbb{1} \;+\; \mathbb{1} \otimes H_B \;+\; H_{Inter} \qquad (2.138)$$

with

$$H_{Inter} \; = \; \sum_\alpha A_\alpha \otimes B_\beta. \tag{2.139}$$

In the derivations of this chapter, following [33], we demand coupling operators A_α and B_β to be hermitian. This will be crucial for applying the secular approximation, which we explain in the following. Formally the time evolution is given by

$$\frac{\partial \rho}{\partial t} \; = \; -i \left[H_S \otimes \mathbb{1} \; + \; \mathbb{1} \otimes H_B \; + \; H_{Inter} \; , \; \rho(t) \right] \tag{2.140}$$

which, as we mentioned before, is not suitable for a numerical implementation due to the bath size. Hence, we perform perturbation theory for the small system in terms of $|H_{Inter}|$. For this purpose we transform equation 2.140 into the interaction picture, which we will denote by the superscript ^{I} :

$$\frac{\partial \rho^I(t)}{\partial t} \; = \; -i \left[H^I_{Inter}(t), \rho^I(t) \right] \tag{2.141}$$

with

$$H^I_{Inter}(t) \; = \; e^{i(H_S+H_B)t} \, H_{Inter} \, e^{-i(H_S+H_B)t} \tag{2.142}$$

and

$$\rho^I(t) \; = \; e^{i(H_S+H_B)t} \, \rho(t) \, e^{-i(H_S+H_B)t} \, . \tag{2.143}$$

The **first approximation** is that the initial density matrix factorises as

$$\rho^I(t=0) \; = \; \rho^I_S(t=0) \otimes \bar{\rho}^I_B \, . \tag{2.144}$$

Furthermore we assume that the bath is so large that it is hardly affected by the interaction with the system and thus does not change with time. A formal expansion in terms of the interaction Hamiltonian then has the form

$$\rho^I(t) \; = \; \rho^I_S(t) \otimes \bar{\rho}^I_B + \mathcal{O}(\lambda) \, , \tag{2.145}$$

with $\lambda \; = \; |H^I_{Inter}|$. We neglect of all terms of higher orders in λ, which is called the **Born approximation**. Taking the partial trace with respect to the baths as well as formally integrating equation 2.141 and re-inserting the solution, gives

$$\begin{aligned} \frac{\partial}{\partial t} \rho^I_S(t) \; = \; & -i \cdot tr_B \left(\left[H^I_{Inter}(t), \rho^I(0) \right] \right) + \\ & \ldots - tr_B \int_0^t \left[H^I_{Inter}(t), \left[H^I_{Inter}(t'), \rho^I_S(t') \otimes \bar{\rho}^I_B \right] \right] dt' + \mathcal{O}(\lambda^3) \, . \end{aligned} \tag{2.146}$$

We point out that by regarding this it comes clear that the Born approximation is formally equivalent to perturbation theory up to second order in terms of the interaction Hamiltonian. The resulting equation (2.146) is non-Markovian because the right hand side also depends on ρ^I_S at times $t' < t$. Nevertheless, it already does preserve trace and

hermiticity of the density matrix. To achieve a Markovian master equation, starting from (2.146), we make use of the fact that one can assume

$$
\begin{aligned}
tr_B \left[H_{Inter}^I(t), \rho^I(0) \right] &= tr_B \sum_\alpha \left[A_\alpha^I(t) \otimes B_\alpha^I(t), \rho_S^I(0) \otimes \bar{\rho}_B^I \right] \\
&= \sum_\alpha \left[A_\alpha^I(t) \rho_S^I(0), tr_B \left(B_\alpha^I(t) \bar{\rho}_B^I \right) \right] \qquad (2.147) \\
&= 0.
\end{aligned}
$$

This holds due to the fact that one can always construct a situation where the single-operator expectation values vanish:

$$
tr_B \left(B_\alpha^I(t) \bar{\rho}_B^I \right) = 0. \qquad (2.148)
$$

This is achieved by simultaneously modifying H_S and B_α as shown in [34]. As a result the first summand on the right hand side of equation (2.146) drops out. We further make two important approximations:

- **First Markovian Approximation:** We assume the bath to be memoryless, which means that the decay time of bath correlations is much smaller than the time-scales in which the density matrix varies. Thus we can replace $\rho_S^I(t')$ by $\rho_S^I(t)$ in (2.146).

- **Second Markovian Approximation:** We extend the integral limit t to infinity. Again this is justified by assuming that the bath correlations functions decay rapidly.

As a result we obtain the Born-Markov master equation

$$
\frac{\partial}{\partial t} \rho_S^I(t) = -tr_B \int_0^\infty \left[H_{Inter}^I(t), \left[H_{Inter}^I(t-\tau), \rho_S^I(t) \otimes \bar{\rho}_B^I \right] \right] d\tau. \qquad (2.149)
$$

It preserves trace, hermeticity of ρ and is markovian [34]. However, it does not preserve the positivity of the density matrix, which might lead to non-physical results, such as negative probabilities [33]. In order to transform the above equation (2.149) into the form of a Lindblad master equation as given in (2.137), we additionally introduce the so called **Secular approximation**. Thereby we basically average over fast oscillating terms in time t. This is done by explicitly calculating the dynamics of the system coupling operators in Schroedinger picture and averaging out the corresponding terms. When doing this we have to demand the coupling operators A_α and B_β to be hermitian, which is ensured using a Jordan-Wigner transformation. A detailed derivation of that is given in [33]. We mention that for the secular approximation we require the coupling strength between system and bath to be significantly smaller than the energy scales in the system. The secular approximation corresponds to the rotating-wave approximation in quantum optics where one makes use of the fact that optical transition frequencies are much larger than decay rates of excited states and hence can be averaged out. We

further introduce the bath correlation functions of the form

$$C_{\alpha\beta}(t) \;=\; tr\left[e^{iH_B t}B_\alpha e^{-iH_B t}B_\beta \bar{\rho}_B\right] \;.\tag{2.150}$$

After applying the secular approximation to equation 2.149 and transforming back to Schrödinger picture we obtain the BMS-ME

$$
\begin{aligned}
\frac{\partial \rho_S(t)}{\partial t} \;=\; &-i\left[H_S + \sum_{ab}\sigma_{ab}\,|a\rangle\,\langle b|\;,\;\rho_S(t)\right] \\
&+ \sum_{a,b,c,d}\gamma_{ab,cd}\left(|a\rangle\,\langle b|\,\rho_S(t)\,(|c\rangle\,\langle d|)^\dagger \;-\; \frac{1}{2}\left\{(|c\rangle\,\langle d|)^\dagger\,|a\rangle\,\langle b|\;,\;\rho_S(t)\right\}\right)
\end{aligned}
\tag{2.151}
$$

where $|a\rangle$ are the Eigenvectors of H_S: $H_S\,|a\rangle \;=\; E_a\,|a\rangle$. The coefficients are given by

$$\sigma_{ab} \;=\; \sum_{\alpha\beta,c}\frac{1}{2i}\tilde{\sigma}_{\alpha\beta}(E_b - E_a)\delta_{E_a,E_b}\,\langle c|\,A_\beta\,|b\rangle\,\langle c|\,A_\alpha\,|a\rangle^*\tag{2.152}$$

and

$$\gamma_{ab,cd} \;=\; \sum_{\alpha\beta}\tilde{\gamma}_{\alpha\beta}(E_b - E_a)\delta_{E_b-E_a,E_d-E_c}\,\langle a|\,A_\beta\,|b\rangle\,\langle c|\,A_\alpha\,|d\rangle^*\tag{2.153}$$

with

$$\tilde{\gamma}_{\alpha\beta}(\omega) \;=\; \int_{-\infty}^{\infty} C_{\alpha\beta}(t)e^{i\omega t}dt\tag{2.154}$$

and

$$\tilde{\sigma}_{\alpha\beta}(\omega) \;=\; \frac{i}{\pi}\mathrm{Pv}\int_{-\infty}^{\infty}\frac{\gamma_{\alpha\beta}(\omega')}{\omega - \omega'}d\omega'.\tag{2.155}$$

The above equation (2.151) is the main result of this section and serves as a recipe for treating open quantum systems numerically. It preserves trace, positivity and hermiticity and further is markovian [34]. Hence, it is a Lindlad-type master equation.

2.7. Hubbard Model

The physical model that we examine within this thesis is the Hubbard model. It was originally introduced to describe electrons in solids with narrow energy bands, such as for example transition metals, where a description by means of plane waves fails to work [35]. Later on it has been of particular interest in the field of hight-temperature superconductivity. This section serves as a brief introduction to the standard Hubbard model and its applications. For a more detailed derivation the reader is referred to [35] and [14].

The Hamiltonian for a solid can formally be written as

$$H_{full} = H_{ion} + H_{el} + H_{e,i}\;,\tag{2.156}$$

containing all terms for electrons H_{el}, ions H_{ion} and their interaction $H_{e,i}$. In a first step the Born-Oppenheimer approximation is applied, which allows to write the wave function as $\Psi_{full} = \Psi_{el} \otimes \Psi_{ion}$. Therefore, the electron part of the system can be solved separately. The Hamilton of interest then is

$$H = H_{e,kin} + H_{e,i} + H_{e,e} \tag{2.157}$$

with

$$
\begin{aligned}
H_{e,kin} &= \sum_j \frac{\mathbf{p}_j^2}{2} \;, \\
H_{e,i} &= \sum_{j,l} V_{e,i}(\mathbf{r}_j - \mathbf{R}_l) \quad \text{the grid potential and} \\
H_{e,e} &= \sum_{j,k} \frac{1}{\mathbf{r}_j - \mathbf{r}_k} \;.
\end{aligned}
$$

We remind that in this chapter the terms are as well written in atomic units with $m_e = \frac{1}{4\pi\epsilon_0} = 1$. In a grid one has a periodicity given as $V_{e,i}(\mathbf{r}_j - \mathbf{R}_l + \mathbf{R}_m) = V_{e,i}(\mathbf{r}_j - \mathbf{R}_l)$ whereby the vectors $\mathbf{R}_m$ define the Bravais lattice. Thus, for the wavefunctions one uses Bloch functions of the form

$$\Psi_{nk}(\mathbf{r}) = \frac{1}{\sqrt{N_i}} \sum_{j=1}^{N_i} e^{i\mathbf{k}\cdot\mathbf{R}_j} \varphi_n(\mathbf{r} - \mathbf{R}_j) \;. \tag{2.158}$$

They are a complete set of orthonormal eigenvectors of the part of the Hamiltonian without the electron-electron interaction,

$$H_0 = H_{e,kin} + H_{e,i} \;,$$

fulfilling

$$H_0 \Psi_{nk}(\mathbf{r}) = \epsilon_n(\mathbf{k}) \Psi_{nk}(\mathbf{r}) \;. \tag{2.159}$$

The subscript n thereby describes a set of quantum numbers, such as for example a distinct orbital or a spin number. As in this chapter we regard materials with narrow energy bands, where the probability of finding an electron is strongly peaked around the sites of the grid and their mobility is small. Then it is advantageous to choose for the amplitude functions $\varphi_n(\mathbf{r})$ in (2.158) the atomic wave functions. From here on we switch to second quantization, where the Bloch states are described in a discrete Fock space $|\mathbf{k}, n\rangle$ with the corresponding ladder operators $a_{k,m}^{(\dagger)}$. The non-interacting Hamiltonian is then written as

$$h_0 = \sum_{\substack{n,n' \\ \mathbf{k},\mathbf{k}'}} \langle \mathbf{k}, n| H_0 |\mathbf{k}', n'\rangle \, a_{k,n}^{\dagger} a_{k',n'} \tag{2.160}$$

which, after using equation (2.159), provides

$$h_0 = \sum_n \epsilon_n(\mathbf{k}) a_{k,n}^\dagger a_{k,n} . \tag{2.161}$$

To identify the hopping terms we perform a Fourier transformation to the real space coordinates of the ladder operators,

$$\tilde{a}_{l,n} = \sum_k e^{i\mathbf{k}\cdot\mathbf{R}_l} a_{k,n} . \tag{2.162}$$

A ladder operator $\tilde{a}_{l,n}^{(\dagger)}$ in this case destroys (creates) a particle at place l. Then the non-interacting Hamiltonian becomes

$$h_0 = \frac{1}{N_l} \sum_{l,m} \sum_{\mathbf{k},n} \epsilon_n(\mathbf{k}) e^{i\mathbf{k}\cdot(\mathbf{R}_l - \mathbf{R}_m)} \tilde{a}_{l,n}^\dagger \tilde{a}_{m,n} = \dots \tag{2.163}$$

$$= \sum_{l,m} \tilde{T}_{lm}\, \tilde{a}_{l,n}^\dagger \tilde{a}_{m,n} . \tag{2.164}$$

In the Hubbard model, as well as in the Tight-binding model, only terms up to nearest neighbouring sites are kept and all others are neglected. That leads to

$$h_0 = \sum_{l,n} \epsilon_l\, \tilde{a}_{l,n}^\dagger \tilde{a}_{l,n} + \sum_{\substack{<l,m> \\ n}} T_{lm}\, \tilde{a}_{l,n}^\dagger \tilde{a}_{m,n} \tag{2.165}$$

where "$< \cdots >$" indicates that only nearest neighbouring indices l,m are taken into account. T_{lm} is the so called hopping integral and ϵ_l an onside energy. This is already the Tight-binding Hamiltonian. To obtain the Hubbard model we further have to regard the interaction term $H_{e,e}$, which in second quantisation is written as

$$h_{e,e} = \sum_{\substack{\mathbf{k}_1,\dots,\mathbf{k}_4 \\ n_1,\dots,n_4}} \langle \mathbf{k}_1, n_1 | \langle \mathbf{k}_2, n_2 | H_{e,e} | \mathbf{k}_3, n_3 \rangle | \mathbf{k}_4, n_4 \rangle\, a_{\mathbf{k}_1,n_1}^\dagger a_{\mathbf{k}_2,n_2}^\dagger a_{\mathbf{k}_3,n_3} a_{\mathbf{k}_4,n_4} \tag{2.166}$$

$$= V(\mathbf{k}_1, n_1; \dots; \mathbf{k}_4, n_4) a_{\mathbf{k}_1,n_1}^\dagger a_{\mathbf{k}_2,n_2}^\dagger a_{\mathbf{k}_3,n_3} a_{\mathbf{k}_4,n_4} . \tag{2.167}$$

$V(\dots)$ is calculated using the atomic wave functions in real space coordinates. From here on we explicitly write out the spin index σ, while the other possible quantum numbers that are contained in the subscript n are omitted for the sake of readability. Due to the fact that $H_{e,e}$ does not depend on spin, we further have $\sigma_1 = \sigma_3 = \sigma$ and $\sigma_2 = \sigma_4 = \sigma'$. This results in:

$$\tilde{V}(a, \sigma; b, \sigma'; c, \sigma; d, \sigma') = \dots$$

$$\dots = \iint d^3\mathbf{r}\, d^3\mathbf{r}'\, \varphi_\sigma^*(\mathbf{r} - \mathbf{R}_a)\varphi_{\sigma'}^*(\mathbf{r}' - \mathbf{R}_b) \frac{1}{\mathbf{r} - \mathbf{r}'} \varphi_\sigma(\mathbf{r} - \mathbf{R}_c)\varphi_{\sigma'}(\mathbf{r}' - \mathbf{R}_d) . \tag{2.168}$$

The overlap of atomic wave functions from different sites is much smaller than that from same sites. In the Hubbard model only the terms at the same sites $\tilde{V}(a, \sigma; a, \sigma'; a, \sigma; a, \sigma')$ are kept. In other words, an interaction between electrons is only accounted for if they are on the same site. This allows to write the Hubbard Hamiltonian in a compact form:

$$H_{Hubbard} = \sum_{\substack{<j,k> \\ \sigma}} T_{jk}\, \tilde{a}_{j,\sigma}^{\dagger} \tilde{a}_{k,\sigma} + \sum_{\substack{j \\ \sigma \neq \sigma'}} U_j \tilde{a}_{j,\sigma}^{\dagger} \tilde{a}_{j,\sigma'}^{\dagger} \tilde{a}_{j,\sigma} \tilde{a}_{j,\sigma'} + \sum_{j,\sigma} \epsilon_j\, \tilde{a}_{j,\sigma}^{\dagger} \tilde{a}_{j,\sigma}\,. \tag{2.169}$$

U_j is the local interaction energy at site j and $< \cdots >$ denotes the summation over nearest neighbours. We mention that in this thesis we parametrise the hopping integral with $t_{jk} = -T_{jk}$. This model allows to study effects arising from the lattice and additionally takes into account short-range two-particle interactions. As stated before, the Hubbard model is well suited to describe electronic properties of materials with narrow energy bands. The inclusion of interaction terms further allows to study many-body effects arising from the electron-electron repulsion, which is of particular interest in the field of strongly correlated many-body physics. We mention that even though the Hubbard Hamiltonian still is rather simple model, a general analytical solution has not yet been found.

3. Master equation based steady-state cluster perturbation theory (ME-CPT)

In this chapter we explain the master equation based steady-state cluster perturbation theory (ME-CPT), following the work in [6]. This hybrid method combines the cluster perturbation theory from section 2.2 with the master equation approach of section 2.6. To explain this method in more detail we show a sketch of a one dimensional chain out of equilibrium in figure 3.1, whereby the chemical potentials and the density of states (DOS) have been drafted. In this case a symmetric bias voltage has been applied that corresponds to a symmetric shift of the chemical potentials in the baths. In principle, the semi-circle shape of the DOS corresponds to a semi-infinite tight binding chain, though figure 3.1 should only serve as a sketch. First we treat this situation with ground-state
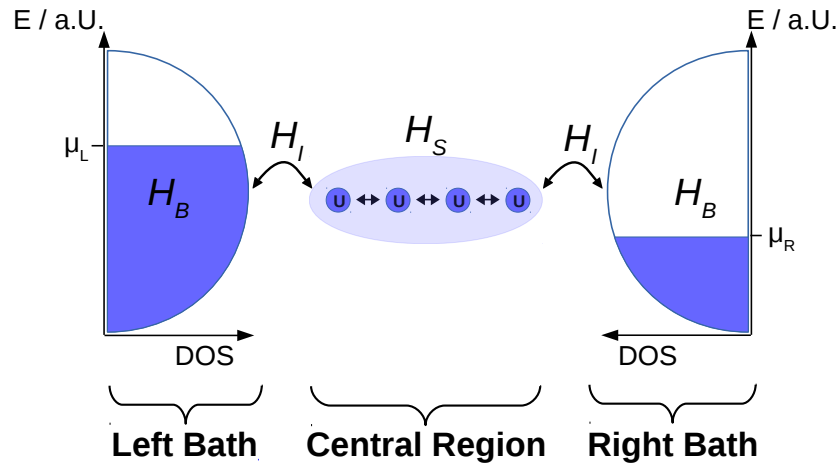
Figure 3.1.: Sketch of a one dimensional chain out of equilibrium. The chemical potentials have been sketched in order to represent an applied voltage.

CPT and use the same three steps as explained in chapter 2.2:

(i) The whole system is divided into a central region and two baths.

(ii) The Green's functions of the isolated central region are calculated in the ground-state by exact diagonalization.

(iii) The interaction with the baths is introduced perturbatively according to Dyson's equation in CPT (2.55).

A crucial problem of this procedure, when applied to a nonequilibrium situation as in figure 3.1, is step (ii). Therein the Green's function is calculated using the ground-state of the central region. This ground-state, however, depends on the chemical potential in the central region, which is unknown for a nonequilibrium situation. A common choice in recent works has been to choose a chemical potential in between the values of the chemical potentials in the baths, μ_L and μ_R [36]. This is still an ad hoc choice as explained in [6]. In addition to that shortcoming, one has the problem that the ground state is a many-body state describing an equilibrium situation. Using this as the reference state for perturbation theory in a nonequilibrium situation is clearly unsatisfactory [27]. We conclude that CPT is only suitable for situations close to an equilibrium, where the applied bias voltage, as well as the temperature, is small. Otherwise, step (ii) leads to inconsistencies. Therewith it comes clear that CPT has to be improved in order to consistently capture situations far from equilibrium.

A promising approach to that was introduced in [6]. Therein, CPT is improved by using in step (ii) a quantum master equation to calculate the nonequilibrium many-body steady-state in the central region. The nonequilibrium steady-state is then used to calculate the Green's functions of the central region. This method is denoted *master equation based steady-state cluster perturbation theory* (ME-CPT). In this work we use the BMS-ME, as explained in section 2.6, to calculate the steady-state. Within ME-CPT the situation of figure 3.1 is treated as follows:

(i) The whole system is divided into a central region and two baths.

(ii) The BMS-ME is implemented for the central region, including the interaction with the baths. It is then solved for the steady-state, which is used to calculate the cluster Green's functions with exact diagonalization methods.

(iii) The interaction with the baths is introduced perturbatively according to Dyson's equation in CPT (2.55).

The improvement, compared to CPT, is that in step (ii) the non-equilibrium situation is taken into account by means of the nonequilibrium steady-state, calculated from the BMS-ME. This nonequilibrium many-body state already takes into account the influence of the baths, including their chemical potentials and temperatures. We do not have to care about choosing a chemical potential for the central region. Thus, there is no inconsistency in the nonequilibrium case any more. Further, the equilibrium case is automatically included in ME-CPT.

In the end of this section we want to refer to the result for the general current formula from section 2.5, given in equation (2.133). Therein we showed that the nonequilibrium distribution inside the central region explicitly plays an important role for calculating the current. Within CPT, however, the nonequilibrium distribution is not accounted for, as shown in formula (2.127) which is of Landauer-type [31]. In ME-CPT, the nonequilibrium distribution is accounted for by means of the steady-state computed from a master equation, in this particular case from the BMS-ME. Even though we have the same Landauer-type current formula (2.127) for ME-CPT, the nonequilibrium distribution is

taken into account in the calculation of the Green's functions. Therefore, ME-CPT is expected to systematically improve the results from CPT for systems out of equilibrium. This was confirmed in [6] for the examples of a quantum diode and a triple quantum dot ring junction.

3.1. Implementation of ME-CPT for the fermionic Hubbard model

In this section we discuss the implementation of the ME-CPT method for the case of a fermionic Hubbard model, as studied in this thesis. All computations are carried out in MATLAB (Version R2018b) of MathWorks $^{©}$.
In this thesis we study one dimensional systems that consist of a small region connected to various baths as depicted in figure 3.1. In particular, we investigate a linear chain containing four Hubbard places connected to two semi-infinite noninteracting baths with a flat density of states (DOS). This is a model for a linear chain of quantum dots, connected with two leads. We show a sketch of such a situation in figure 3.2.
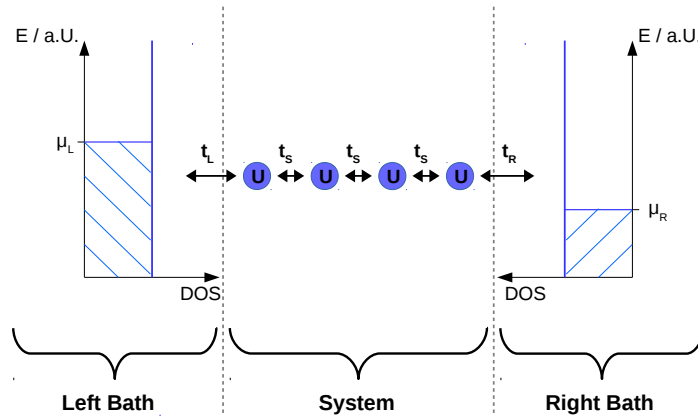
Figure 3.2.: Sketch of a linear chain with four Hubbard sites connected to two baths. The local interaction inside the cluster is denoted with U and the hopping inside the system with t_S. The hopping between system and bath is denoted with $t_{L/R}$. The baths are assumed to have a flat DOS and the nonequilibrium situation is indicated with different chemical potentials $\mu_{L/R}$.

We write the Hamiltonian of this situation as

$$H \;=\; H_S + H_B + H_{SB} \;, \tag{3.1}$$

with H_S the Hamiltonian describing the system, H_B the baths and H_{SB} the hopping between them. The system is described by the Hubbard model

$$H_S = -\sum_{\substack{<j,k> \\ \sigma}} t_{jk}\, c^\dagger_{j,\sigma} c_{k,\sigma} + \sum_j U \left(c^\dagger_{j,\uparrow} c_{j,\uparrow} - \frac{1}{2} \right) \left(c^\dagger_{j,\downarrow} c_{j,\downarrow} - \frac{1}{2} \right) . \tag{3.2}$$

Therein t_{jk} correspond to the hopping parameters inside the system t_S, that do not have to be homogeneous. The Hamiltonian of (2.169) has been modified such that particle-hole symmetry is ensured. $c^{(\dagger)}$ are the fermionic annihilation (creation) operators inside the system and $\sigma = \uparrow / \downarrow$ is the spin index. The environment consists of noninteracting electronic leads described by

$$H_B = \sum_{\substack{<j,k> \\ \sigma}} t'_{j,k}\, b^\dagger_{j,\sigma} b_{k,\sigma} + \sum_{j,\sigma} \epsilon'_j\, b^\dagger_{j,\sigma} b_{j,\sigma} \tag{3.3}$$

with fermionic annihilation (creation) operators $b_j^{(\dagger)}$ inside the baths. The coupling between system and environment is given by an instantaneous single-particle hopping of the form

$$H_{SB} = \sum_{\substack{l,m \\ \sigma}} t^I_{l,m}\, b^\dagger_{l,\sigma} c_{m,\sigma} + \text{h.c.}, \tag{3.4}$$

whereby in the present case $t^I_{l,m}$ corresponds to $t_{L/R}$.

3.1.1. Implementation of the baths

In this work we assume the baths to be noninteracting, infinitely large and in thermal equilibrium. We used a constant density of states, mimicking a wide band limit, as sketched in figure 3.2. Following [6, 37], we modelled that with a local retarded Green's function of the form

$$g^{ret}(\omega) = -\frac{1}{2D} \ln \left(\frac{\omega + i0^+ - D}{\omega + i0^+ + D} \right) , \tag{3.5}$$

with D a half-bandwidth, chosen to be larger than all energy scales of the system. From that we can calculate all other Green's functions, since the leads are at thermal equilibrium.

3.1.2. Implementation of the BMS-ME

In order to implement the BMS-ME as derived in section 2.6, we have to do the following:

1. Rewrite the coupling between system and bath in the form

$$H_{SB} = \sum_\alpha A_\alpha \otimes B_\beta , \tag{3.6}$$

with hermitian operators A_α and B_β.

2. Calculate the even and odd Fourier transform of the bath correlation functions given by (2.150).

3. Diagonalize the matrix representation of the system Hamiltonian.

Equation (3.6) is a sum over tensor products which implies that $[A_\alpha, B_\beta] = 0$ holds, whereas for the ladder operators in (3.4) we have $\left[b_{l,\sigma}^\dagger, c_{m,\sigma}\right] = 2b_{l,\sigma}^\dagger c_{m,\sigma}$ due to their fermionic nature. In order to rewrite (3.4) in the form of (3.6) we have to use a Jordan-Wigner transformation that maps the situation onto Pauli matrices that act on a spin chain [33]. We denote the Pauli matrices as $\hat{s}$ which gives:

$$b_{l,\sigma} = \big(\underbrace{\hat{s}_z \otimes \hat{s}_z \otimes \cdots \otimes \hat{s}_z}_{l-1} \otimes \hat{s}_- \otimes \underbrace{\mathbb{1} \otimes \cdots \otimes \mathbb{1}}_{N^{\text{bath}}-l} \otimes \underbrace{\mathbb{1} \otimes \cdots \otimes \mathbb{1}}_{N^{\text{sys}}}\big)_\sigma \otimes \big(\underbrace{\mathbb{1} \otimes \cdots \otimes \mathbb{1}}_{N^{sys}+N^{bath}}\big)_{\bar{\sigma}} \quad (3.7)$$

$$c_{m,\sigma} = \big(\underbrace{\hat{s}_z \otimes \cdots \otimes \hat{s}_z}_{N^{\text{bath}}} \otimes \underbrace{\hat{s}_z \otimes \hat{s}_z \otimes \cdots \otimes \hat{s}_z}_{m-1} \otimes \hat{s}_- \otimes \underbrace{\mathbb{1} \otimes \cdots \otimes \mathbb{1}}_{N^{\text{sys}}-k}\big)_\sigma \otimes \big(\underbrace{\mathbb{1} \otimes \cdots \otimes \mathbb{1}}_{N^{sys}+N^{bath}}\big)_{\bar{\sigma}} \ . \quad (3.8)$$

We denoted therein with $\bar{\sigma}$ the spin antiparallel to σ. This relations preserve the fermionic anti-commutator relation $\left\{b_{l,\sigma}, b_{n,\sigma}^\dagger\right\} = \delta_{l,n}\mathbb{1}$ for all bath and system operators. The order in the nonlocal Jordan-Wigner transformation can be chosen as convenient [33]. In our case it is thereupon advantageous to introduce fermionic operators, which are defined for bath and system separately:

$$\tilde{b}_{l,\sigma} = \big(\underbrace{\hat{s}_z \otimes \hat{s}_z \otimes \cdots \otimes \hat{s}_z}_{l-1} \otimes \hat{s}_- \otimes \underbrace{\mathbb{1} \otimes \cdots \otimes \mathbb{1}}_{N^{\text{bath}}-l}\big)_\sigma \otimes \big(\underbrace{\mathbb{1} \otimes \cdots \otimes \mathbb{1}}_{N^{bath}}\big)_{\bar{\sigma}} \quad (3.9)$$

$$\tilde{c}_{m,\sigma} = \big(\underbrace{\hat{s}_z \otimes \hat{s}_z \otimes \cdots \otimes \hat{s}_z}_{m-1} \otimes \hat{s}_- \otimes \underbrace{\mathbb{1} \otimes \cdots \otimes \mathbb{1}}_{N^{\text{sys}}-l}\big)_\sigma \otimes \big(\underbrace{\mathbb{1} \otimes \cdots \otimes \mathbb{1}}_{N^{sys}}\big)_{\bar{\sigma}} \ . \quad (3.10)$$

This finally allows us to rewrite the interaction Hamiltonian in a compact way:

$$H_{SB} = \sum_{\substack{l,m \\ \sigma}} t_{l,m}^I \cdot \tilde{b}_{l,\sigma}^\dagger \otimes \tilde{c}_{m,\sigma} + \text{h.c.} \ , \quad (3.11)$$

which has the same form as the original H_{SB} in terms of the new operators 3.9 and 3.10. For the Hubbard model it turns out that the rewritten system Hamiltonian again has the same form as the original one, in terms of the new operators. It further turns out that for an environment that preserves particle number, the bath correlation functions, as defined in equation (2.150), have the same form in terms of the new operators as well [6, 33]. Thus, when calculating the BMS-ME for a situation as given in figure 3.2, with large noninteracting leads, we can omit the Jordan-Wigner transformation and perform all calculations with the original fermionic latter operators. We then rewrite

the Hamiltonian H_{SB} with hermitian coupling operators defined by

$$A_{m,\sigma} = \frac{1}{\sqrt{2}} \left(c_{m,\sigma} + c_{m,\sigma}^{\dagger} \right) \tag{3.12}$$

$$\bar{A}_{m,\sigma} = \frac{i}{\sqrt{2}} \left(c_{m,\sigma} - c_{m,\sigma}^{\dagger} \right) \tag{3.13}$$

and

$$B_{l,\sigma} = t_{l,\sigma}^{I} \cdot \frac{1}{\sqrt{2}} \left(b_{l,\sigma} + b_{l,\sigma}^{\dagger} \right) \tag{3.14}$$

$$\bar{B}_{l,\sigma} = t_{l,\sigma}^{I} \cdot \frac{i}{\sqrt{2}} \left(b_{l,\sigma} - b_{l,\sigma}^{\dagger} \right) \tag{3.15}$$

as

$$H_{SB} = \sum_{l,m;\sigma} \left(A_{m,\sigma} \otimes B_{l,\sigma} + \bar{A}_{m,\sigma} \otimes \bar{B}_{l,\sigma} \right) . \tag{3.16}$$

From here on we omit the spin index σ for the sake of readability. With equation (3.16) we have achieved the above mention first step for implementing the BMS-ME. We further have to calculate the bath correlation functions, given by

$$C_{kl}^{B\bar{B}}(t) = tr \left\{ B_k(t) \bar{B}_l \bar{\rho}_b \right\} . \tag{3.17}$$

For that purpose we recall that the environment is given by various baths that initially, prior to being connected with the central region, do not interact under each other. Furthermore, when deriving the BMS-ME, it was assumed that they are not influenced by the comparatively small system. As a result, the bath density matrix $\bar{\rho}_B$ can be factorised as a tensor product of the different baths

$$\bar{\rho}_b = \bar{\rho}_{b_1} \otimes \bar{\rho}_{b_2} \otimes \cdots \otimes \bar{\rho}_{b_N} . \tag{3.18}$$

We already explained in section 2.6, equation (2.148), that we can assume all single-operator expectation values to vanish. Due to that, no bath correlation functions between different baths occur in the master equation. Thus, we can treat each bath separately in the calculation of the BMS-ME. Regarding equation (3.17), we have four possible bath correlation functions for each fixed index kl in every bath:

$$C_{kl}^{BB}(t) \quad , \quad C_{kl}^{B\bar{B}}(t) \quad , \quad C_{kl}^{\bar{B}B}(t) \quad \text{and} \quad C_{kl}^{\bar{B}\bar{B}}(t) . \tag{3.19}$$

We write the first one out explicitly with:

$$
\begin{aligned}
C_{kl}^{BB}(t) &= \frac{(t_l^I)^2}{2} tr\left\{ \left(b_k(t)b_l + b_k(t)b_l^\dagger + b_k^\dagger(t)b_l + b_k^\dagger(t)b_l^\dagger \right) \bar\rho_b \right\} \\
&= \frac{(t_l^I)^2}{2} \left(tr\left\{ b_k(t)b_l^\dagger \, \bar\rho_b \right\} + tr\left\{ b_k^\dagger(t)b_l \, \bar\rho_b \right\} \right) \\
&= \frac{(t_l^I)^2}{2} \left(G_{kl}^>(t) + G_{lk}^<(-t) \right) \\
&= C_{kl}^{\bar B \bar B}(t)
\end{aligned}
\tag{3.20}
$$

For the second one we obtain

$$
\begin{aligned}
C_{kl}^{B\bar B}(t) &= i\frac{(t_l^I)^2}{2} tr\left\{ \left(b_k(t)b_l - b_k(t)b_l^\dagger + b_k^\dagger(t)b_l - b_k^\dagger(t)b_l^\dagger \right) \bar\rho_b \right\} \\
&= i\frac{(t_l^I)^2}{2} \left(tr\left\{ b_k(t)b_l^\dagger \, \bar\rho_b \right\} + tr\left\{ b_k^\dagger(t)b_l \, \bar\rho_b \right\} \right) \\
&= i\frac{(t_l^I)^2}{2} \left(-G_{kl}^>(t) + G_{lk}^<(-t) \right) \\
&= -C_{kl}^{\bar B B}(t)
\end{aligned}
\tag{3.21}
$$

In the above relations we again used that the baths preserve the particle number. From relations (3.20) and (3.21) we see that all bath correlation functions necessary are given by the greater and lesser Green's functions of the baths. For computing the coefficients $\tilde\gamma_{kl}$ and $\tilde\sigma_{kl}$ in the BMS-ME according to equations (2.154) and (2.155) we further have to calculate the even and odd Fourier transformations thereof. The even Fourier transform is given by

$$
\tilde C_{kl}^{BB}(\omega) = \frac{(t_l^I)^2}{2} \left(\tilde G_{kl}^>(\omega) + \tilde G_{lk}^<(\omega) \right)
\tag{3.22}
$$

$$
\tilde C_{kl}^{B\bar B}(\omega) = \frac{(t_l^I)^2}{2} \left(-\tilde G_{kl}^>(\omega) + \tilde G_{lk}^<(\omega) \right) .
\tag{3.23}
$$

We calculate the greater and lesser Green's functions of the baths using equation (3.5). For the coefficients $\tilde\sigma_{kl}(\omega)$ we have to calculate the odd Fourier transform of (3.20) and (3.21) which can be calculated with the Cauchy Principal Value of the even Fourier transform. The Cauchy Principal Values is an integral of the form

$$
I(\omega) = \mathrm{Pv} \int_{-\infty}^{\infty} \frac{f(\omega')}{\omega - \omega'} d\omega'.
\tag{3.24}
$$

which is a numerically challenging problem due to the poles at $\omega = \omega'$. Particularly in this work, when implementing the self consistent iteration schemes, the bath Green's functions are given solely numerically. To solve this, we recast the above integral (3.24)

into the expression

$$I(\omega) = \int\limits_0^\infty \frac{f(\omega - x) - f(\omega + x)}{x} dx .$$ (3.25)

This is numerically more stable and has a good convergence when reducing the increments in ω-space [38]. We use this to compute the odd Fourier transform of the bath correlation functions which finally provides us the coefficients $\tilde{\sigma}_{kl}$, needed for setting up the BMS-ME. Further we exploited the following symmetries:

$$\tilde{\sigma}_{kl} = -\tilde{\sigma}_{lk}^*$$ (3.26)
$$\tilde{\gamma}_{kl} = \tilde{\gamma}_{lk}^*$$ (3.27)

As a result we have all coefficients that we need to set up the BMS-ME according to (2.151). The remaining task is to diagonalize the system Hamiltonian. For that purpose we use the Matlab internal routine "eigs" that provides the eigenvalues and eigenvectors of sparse matrices.

3.1.3. Calculation of the Steady State

Within this thesis we use the BMS-ME to calculate the steady state for the ME-CPT method as explained in section 3. For that purpose we rewrite equation (2.151) with the help of a so-called *superoperator*. A superoperator is defined as a linear operator acting on a vector space of linear operators [39]. In this work we write the BMS-ME from equation (2.151) as a superoperator acting on the density operator:

$$\dot{\hat{\rho}} = \hat{\hat{\mathcal{L}}}\hat{\rho} .$$ (3.28)

The hat therein indicates an operator and the double-hat a superoperator. In this compact form the steady state fulfils the following relation

$$\hat{\hat{\mathcal{L}}}\hat{\rho}_{sts} = \hat{0} .$$ (3.29)

This has the form of an eingenvalue equation for the superoperator. To solve this we have to find a matrix representation of the superoperator and rewrite equation (3.29) as a matrix-vector multiplication. We achieve this by vectorization, which converts matrices into column vectors by simply stacking their columns upon each other. To explain this in more detail we show an example for a general 2x2 matrix:

$$\text{vec} \begin{pmatrix} a & b \\ c & d \end{pmatrix} = \begin{pmatrix} a \\ c \\ b \\ d \end{pmatrix} .$$ (3.30)

We denote the vectorization by "vec" or an " $\vec{}$ " on top of the matrix. To obtain the matrix representation of the BMS-ME superoperator from equation (2.151), we have to

use the following important relation:

$$\text{vec}\,(ABC) \;=\; \left(C^T \otimes A\right) \cdot \text{vec}\,(B) \,. \tag{3.31}$$

It is valid for general quadratic matrices A, B and C. $\otimes$ is the Kronecker product. This allows to rewrite the BMS-ME as a matrix multiplication of a superoperator onto a vectorized density matrix:

$$\mathcal{L} \cdot \vec{\rho}_{sts} \;=\; \vec{0}\,. \tag{3.32}$$

This has the form of an eigenvalue problem, which has to be solved for the Eigenvector corresponding to the eigenvalue 0. In this work we again solve this in Matlab with the internal routine "eigs". We point out that the size of the superoperator matrix is equal to the size of the Hamiltonian matrix squared. This comes clear considering equation (3.30). The numerical treatment, in particular solving the eigenvalue problem, thus requires a huge amount of memory. In order to be able to study large systems, we have to exploit symmetries that allow to reduce the dimension of the matrix representation of the superoperator. As explained in chapter 2.6 the BMS-ME preserves trace, hermiticity and positivity. If additionally the system Hamiltonian commutes with the operator of total spin, $\hat{S}$, and particle number, $\hat{N}$, as it is the case for the Hubbard model, it is possible to show that the superoperator commutes with $(\hat{N} \otimes \mathbb{1} - \mathbb{1} \otimes \hat{N})$ and $(\hat{S} \otimes \mathbb{1} - \mathbb{1} \otimes \hat{S})$. This leads to a block-diagonal form of the superoperator matrix representation in the vectorized space, which allows to immensely reduce the memory requirements for the diagonalization [40].

3.1.4. Implementation of the Green's functions

In order to compute the Green's functions, we use the Lehmann representation as explained in section 2.1.2. The self energy describing the instantaneous hopping between system and bath is of the form

$$\Sigma \;=\; \begin{pmatrix} V^{ret} & 0 \\ 0 & V^{adv} \end{pmatrix} \tag{3.33}$$

with $V^{ret} = V^{adv}$ being the matrix form of H_{SB} in Wannier representation.

4. Results from ME-CPT

In this chapter we present the results from ME-CPT calculations. We study a linear chain containing four quantum dots which is connected to two leads. A sketch of this situation is given in figure 4.1. The linear chain is described by the Hubbard model as explained in chapter 2.7:

$$H_{Sys} \;=\; - \sum_{\substack{<j,k> \\ \sigma}} t_{jk}\, a^{\dagger}_{j,\sigma} a_{k,\sigma} \;+\; \sum_{j} U \left(a^{\dagger}_{j,\uparrow} a_{j,\uparrow} - \frac{1}{2} \right) \left(a^{\dagger}_{j,\downarrow} a_{j,\downarrow} - \frac{1}{2} \right) . \tag{4.1}$$

Again we choose the Hubbard Hamiltonian to ensure particle-hole symmetry. According to figure 4.1 we denote the hopping terms $t_{12} = t_{21} = t_{34} = t_{43}$ with t_{Sys} and $t_{34} = t_{43}$ with t'_{Sys}. The repulsive interaction U is chosen to be the same on all sites, modelling a local coulomb repulsion between electrons. Further, both baths are described by a flat density of states (DOS) according to equation (3.5) and are assumed to initially be in thermal equilibrium with a given temperature and chemical potential $\mu_{L/R}$. These chemical potentials are shifted due to a symmetrically applied, external bias voltage: $\mu_L = \frac{V_b}{2}$, $\mu_R = -\frac{V_b}{2}$. The coupling to the system is described by an instantaneous single-particle hopping with amplitude $t_{Right/Left}$, as shown in figure 4.1. The latter is calculated from a correspondingly chosen hybridization parameter Γ with

$$\Gamma_{R/L} \;=\; \pi |t^2_{Right/Left}| \frac{1}{2D} \; . \tag{4.2}$$

D is the half-bandwidth according to equation (3.5). We do all implementations in Matlab as described in chapter 3.1 and calculate the current and charge densities with the formulas derived in chapter 2.3. For the following analysis of the ME-CPT method we choose two different configurations of the central region:

- **Two double quantum dots connected in series:** We model this by setting the hopping parameters inside the system $|t'_{Sys}| = 0.1 \cdot |t_{Sys}|$. In doing so the we divide the system into two clusters, each containing one double quantum dot. Thereby the correlations across the two double quantum dots become small compared to the correlations inside the double quantum dots. This is particularly important for the applicability of the iteration schemata, presented in the subsequent chapters 5.1 and 5.2, since they are based on a slitting of large systems into sub-clusters.

- **Serial quadruple quantum dot:** We model this by setting the hopping parameters inside the system $|t'_{Sys}| = |t_{Sys}|$. Therewith the central region consisted of a linear homogeneous chain of quantum dots. We use the results of this situation to study the limits of the applicability of the later presented iteration schemata.
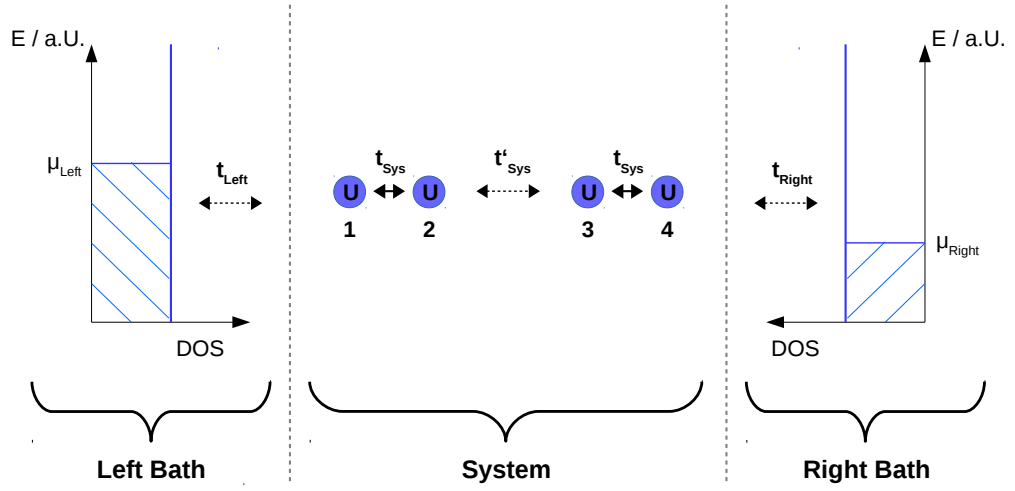
Figure 4.1.: Sketch of the linear chain with four Hubbard places connected to two baths with flat density of states. t_{Left}, t_{Right} and t_{Sys}, t'_{Sys} are the hopping terms to the left bath, right bath and within the system. On each place there is a local repulsive interaction U. For $|t'_{Sys}| = |t_{Sys}|$ the system is denoted as a *serial quadruple quantum dot* and for $|t'_{Sys}| < |t_{Sys}|$ as *two double quantum dots connected in series*. The chemical potentials in the baths are shifted symmetrically.

4.1. Two double quantum dots connected in series

In this section we discuss the results from ME-CPT for the configuration of two double quantum dots connected in series. We compare them to the results from ground-state CPT (GS-CPT) calculations. The system is described by the Hubbard Hamiltonian, according to equation (4.1). The hopping parameters are chosen to be $|t'_{Sys}| = 0.1 \cdot |t_{Sys}|$. For the repulsive interaction parameter U we discuss two different cases:

- Weak local repulsion between the fermions with $U = 0.1 \, |t_{Sys}|$.

- Strong local repulsion with $U = 3 \, |t_{Sys}|$.

The results are given in figure 4.2 and 4.3. We first discuss the results for weakly interacting particles with $U = 0.1 \, |t_{Sys}|$ that are shown in figure 4.2. In figure 4.2 (a) the current between the left bath and site one, I_L, is plotted versus the applied external bias voltage, V_b. In figure 4.2 (b) the corresponding expectation value of the density operator at site one, $\langle n_1 \rangle$, is plotted against the applied bias voltage. The current curves for ME-CPT and GS-CPT both are symmetric around $|V_b| = 0$ and have a distinct step

(a) Current characteristic I_L for U = 0.1   (b) Density $\langle n_1 \rangle$ for U = 0.1
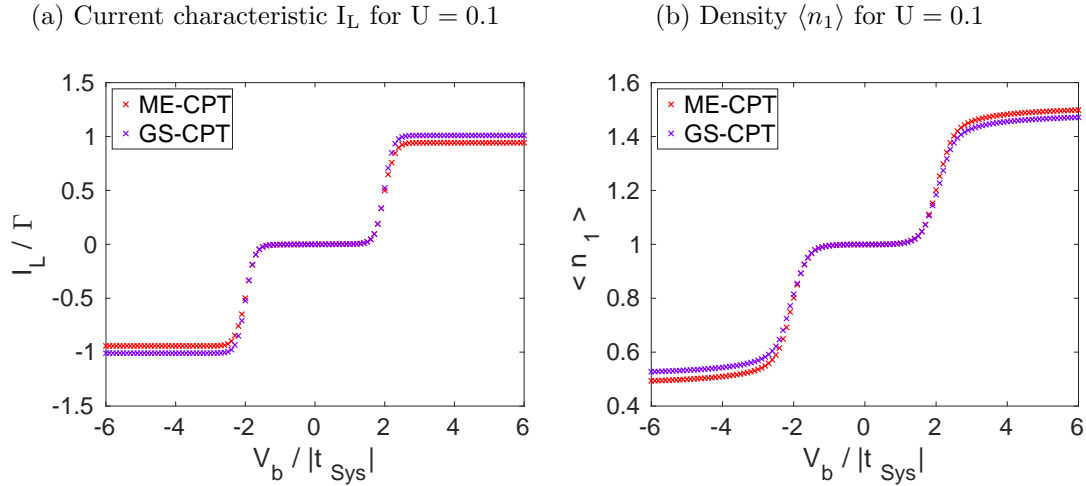
Figure 4.2.: Two interacting double quantum dots: Current characteristic and local densities for GS-CPT and ME-CPT. System Hamiltonian as defined in equation (4.1) for the situation depicted in figure 4.1. (a) Current flowing between left bath and the central region: I_L. (b): Density at site one: $\langle n_1 \rangle$. Parameters are as follows: U = $0.1 \, |t_{Sys}|$, $|t'_{Sys}| = 0.1 \, |t_{Sys}|$, $\Gamma_L = \Gamma_R = \Gamma = 0.1 \, |t_{Sys}|$ and the temperature in the leads T = $0.05 \, |t_{Sys}|$. Chemical potentials of the leads are shifted symmetrically by the bias voltage: $\mu_L = \frac{V_b}{2}$, $\mu_R = -\frac{V_b}{2}$.

at $|V_b| = 2|t_{Sys}|$. The data for the density at site one shows the same behaviour, whereby the step-like shape is more smeared out. This step comes from the energy gap inside the system, which for small U approximately has the value $2 \cdot |t_{Sys}|$. If the transport window is within this gap, no current can flow. For applied bias voltages of about $|V_b| = 2|t_{Sys}|$ a transport channel is reached and the current shows a steep ascent. It ends in a plateau which origins in the Pauli exclusion principle. This is explained regarding the density data in figure 4.2 (b), which, as well, reaches a plateau for large applied bias voltages. Therein, when the plateau is reached, the density at site one increases by approximately 0.5. The obtained data for the density at site two is exactly the same as for site one and thus, in total, one electron is added to the left double quantum dot. The further addition of an electron is then suppressed by the Pauli exclusion principle, since an additional electron can not occupy the exact same state in the transport channel. The comparison of the ME-CPT and the GS-CPT curves, for the current as well as for the density, shows that they are in good concordance. The deviation of the GS-CPT results from ME-CPT is small, even for large applied bias voltages. This is explained by the fact that GS-CPT provides the exact Green's functions in the case of U $\to$ 0 [27]. Consequently, for a small repulsive interaction, as in the calculations of figure 4.2, GS-CPT provides a good approximation for the observables.

In contrast to that, for a strong interaction between the electrons with U = $3 \, |t_{Sys}|$, the current and density curves from GS-CPT and ME-CPT differ considerably from each
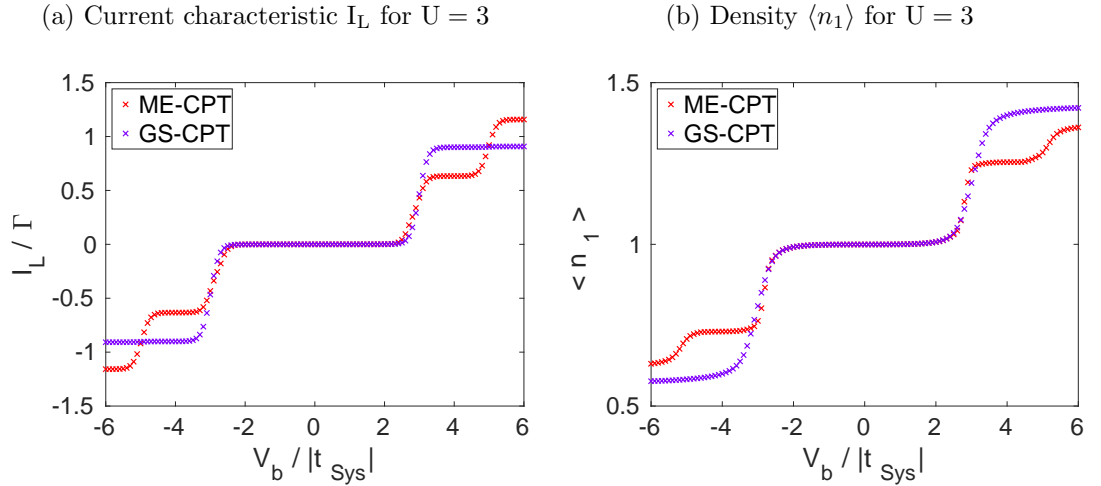
Figure 4.3.: Two interacting double quantum dots: Current characteristic and density for GS-CPT and ME-CPT. System Hamiltonian as defined in equation (4.1) for the situation depicted in figure 4.1. (a) Current flowing between left bath and the central region: I_L. (b): Density at site one: $\langle n_1 \rangle$. Parameters are as follows: $U = 3\,|t_{Sys}|$. All other parameters are the same as in the previous calculations for figure 4.2.

other. We show the results in figure 4.3. The current I_L from GS-CPT has a similar shape as in the case of $U = 0.1\,|t_{Sys}|$, with the difference that the step occurs at larger applied bias voltages of about $V_b = 3\,|t_{Sys}|$. This shift is explained by the coulomb repulsion due to the parameter U in the Hubbard Hamiltonian: Parallel to the steep increase of the current in figure 4.3 (a), the density at site one also increases significantly at $V_b = 3\,|t_{Sys}|$. This leads to an increase of charge and the electrons have to overcome a higher potential to jump onto site one. The current I_L obtained from ME-CPT also shows a steep increase at an applied bias voltage of about $V_b = 3\,|t_{Sys}|$. However, it reaches a plateau prior to the GS-CPT curve and exhibits another step between $V_b = 4\,|t_{Sys}|$ and $V_b = 6\,|t_{Sys}|$. This deviation between ME-CPT and GS-CPT is explained by the fact that within ME-CPT we take into account the nonequilibrium distribution inside the system when calculating the Green's functions. Within GS-CPT this is not the case. In the following we discuss this in more detail. For that purpose we show in figure 4.4 a detailed view of the bias voltage range between $V_b = 0$ and $V_b = 6\,|t_{Sys}|$. Further, for two different values of V_b, we show a schematic representation of the steady-state density matrix which is used in the ME-CPT calculations. We do this by plotting the corresponding weights of the density matrix in the eigenbasis of the system Hamiltonian against the energy relative to the ground-state energy ($E_j - E_0$). In figure 4.4 (c) we show the density matrix for the applied bias voltage of $V_b = 3\,|t_{Sys}|$ and in figure 4.4 (d) for $V_b = 4\,|t_{Sys}|$. In the current and density curves in 4.4 (a) and (b) we indicate the data points corresponding to this values of V_b with arrows (c) and (d). Figure 4.4, (c)

(a) Current I_L (b) Density $\langle n_1 \rangle$

(c) ρ_{jj} at $V_b = 3\,|t_{Sys}|$ (d) ρ_{jj} at $V_b = 4\,|t_{Sys}|$
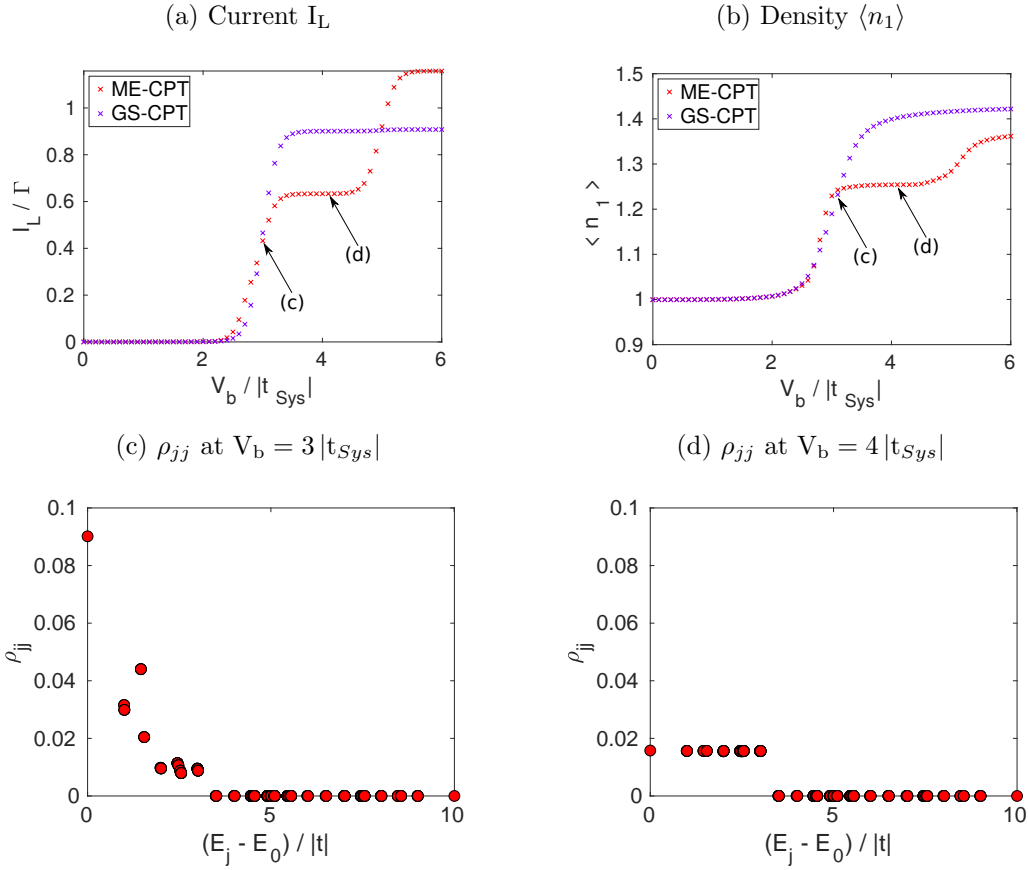
Figure 4.4.: Detailed view of current characteristic (a) and density (b) for $V_b > 0$ of figure 4.3 with parameter U = 3. (c) and (d) are the steady state density matrices for the two different bias voltages $V_b = 3\,|t_{Sys}|$ and $V_b = 4\,|t_{Sys}|$, indicated by arrows (1) and (2). Plotted are the diagonal entries of $\hat{\rho} = \sum_j \rho_{jj}\,|j\rangle\,\langle j|$, with $|j\rangle$ the eigenstates of the system Hamiltonian, against their corresponding eigenenergies E_j. E_0 thereby is the ground-state energy.

shows that for $V_b = 3\,|t_{Sys}|$ the steady-state does already not correspond to the ground-state any more. We have an occupation of energetically higher states as well. These states contribute to the transport channel, which is responsible for the steep ascent in the current and density curves in figure 4.4 (a) and (b). An increasing population therein hinders further electrons in using these excited states for the hopping process through the central region. As a result the current and density curves flatten. For $V_b = 4\,|t_{Sys}|$ the weights in the energetically higher states have further increased and the weight of the ground state further decreased, as shown in figure 4.4, (d). As a result, due to the increased population in the transport channel, additional electrons get blocked in hopping through the central region. This circumstance explains the plateau between $3|t_{Sys}| < V_b < 5|t_{Sys}|$ in the ME-CPT curves. It does not occur in the GS-CPT results,

because therein we do not take into account the nonequilibrium distribution inside the system. In the ME-CPT data, subsequent to the first plateau, another step occurs in the current curve for $V_b \approx 5|t_{Sys}|$. For this corresponding large voltages the weights in the density matrix shift to energetically even higher lying states, thereby decreasing the weights in the channel mentioned before. As a result we obtain a steep ascent in the current curve until the new distribution of weights in the steady-state density matrix stays constant and another plateau is reached. The latter lies remarkably above the broad plateau of the ground-state calculations. An explanation of that is given by regarding the local density curves in figure 4.3 (b): ME-CPT predicts a smaller density of electrons at site one than in GS-CPT. Thus, the effect of coulomb blocking among the electrons is smaller. We conclude that also for a simple one dimensional model, as studied in this chapter, ME-CPT remarkably improves the results of GS-CPT for transport properties in the nonequilibrium case. This substantiates the analytic results of chapter 2.5: For finite temperatures and finite applied bias voltages the nonequilibrium distribution within the cluster explicitly plays a role for the calculation of the current.

4.2. Serial quadruple quantum dot

In this section we discuss the results from ME-CPT for the serial quadruple quantum dot and compare them to the GS-CPT calculations. The situation is in principle the same as in the previous section 4.1, depicted in figure 4.1, with the only difference that inside the system we have $|t'_{Sys}| = |t_{Sys}|$. We study this situation, since it will be important for the investigation of the self-consistent iteration schemes in chapters 5.1 and 5.2. Within this iteration schemes the system is divided into clusters. For the case of two interacting double quantum dots this is rather justified than for the serial quadruple quantum dot. It will be interesting to what extent the schemata are able to reproduce the ME-CPT results for both cases. In the following we discuss the case of strongly interacting electrons with $U = 3 |t_{Sys}|$. We have already discussed in the previous section that for $U = 0.1 |t_{Sys}|$ the results from GS-CPT and ME-CPT have a good agreement. We show the results in figure 4.5, (a) and (b). The current characteristics from ME-CPT, as well as from GS-CPT, in figure 4.5 (a) show that the system has a gap. For applied bias voltages $V_b < 2 |t_{Sys}|$, the current is suppressed since the transport window is inside the system gap. With increasing bias voltage $V_b \geq 2 |t_{Sys}|$, we obtain a staircase-like shape for the current characteristics. Compared to the results for the serial double quantum dots of figure 4.3, the plateaus are much less pronounced. Further, in the results of GS-CPT and ME-CPT in figure 4.5 (b), the density at site one only shows a minor deviation from the half-filling level within the whole range of bias voltage. This is in contrast to the results for the two serial double quantum dots in figure 4.3 (b). It is explained by the fact that in the present case the hopping between all sites is of the same order ($|t'_{Sys}| = |t_{Sys}|$). Thus, correlations, as well as entanglements, across the whole system substantially influence the transport characteristics. For the two serial double quantum dots, with ($|t'_{Sys}| = 0.1 \cdot |t_{Sys}|$), this is not the case since correlations between the two double quantum dots are significantly smaller than those inside them. The results have
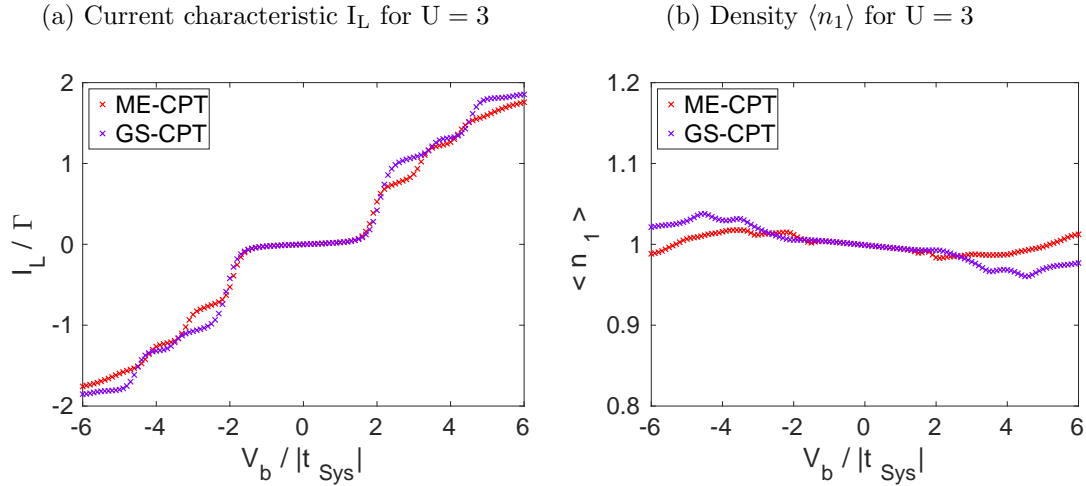
Figure 4.5.: Serial quadruple quantum dot: Current characteristic and densities for GS-CPT and ME-CPT. System Hamiltonian as defined in equation (4.1) for the situation depicted in figure 4.1. (a) Current flowing between left bath and the central region I_L. (b): Density at site one $\langle n_1 \rangle$. Parameters are as follows: $U = 3 |t_{Sys}|$, $|t'_{Sys}| = |t_{Sys}|$. All other parameters are the same as in the previous calculations for figure 4.2 and 4.3.

shown that the density $\langle n_1 \rangle$ increases in the same way as the current, as depicted in figure 4.3 (b). The staircase-like shape for the quadruple quantum dot in figure 4.5 (a) mainly comes from the corresponding transport channels that lie at many-body excitations inside the whole system. Comparing the current curves from ME-CPT and GS-CPT in figure 4.5 (a), we see that for $V_b > 2 |t_{Sys}|$ there is a remarkable difference between them. This is explained by recalling that within ME-CPT we take into account the nonequilibrium distribution inside the system by means of a master equation. This nonequilibrium distribution already predicts a finite occupation of excited states that lie in the transport channel, especially for large applied bias voltages. The result is a suppression of the current, since electrons get hindered in using this states for their hopping processes. Within GS-CPT we do not consider the nonequilibrium steady-state of the system when calculating the Green's functions, which has the consequence that GS-CPT overestimates the current in figure 4.5 (a). We conclude that also for the example of a serial quadruple quantum dot, ME-CPT significantly improves the results from GS-CPT for the current characteristics.

5. Self-consistent iteration scheme

We have shown with the results of the previous chapters 4.1 and 4.2, that ME-CPT notably improves the results of GS-CPT for observables in a one dimensional Hubbard chain in the nonequilibrium case. This Hubbard chain is a model for a one dimensional system of interacting quantum dots. With the Hubbard model and its enhancements, it is moreover possible to model complex, two- or three-dimensional structures, such as large clusters of molecules. In recent experimental research there has been a vast progress in assembling and performing measurements on such systems, opening new paths towards possible molecule-based electronic devices [1, 2, 4, 8, 9]. Therefore, the theoretical description of them, especially in the nonequilibrium case, is of major importance. The treatment of such complex systems within ME-CPT, however, is limited by the exponential growth of the many-body Hamiltonian with system size. A full diagonalization thereof demands an enormous amount of memory. Thus, with ME-CPT as it was introduced in [6], it is not possible to capture large two- or three dimensional systems. In this thesis we present a modification of ME-CPT that allows to divide the system into sub-clusters in the nonequilibrium case, similar to the procedure in GS-CPT for the equilibrium case [27]. As a result we solely have to diagonalize the Hamiltonians of the small sub-clusters, which makes large, composite systems accessible. The crucial point therein is, that in ME-CPT when setting up the master equation, we have to know the Green's functions of the baths. In the previous chapters 4.1 and 4.2 we had noninteracting baths, described by a flat DOS. When setting up the BMS-ME for a cluster inside an interacting region, however, we do not know all Green's functions of the neighbouring environment. We propose a solution for this with the help of a self-consistent iteration scheme. As a benchmark we choose the situation of two serial double quantum dots as depicted in figure 4.1. The advantage thereby is, that this system is still small enough to be treated with ME-CPT and yet can be separated into two clusters. The requirement for the iteration schemata then is to reproduce the results of the ME-CPT calculations.

5.1. Iteration Scheme A

In this section we present our first proposed iteration scheme. As we have mentioned above, when calculating Green's functions within the ME-CPT approach one needs to know all Green's functions of the corresponding environment to set up the master equation. In this iteration scheme we divide the system into two clusters, each containing one double quantum dot. A sketch thereof is given in figure 5.1. The aim is to calculate the Green's functions for each cluster separately within ME-CPT. In doing so we have to know the Green's functions of the adjacent sites, also of those from inside the system. However, prior to our calculations they are unknown. Our proposal is to treat

the clusters within ME-CPT iteratively, always using the previously calculated Green's functions from inside the system to describe the corresponding baths. This is repeated alternating for the two double quantum dots until convergence is reached. As a starting point we connect one of the clusters to both of the initially given external baths. This starting point, of course, must not influence the final result.

In the following we discuss this in detail by means of the system sketched in figure 5.2. For iteration scheme A the central region is divided into clusters one and two, each containing two sites, as shown in figure 5.1. In the first step we start with cluster one and
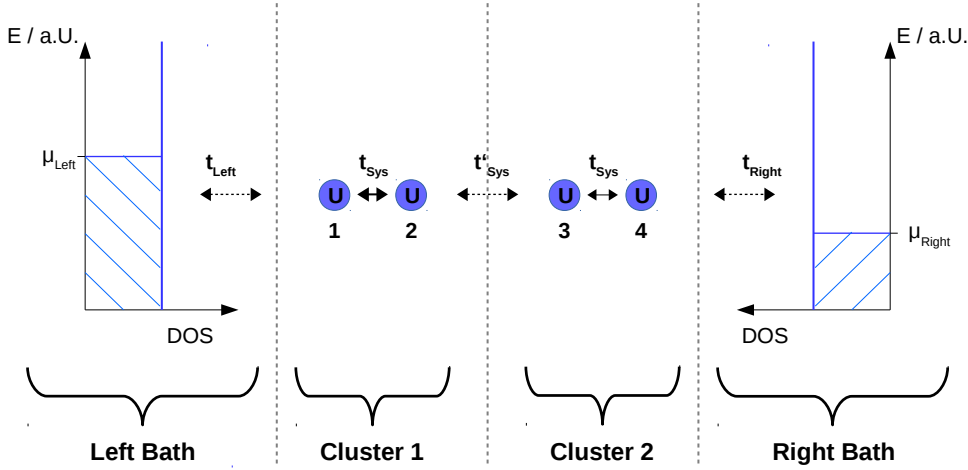
Figure 5.1.: Formal separation of a cluster with four Hubbard places into two clusters with two Hubbard places each.

simply connect it to both baths with the flat DOS. A sketch thereof is given in figure 5.2 (a). We calculate the Green's functions within the ME-CPT approach as described in section 3 and again implement the calculations in Matlab as explained in 3.1. Then, in the subsequent step, we connect cluster two on the right side to the right bath and on the left side to cluster one, as depicted in figure 5.2 (b), step (n). Thereby the Green's functions obtained from the previous step are used to describe the left sided bath in the ME-CPT calculation for setting up the BMS-ME. In the subsequent third step we perform this calculations again for cluster one. We sketch this as well in figure 5.2. The resulting Green's functions for cluster one then differ from those obtained in the first step. This deviation is taken as the convergence criteria by computing the absolute difference of the ω-dependent greater and lesser Green's functions as

$$(\delta_j)^{>/<,(n)} = \frac{\int |G_j^{>/<,(n)}(\omega) - G_j^{>/<,(n-1)}(\omega)|\,d\omega}{\int |G_j^{>/<,(n)}(\omega)|\,d\omega} \qquad (5.1)$$

(a) **First step**

(b) **Steps in the iteration**
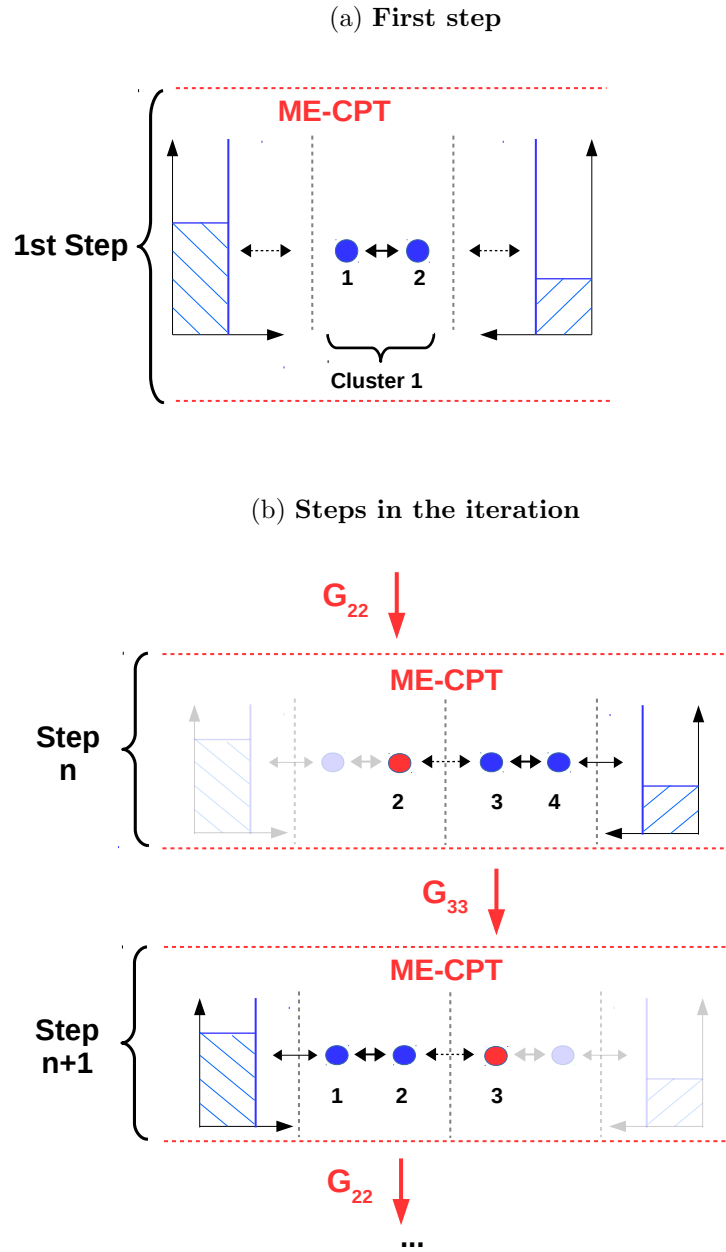
Figure 5.2.: **Iteration scheme A:** (a) In the first Step cluster number 1 is directly connected to both leads and Green's functions are calculated with ME-CPT. The local greater and lesser Green's functions of site number 2 are stored for the next step. (b) In the iteration the local Green's functions from the adjacent site of the corresponding cluster are used to describe the environment within the central region. On the opposite side it is connected to the given lead. In every step the Green's functions required for the consecutive step are stored.

with n numbering the steps and j the site-index of figure 5.1. We carry on the iteration in an alternating way for cluster one and two, until convergence is reached according to

$$(\delta_j)^{>/<,(n)} \leq \epsilon \qquad \text{for} \quad j = 1, 2, 3, 4 \,, \tag{5.2}$$

with ϵ a properly chosen small number. The iterative pattern is depicted in figure 5.2 (b). After convergence is reached, we calculate current and charge densities from the obtained Green's functions as described in chapter 2.3.

5.1.1. Results for two double quantum dots connected in series

In the following we apply iteration scheme A to the system of two double quantum dots connected in series. A sketch of the situation is depicted in figure 5.1. The results are compared to those from the ME-CPT calculations of chapter 4. We consider the case of strong interacting electrons with $U = 3\,|t_{Sys}|$, since for that case the advantages of ME-CPT, compared to GS-CPT, are more apparent. For the convergence parameter we take $\epsilon = 10^{-8}$. Therewith, we reached convergence according to (5.1) for each data point of figure 5.3 within 100 steps or less. We show the results in figure 5.3. The current

(a) Current characteristic I_L for $U = 3$ (b) Density $\langle n_1 \rangle$ for $U = 3$
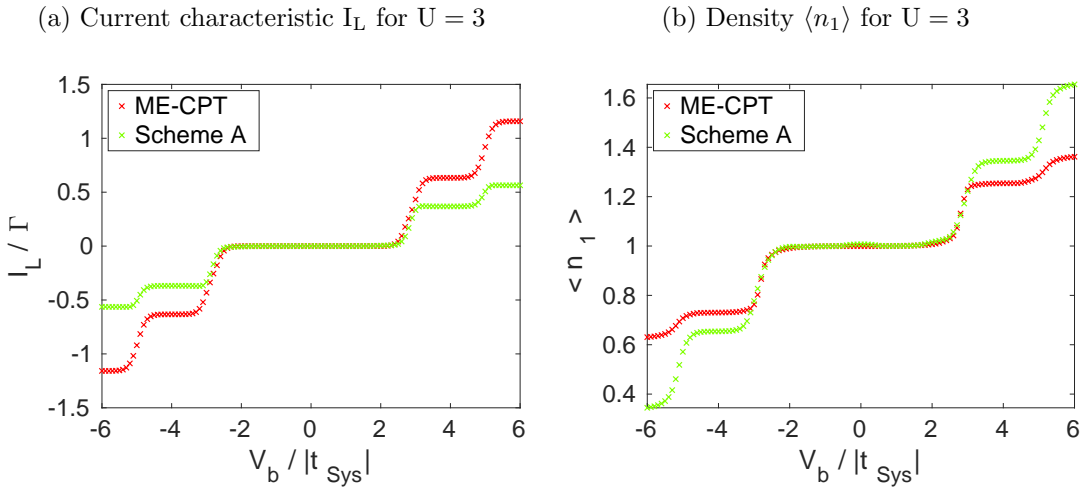
Figure 5.3.: Two interacting double quantum dots: Iteration scheme A is compared to ME-CPT. (a): Current flowing between left bath and the central region: I_L. (b): Density at site one $\langle n_1 \rangle$. System Hamiltonian as defined in equation (4.1) for the situation depicted in figure 5.1. Parameters are as follows: $U = 3\,|t_{Sys}|$, $|t'_{Sys}| = 0.1\,|t_{Sys}|$, $\Gamma_L = \Gamma_R = \Gamma = 0.1\,|t_{Sys}|$, and the temperature in the leads $T = 0.05\,|t_{Sys}|$. Chemical potentials of the baths are shifted symmetrically by the bias voltage: $\mu_L = \frac{V_b}{2}$, $\mu_R = -\frac{V_b}{2}$.

characteristic in (a), as well as the the density curve in (b), obtained from scheme A both show a stair-case like shape, similar to the ME-CPT results. The steps occur at the same values of applied bias voltage in scheme A and ME-CPT. However, there

is a significant offset between the two methods, which grows with increasing absolute values of the bias voltage. In the curves for the density in figure 5.3 (b), we see that scheme A overestimates the density for large V_b. This leads to an overestimation of the repulsive effects between electrons, coming from the coulomb repulsion. This results in an underestimation of the current, which is shown in the results of figure 5.3 (a). In order to explain this discrepancy we have to recall the approximations that are made in scheme A, compared to those in ME-CPT. The crucial difference between this methods is that in scheme A the system itself is further split up into two sub-clusters. In scheme A we perform the ME-CPT calculations for each of the sub-clusters during the self consistent iteration. Thereby, when computing the BMS-ME as in chapter 2.6 in order to obtain the nonequilibrium steady-state, we apply the corresponding approximations *inside* the system. For the BMS-ME this approximations require important assumptions concerning the baths, such as a rapid decay of the bath correlation functions or that they are hardly effected by the system. In order to explain this in more detail, we recap the approximations from the derivation of the BMS-ME equation in 2.6:

(i) The **first approximation** is to factorize the density matrix as

$$\rho(t) \;=\; \rho_S(t) \otimes \bar{\rho}_B \;, \tag{5.3}$$

which means assuming the baths to be so large that they are hardly effected by the system. Of course, inside the system the sub-clusters do effect each other. The idea in scheme A is that the self-consistency in the iteration takes this effects into account.

(ii) Within the **Markov approximation**, it is assumed that the bath correlation functions decay rapidly compared to timescales in which the density matrix varies. The correlation functions of the clusters inside the system, however, vary in the same timescales. Thus, when using a cluster to describe a bath, all correlation functions that do not rapidly decay therein are neglected.

(iii) To receive a master equation of Lindblad form, one applies the **secular approximation** and neglects all fast oscillating terms in the coupling operators. This is legitimate in the iteration scheme as long as the hopping parameter between the clusters is small.

We expected iteration scheme A to fulfil the above approximations (i-iii) for the current example of two serial double quantum dots, as depicted in figure 5.1, with $|t'_{Sys}| = 0.1 \cdot |t_{Sys}|$. However, the results in figure 5.3 show that the ME-CPT current and density curves are not reproduced sufficiently. We explain this by the fact that there is still an inconsistency when applying ME-CPT to each cluster, or double quantum dot of figure 5.1: In doing so we connect the clusters in each step on both sides with corresponding baths. From that we obtain Green's functions that describe a system which is connected on both sides with an environment. In the subsequent step, however, we use this Green's functions to describe the environment of a cluster on only one side. Thus, in scheme A we actually use Green's functions describing a system connected on

both sides with an environment, to describe baths on only one side. This inconsistency of scheme A points out that we have to modify it, in order to be able to reproduce the results from ME-CPT. We do this in the following chapter and present a new scheme B.

5.2. Iteration Scheme B

In iteration scheme A we perform a ME-CPT calculation for each cluster and use the resulting Green's functions to describe a bath in a subsequent step. This, however, leads to the inconsistency that a Green's functions from a system between two baths is used to describe a one-sided bath. In the ME-CPT calculations we have a small system, connected to two semi-infinite baths, as depicted in figure 4.1. The idea of iteration scheme B is to modify scheme A in such a way that during the iteration the clusters are always connected to semi-infinite baths on both sides. To explain this in more detail we recap the steps of ME-CPT for the example of the two serial double quantum dots of figure 4.1:

 (i) The whole situation is divided into a system and two baths.

 (ii) The BMS-ME is implemented for the system, including the hopping terms to the baths. It is then solved for the steady-state, which is used to calculate the cluster Green's functions with exact diagonalization methods.

 (iii) The interaction with the baths is introduced perturbatively according to Dyson's equation in CPT (2.55).

In iteration scheme A steps (ii) and (iii) are applied to each cluster of figure 5.1 in an iterative pattern. In scheme B this is modified. We explain this in the following with the help of the drawings in figures 5.4 and 5.5. We start with the first step of the iteration, which is depicted in figure 5.4. The separation of the two double quantum dots into two clusters and two baths is the same as in scheme A, shown in figure 5.1. In the first step we start with cluster one and connect it to both baths with flat DOS as shown in figure 5.4 (a). For this situation we implement the BMS-ME as described in chapter 3.1. The obtained nonequilibrium steady-state density matrix is then used to calculated the Green's function of the isolated cluster. Until here this is still the same as in scheme A. The important difference is that for the strong coupling perturbation theory in ME-CPT we only consider the hopping to the left bath. We show a sketch thereof in figure 5.4 (b). In doing so we obtain Green's functions that describe a semi-infinite system, consisting of the left bath which is connected with cluster one. This is the crucial difference compared to scheme A. The influence of the right bath thereby is still considered by means of the nonequilibrium density matrix. In the subsequent step we use the Green's functions obtained from step one to describe the left sided bath of cluster two. A sketch thereof is given in figure 5.5 step n, (a). As before we set up the BMS-ME considering the environment on both sides of cluster two. The environment on the left side thereby is given by the Green's functions from the previous step. The
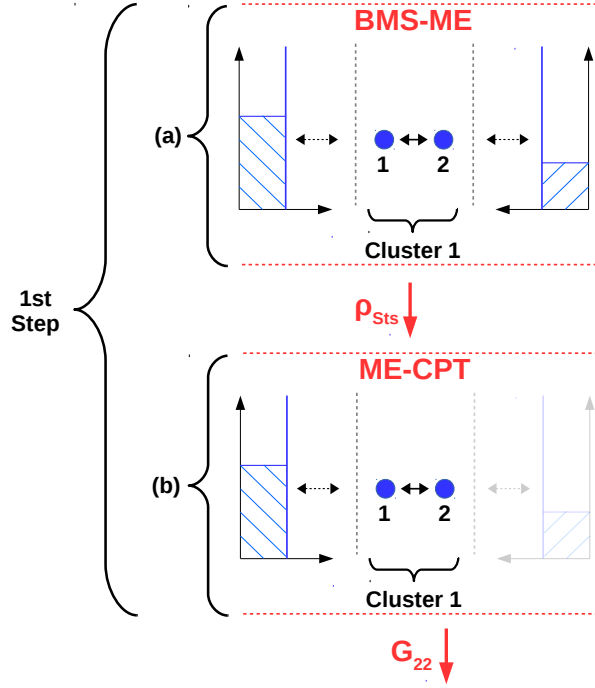
Figure 5.4.: **First step of iteration scheme B**: **(a)**: Cluster one is connected to both baths when implementing the BMS-ME. **(b)**: The obtained nonequilibrium density matrix is used to calculate the isolated cluster Green's function. For the strong coupling perturbation theory only the hopping to the left sided bath is considered.

important advantage compared to scheme A is that in scheme B this Green's functions describe a semi-infinite bath, which is consistent with the physical situation. As in step one we use the BMS-ME to calculate the nonequilibrium density matrix and from that we compute the Green's functions of the isolated cluster. For the strong coupling perturbation theory we again solely consider the initially given bath which is on the right side of cluster two. A sketch thereof is give in figure 5.5 in step n, (b). This pattern is then repeated for cluster one and two in an alternating way until convergence for the obtained Green's functions is reached. The convergence criteria is again calculated with formula (5.1). From this iteration scheme we obtain Green's functions that describe a semi-infinite system and that consider the nonequilibrium situation by means of a nonequilibrium density matrix. Thus, in order to describe the nonequilibrium situation containing both clusters, we have to connect them in one final step. We do this with perturbation theory according to CPT, using Dysons equation in Keldysh space:

$$\mathbf{G}(\omega) \; = \; \mathbf{g}(\omega) \; + \; \mathbf{g}(\omega)\, \mathbf{V}(\omega)\, \mathbf{G}(\omega)\,. \tag{5.4}$$
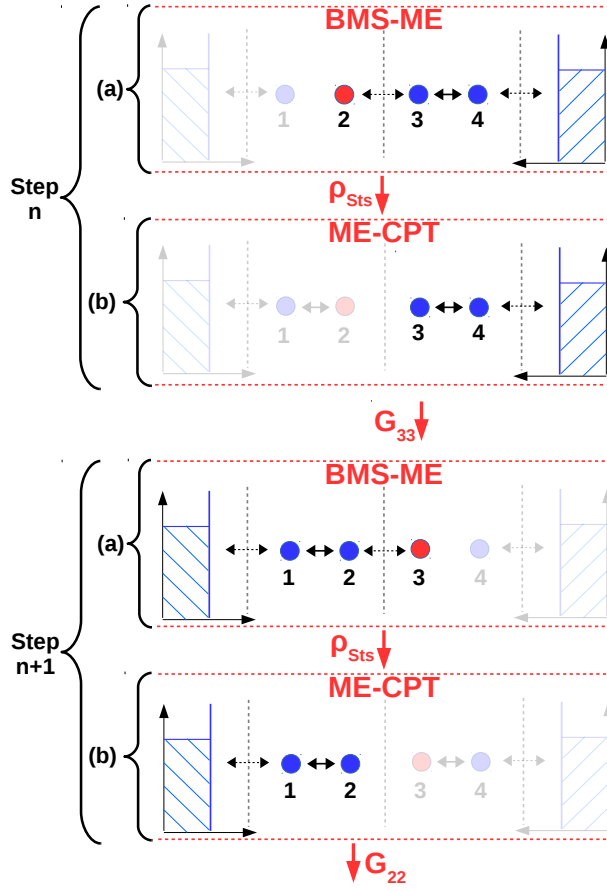
Figure 5.5.: **Steps in iteration scheme B:** Every step of scheme B is divided into parts (a) and (b). **(a)**: The BMS-ME is implemented regarding the baths on both sides. On the side that lies inside the system the Green's functions from the previous step are used for this. **(b)**: The obtained nonequilibrium density matrix is used to calculate the isolated cluster Green's function. For the strong coupling perturbation theory only the hopping to the initially given bath with flat DOS is considered.

Thereby $\mathbf{g}$ contains the Green's functions obtained from the iteration scheme as follows:

$$\mathbf{g} = \begin{pmatrix} G_{11} & G_{12} & 0 & 0 \\ G_{21} & G_{22} & 0 & 0 \\ 0 & 0 & G_{33} & G_{34} \\ 0 & 0 & G_{43} & G_{44} \end{pmatrix}. \tag{5.5}$$

The inter-cluster hopping is introduced with

$$\mathbf{V} \;=\; \begin{pmatrix} 0 & 0 & 0 & 0 \\ 0 & 0 & V_{23} & 0 \\ 0 & V_{32}^{\dagger} & 0 & 0 \\ 0 & 0 & 0 & 0 \end{pmatrix}, \tag{5.6}$$

whereas V_{23} contains the hopping term $|t'_{Sys}|$ of figure 5.1 in Wannier representation. We mention that due to the nonequilibrium situation, all terms in the above matrices in (5.5) and (5.6) are 2x2 matrices in Keldysh space according to equation (2.86). From the finally obtained Green's functions we calculate the current and density as described in chapter 2.3.

5.2.1. Results for two double quantum dots connected in series

In this section we apply iteration scheme B to the system of two double quantum dots connected in series as depicted in figure 5.1. We compare the results to those from the ME-CPT calculations of chapter 4.1. We discuss the case of strong interacting electrons with $U = 3\,|t_{Sys}|$ and all other parameters are the same as in the calculations of chapter 4.1. For the convergence parameter of equation (5.1) we take $\epsilon = 10^{-8}$. We show the results in figure 5.6. For each data point we reached convergence within 50 steps or

(a) Current Characteristic I_L for $U = 3$ (b) Density $\langle n_1 \rangle$ for $U = 3$
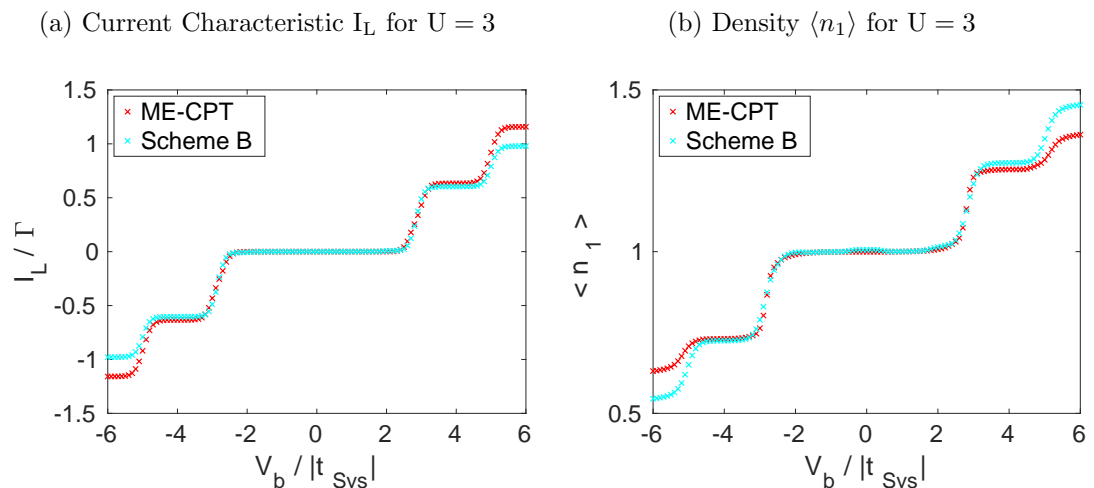
Figure 5.6.: Two interacting double quantum dots: Iteration scheme B is compared with the ME-CPT calculation. (a): Current flowing between left bath and the central region I_L. (b): Density at site one $\langle n_1 \rangle$. System Hamiltonian as defined in equation (4.1) for the situation depicted in figure 5.1. The parameters are the same as in figure 5.3

less. The current characteristic in figure 5.6 (a), as well as the local density in 5.6 (b), show that they are in good concordance with the results from ME-CPT. Only for very

large applied bias voltages with $|V_b| > 4\,|t_{Sys}|$ the curves show a discrepancy. In figure 5.6 (b), scheme B overestimates the density for $V_b > 4\,|t_{Sys}|$ compared to ME-CPT. Following the same argumentation as in chapter 5.1.1 for scheme A, this leads to an overestimation of the repulsive effects between the electrons. The result is that in this range of bias voltage ($V_b > 4\,|t_{Sys}|$) the current is underestimated compared to ME-CPT, as shown in figure 5.6 (a). We point out that this discrepancy solely occurs for very large absolute values of applied bias voltage. In the experimental realization of quantum dots or molecular junctions, as for example in [1, 8] or [9], the application of such a large bias voltage would lead to the destruction of the microscopic components. Thus, within the range of bias voltage that is physically relevant, we achieved a good reproduction of the results from ME-CPT with iteration scheme B. Thereby we were able to drastically reduce the memory requirements for the numerical implementations. This allows for a treatment of much larger systems that consist of clusters with a small correlation in between them. Within ME-CPT the treatment of large systems is not possible since it requires to set up the BMS-ME for the whole interacting region.

5.2.2. Results for the serial quadruple quantum dot

In this chapter we apply iteration scheme B to the serial quadruple quantum dot. We want to investigate if the self-consistent iteration permits a division into clusters for a system with strong correlations between the clusters. The situation is in principle the same as in the previous section 5.2.1, depicted in figure 5.1. The only difference is that the hopping parameter between the clusters is equal to the hopping parameter inside the clusters: $|t'_{Sys}| = |t_{Sys}|$. All other parameters are the same. We compare scheme B with the ME-CPT calculations of section 4.2 and show the results in figure 5.7. We obtained a convergence for each data point in scheme B within 150 steps or less. The curves in figure 5.7 show that for an applied bias voltage, larger than $V_b = 3\,|t_{Sys}|$, there is a significant discrepancy between ME-CPT and iteration scheme B. In figure 5.7 (b), between $V_b = 2\,|t_{Sys}|$ and $V_b = 4\,|t_{Sys}|$, the density from scheme B features a sharp increase. This increase is so large that, due to the repulsive interaction between the electrons as well as the Pauli exclusion principle, the current from scheme B gets substantially suppressed. This is shown in figure 5.7 (a). The current even decreases for $3\,|t_{Sys}| < V_b < 4\,|t_{Sys}|$, which describes a negative differential conductance. This is in contrast to the ME-CPT results, which predict that at site one the density does not significantly derivate from $\langle n_1 \rangle = 1$ in the whole range of applied bias voltage. Further, the current obtained from ME-CPT does not feature negative differential conductance, as shown in figure 5.7. We explain this discrepancy between ME-CPT and scheme B for the situation of a quadruple quantum dot by considering the correlations across cluster one and two of figure 5.1. Since the hopping parameter $|t'_{Sys}|$ between the clusters is the same as the hopping parameter $|t_{Sys}|$ inside them, the correlations between the clusters are of the same order as the correlations inside them. In ME-CPT this is accounted for since the system Hamiltonian, describing cluster one and two, is solved at once. Especially the BMS-ME, that gives us the steady-state, is set up for the system containing both clusters. In contrast to that, in scheme B we solve the Hamiltonian, as

(a) Current Characteristic I_L for $U = 3$ (b) Density $\langle n_1 \rangle$ for $U = 3$
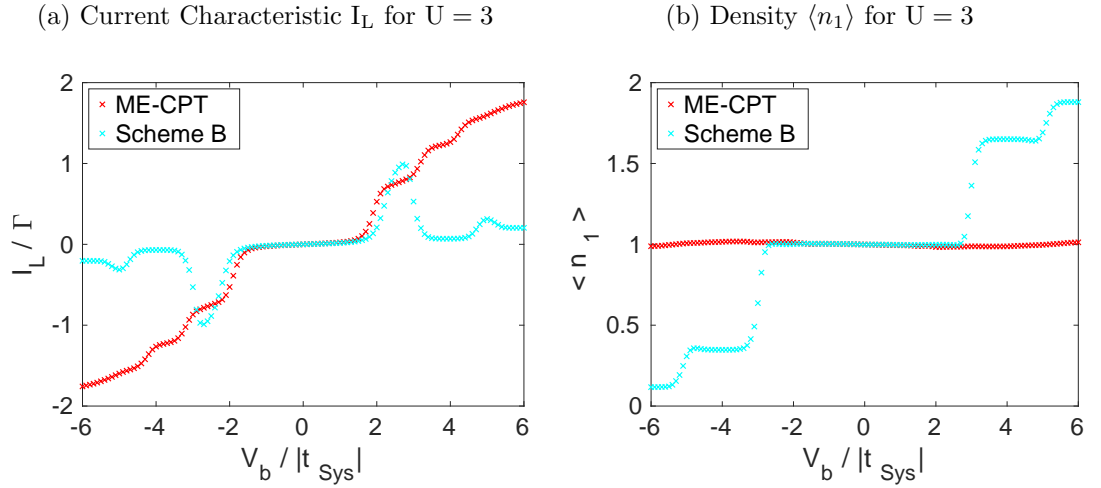
Figure 5.7.: Serial quadruple quantum dot: Comparison of iteration scheme B with ME-CPT. (a): Current flowing between left lead and the central region I_L. (b): Density at site one $\langle n_1 \rangle$. System Hamiltonian as defined in equation (4.1) for the situation depicted in figure 5.1. Parameters are as follows: $|t_{Sys}| = |t'_{Sys}|$. All other parameters are the same as in figure 5.6.

well as the BMS-ME, for each cluster separately and in an iterative way. Therein, when calculating the steady state in each of the two clusters, the correlations across them are solely considered perturbatively according to the Born-Markov-Secular approximations as described in chapter 2.6. Further, in the last additional step, the two clusters are connected perturbatively according to Dyson's equation from CPT. As explained in [27] and chapter 2.2, CPT likewise treats correlations across different clusters solely perturbatively. These considerations explain the results of figure 5.7, which show that for the case of a serial quadruple quantum dot, iteration scheme B does not reproduce the results from ME-CPT sufficiently. Thus, we summarize that iteration scheme B requires spatial correlations across different clusters to be small. In the equilibrium case, one has the same requirement for CPT calculations [28, 27]. Therefore, we expect that systems which can be treated within CPT in the equilibrium case, provide reliable results within scheme B in the nonequilibrium case. What is more, scheme B allows to capture large systems, which can not be studied within ME-CPT due to the enormous memory requirements in the latter.

6. Summary and Conclusion

In this work we have presented a new self-consistent iteration scheme, based upon ME-CPT. The aim has been to drastically reduce the memory requirements by dividing the correlated region into clusters and include the nonequilibrium steady-state in a self-consistent way. The self-consistent ME-CPT approach should allow for the treatment of systems with a large correlated region, which would be impossible to treat via plain ME-CPT.

The main disadvantage of plain ME-CPT is that it requires to solve the Hamiltonian as well as the BMS-ME for the entire central region. Due to the exponential growth of the many-body space with system size, this demands an enormous amount of memory and makes it impossible for ME-CPT to capture large complex structures. The motivation of this thesis has been to formulate a method within the framework of ME-CPT that allows to divide the correlated central region into clusters. The Hamiltonian, as well as the BMS-ME, then solely has to be solved for the small clusters. In order to obtain a consistent nonequilibrium distribution inside these clusters, the method is based on a self-consistent procedure.

In chapter 2.3, we have shown analytically that the nonequilibrium distribution inside of the correlated central region explicitly occurs in the general current formula. This result emphasizes the advantages of ME-CPT with respect to GS-CPT. Within GS-CPT the current is given by a Landauer-type formula, which does not take into account the nonequilibrium distribution within the correlated region. Thus, it is not expected to provide reliable results for systems far from equilibrium. Within ME-CPT one formally obtains the same Landauer-type formula. The crucial improvement compared to GS-CPT is that Green's functions are calculated taking into account the nonequilibrium distribution inside the central region by means of a master equation.

As a benchmark of the new iteration scheme we have chosen a system that is still small enough to be captured with ME-CPT. Thus, the key requirement for the presented scheme is to reproduce the results of the ME-CPT calculations. In this work we have used a linear chain with four sites, described by the Hubbard model, that is connected to two semi-infinite baths. This is a model for a linear chain of quantum dots which are out of equilibrium. We have studied two different configurations:

- **Two double quantum dots connected in series:** The system consists of two double quantum dots that are weakly coupled with each other.

- **Serial quadruple quantum dot:** The coupling between all quantum dots in the system is the same.

The two double quantum dots connected in series are a system that already consists of two clusters, each containing one double quantum dot. Correlations across the clusters

are comparably small and therefore we expect this situation to be well suited for an iteration that treats each cluster separately. In contrast to that, the correlations across the clusters in the serial quadruple quantum dot are not small. We have studied this situation to show whether the proposed iteration scheme is capable of reproducing the ME-CPT results for this case as well.

In chapter 4 we have applied ME-CPT to both configurations and compared the results for current and density to those of GS-CPT. We have shown that also for this simple, one dimensional model, ME-CPT remarkably improves the results of GS-CPT. This substantiates the statements of chapter 2.3.

In chapter 5.1 we have studied the first proposed iteration scheme, designated as **scheme A**. Therein we perform an ME-CPT calculation for each sub-cluster iteratively, until convergence is reached. To describe the environment inside of the central region we use the Green's functions of the corresponding adjacent site, calculated in the previous step. In chapter 5.1.1 we have applied scheme A to the two double quantum dots connected in series and compared results for current and density to those of ME-CPT. In the obtained figures we have shown that scheme A does not sufficiently reproduce the ME-CPT outcomes. Even though the shape of the current and density curves have been qualitatively reproduced, there has been an offset compared to ME-CPT that grows with increasing applied bias voltage. We have explained this by the fact that in scheme A there is an inconsistency: During the self-consistent iteration Green's functions from a system between two baths are used to describe a one-sided bath.

To resolve this issue we have modified scheme A in such a way that all baths, used during the iteration, describe semi-infinite systems. We have designated this new approach as **scheme B**. In chapter 5.2.1 we have applied scheme B to the case of two double quantum dots connected in series. The obtained results have shown that the current and density curves from ME-CPT and scheme B are in a good concordance. Solely in the case of very large applied bias voltages we have observed that the density was slightly overestimated and the current underestimated. However, we have pointed out that in the experimental realization of such systems, as for example in [1, 4, 8], the application of such a large bias voltage would destroy the microscopic components. Thus, in the physically relevant range of applied bias voltage, we have achieved a good reproduction of the ME-CPT results with iteration scheme B. Thereby, the memory requirements for implementing the two double quantum dots have been drastically reduced.

In the case of the two double quantum dots connected in series, the division into the corresponding cluster has been evident. The correlations across these clusters are comparably small and thus it is justified to treat them perturbatively. Nevertheless, it is interesting to what extent the self-consistency in iteration scheme B reproduces the ME-CPT results for the case of stronger correlations between the clusters. This has been studied in chapter 5.2.2, where we have applied iteration scheme B to the serial quadruple quantum dot. The results have shown that iteration scheme B does not reproduce sufficiently the results for current and density. Thus, we have concluded that iteration scheme B requires spatial correlations beyond the extent of the corresponding clusters to be small.

We conclude that scheme B is able to capture systems in the nonequilibrium case

that consist of weakly coupled clusters. It is expected that therewith also systems, that are too large to be treated within plain ME-CPT, are accessible. An important example are large structures of interacting molecules, which may provide building blocks for novel molecular scale electronic devices. They are the subject of up-to-date experimental studies. To quote some of the recent achievements: In [3] the controlled assembly of molecular building blocks onto gold surfaces has been achieved. A method to manufacture molecular junctions with diameter up to 100 μm has been developed [5]. Further, nanostructures consisting of interacting quantum dots have been realised recently [9]. The latter have been proposed for the implementation of universal qubit gates in quantum computers [10]. The explicit study of such complex systems, however, goes beyond the scope of this master thesis, which serves as a first introduction of a method which could be used to investigate their properties within the approximations of ME-CPT.

A. Appendix

In the following we show that the Keldysh component of the inverse of the isolated cluster Green's function, denoted as $(\mathbf{g}^{-1})^{kel}$, is a term proportional to 0^+ and can be neglected within CPT and ME-CPT if there are no bound states. This fact was used in the derivations of chapter 2.4. For the sake of better readability, in this section the subscript "cl" is omitted. We first recall the *Lehmann representation* of Green's functions as explained in chapter 2.1.2. The greater and lesser Green's function then have the form

$$g^{>}_{\alpha,\beta}(\omega) \;=\; -i \sum_{nab} \rho_{ab} \, \langle b| \, \hat{c}_{\alpha} \, |n\rangle \, \langle n| \, \hat{c}^{\dagger}_{\beta} \, |a\rangle \cdot 2\pi \, \delta(\omega - (\omega_n - \omega_b)) \tag{A.1}$$

and

$$g^{<}_{\alpha,\beta}(\omega) \;=\; i \sum_{nab} \rho_{ab} \, \langle b| \, \hat{c}^{\dagger}_{\beta} \, |n\rangle \, \langle n| \, \hat{c}_{\alpha} \, |a\rangle \cdot 2\pi \, \delta(\omega - (\omega_a - \omega_n)) \,. \tag{A.2}$$

The Lehmann representation of the retarded Green's function reads as follows:

$$g^{ret}_{\alpha\beta}(\omega) \;=\; \sum_{nab} \rho_{ab} \left(\frac{\langle b| \, \hat{c}_{\alpha} \, |n\rangle \, \langle n| \, \hat{c}^{\dagger}_{\beta} \, |a\rangle}{\omega + i0^+ - (\omega_n - \omega_b)} + \frac{\langle b| \, \hat{c}^{\dagger}_{\beta} \, |n\rangle \, \langle n| \, \hat{c}_{\alpha} \, |a\rangle}{\omega + i0^+ - (\omega_a - \omega_n)} \right) . \tag{A.3}$$

To calculate the Keldysh part of the inverse of the Green's function inside the central region we exploit the relation

$$(g^{-1}_{\alpha\beta})^{kel} \;=\; (g^{-1}_{\alpha\beta})^{ret} \, g^{kel}_{\alpha\beta} \, (g^{-1}_{\alpha\beta})^{adv} \,, \tag{A.4}$$

which is generally valid in Keldysh space. For writing the Keldysh part of the Green's function, given by

$$g^{kel}_{\alpha\beta}(\omega) \;=\; g^{>}_{\alpha,\beta}(\omega) + g^{<}_{\alpha,\beta}(\omega) \,, \tag{A.5}$$

in the Lehmann representation, we write the Delta-distribution of equations (A.1) and (A.2) as a Lorentzian:

$$\delta(\omega - (\omega_n - \omega_b)) \;=\; \lim_{0^+ \to 0} \frac{1}{\pi} \frac{0^+}{(\omega - (\omega_n - \omega_b))^2 + (0^+)^2} \tag{A.6}$$

$$=\; \lim_{0^+ \to 0} \frac{1}{\pi} \frac{0^+}{[(\omega - (\omega_n - \omega_b)) + i0^+] \, [(\omega - (\omega_n - \omega_b)) - i0^+]} \,. \tag{A.7}$$

Using this relation we obtain for the Keldysh part of the Green's function

$$g_{\alpha\beta}^{kel}(\omega) = \sum_{nab} \frac{0^+ \cdot A_{\alpha\beta}^{(n,a,b)}}{[(\omega - (\omega_n - \omega_b)) + i0^+]\,[(\omega - (\omega_n - \omega_b)) - i0^+]} + \cdots$$

$$+ \sum_{nab} \frac{0^+ \cdot B_{\alpha\beta}^{(n,a,b)}}{[(\omega - (\omega_a - \omega_n)) + i0^+]\,[(\omega - (\omega_a - \omega_n)) - i0^+]}\ ,$$

(A.8)

with corresponding coefficients A and B. For the retarded part of the inverse of the Green's function, the relation $(g_{\alpha\beta}^{-1})^{ret} = (g_{\alpha\beta}^{ret})^{-1}$ holds in Keldysh space. Using this relation we calculate the inverse of g^{ret} in the Lehmann representation and put it into equation A.4. For the inverse of the retarded Green's function, as given in equation (A.3), we obtain

$$(g_{\alpha\beta}^{ret}(\omega))^{-1} = \frac{\prod_{nab} ((\omega + i0^+ - (\omega_n - \omega_b))(\omega + i0^+ - (\omega_a - \omega_n)))}{\sum_{nab} C_{\alpha\beta}^{(n,a,b)}}\ ,$$

(A.9)

after bringing it to a common denominator, with a sum over corresponding constants C. The inverse of the advanced Green's function, which is simply the conjugate transpose of equation (A.9), has the same form

$$(g_{\alpha\beta}^{-1}(\omega))^{adv} = \frac{\prod_{nab} ((\omega - i0^+ - (\omega_n - \omega_a))(\omega + i0^+ - (\omega_b - \omega_n)))}{\sum_{nab} D_{\alpha\beta}^{(n,a,b)}}\ .$$

(A.10)

We put this results of equations (A.8), (A.9) and (A.10) into equation (A.4). When doing this, we see that every summand in g^{kel} of equation (A.8) is multiplied with both products from (A.9) and (A.10). Consequently, all denominators of g^{kel} in the sum in (A.8) are cancelled out with the corresponding factors in the numerators of g^{ret} and g^{adv} of equations (A.9) and (A.10). The result is that $(g_{\alpha\beta}^{-1}(\omega))^{kel}$ consists of a sum of finite factors multiplied by 0^+. Thus, we have shown that within an isolated cluster one has

$$(g_{\alpha\beta}^{-1}(\omega))^{kel} \propto 0^+\ .$$

Bibliography

[1] Leonhard Grill et al. "Nano-architectures by covalent assembly of molecular building blocks". In: *Nature Nanotechnology* 2.11 (Nov. 2007), pp. 687–691. ISSN: 17483395. DOI: `10.1038/nnano.2007.346`. URL: `http://www.nature.com/articles/nnano.2007.346`.

[2] Wenjie Liang et al. "Kondo resonance in a single-molecule transistor". In: *Nature* 417.6890 (June 2002), pp. 725–729. ISSN: 0028-0836. DOI: `10.1038/nature00790`. URL: `http://www.nature.com/articles/nature00790`.

[3] Hylke B. Akkerman et al. "Towards molecular electronics with large-area molecular junctions". en. In: *Nature* 441.1 (May 2006), pp. 69–72. ISSN: 14764687. DOI: `10.1038/nature04699`. URL: `https://www.nature.com/articles/nature04699`.

[4] Christophe Nacci et al. "Covalent Assembly and Characterization of Nonsymmetrical Single-Molecule Nodes". In: *Angewandte Chemie - International Edition* 55.44 (2016), pp. 13724–13728. ISSN: 15213773. DOI: `10.1002/anie.201605421`.

[5] Abraham Nitzan and Mark A. Ratner. "Electron Transport in Molecular Wire Junctions". In: *Science* 300 (5624 May 2003), pp. 1384–1389. DOI: `10.1126/science.1081572`.

[6] Martin Nuss et al. "Master equation based steady-state cluster perturbation theory". In: *Physical Review B* 92.125128 (2015). DOI: `10.1103/PhysRevB.92.125128`.

[7] Sara M. Cronenwett, Tjerk H. Oosterkamp, and Leo P. Kouwenhoven. "A tunable Kondo effect of quantum dots". In: *Science* 281.5376 (July 1998), pp. 540–544. ISSN: 00368075. DOI: `10.1126/science.281.5376.540`. URL: `http://science.sciencemag.org/content/281/5376/540/tab-pdf`.

[8] W. G. van der Wiel et al. "Electron transport through double quantum dots". In: *Reviews of Modern Physics* 75.1 (Dec. 2002), pp. 1–22. ISSN: 0034-6861. DOI: `10.1103/RevModPhys.75.1`. URL: `https://link.aps.org/doi/10.1103/RevModPhys.75.1`.

[9] D. Schröer et al. "Electrostatically defined serial triple quantum dot charged with few electrons". In: *Physical Review B* 76.7 (Aug. 2007), p. 075306. ISSN: 1098-0121. DOI: `10.1103/PhysRevB.76.075306`. URL: `https://link.aps.org/doi/10.1103/PhysRevB.76.075306`.

[10] Daniel Loss and David P. DiVincenzo. "Quantum computation with quantum dots". In: *Phys. Rev. A* 57 (1 Jan. 1998), pp. 120–126. DOI: `10.1103/PhysRevA.57.120`. URL: `https://link.aps.org/doi/10.1103/PhysRevA.57.120`.

[11] Frithjof B. Anders. "Steady-State Currents through Nanodevices: A Scattering-States Numerical Renormalization-Group Approach to Open Quantum Systems". In: *Phys. Rev. Lett.* 101 (6 Aug. 2008), p. 066804. DOI: `10.1103/PhysRevLett.101.066804`. URL: `https://link.aps.org/doi/10.1103/PhysRevLett.101.066804`.

[12] S Andergassen et al. "Charge transport through single molecules, quantum dots and quantum wires". In: *Nanotechnology* 21.27 (June 2010), p. 272001. DOI: `10.1088/0957-4484/21/27/272001`. URL: `https://doi.org/10.1088%2F0957-4484%2F21%2F27%2F272001`.

[13] Ulrich Schollwöck. "The density-matrix renormalization group in the age of matrix product states". In: *Annals of Physics* 326.1 (2011). January 2011 Special Issue, pp. 96–192. ISSN: 0003-4916. DOI: `https://doi.org/10.1016/j.aop.2010.09.012`. URL: `http://www.sciencedirect.com/science/article/pii/S0003491610001752`.

[14] Wolfgang Nolting. *Grundkurs Theoretische Physik 7. Viel-Teilchen-Theorie.* Ed. by Springer-Verlag Berlin Heidelberg. Vol. 8. 2015. ISBN: 978-3-642-25807-7.

[15] Mariana M. Odashima, Beatriz G. Prado, and E. Vernek. "Pedagogical introduction to equilibrium Green's functions: condensed-matter examples with numerical implementations". In: *Rev. Bras. Ensino Fis* 39.1 (2016). DOI: `10.1590/1806-9126-RBEF-2016-0087`.

[16] Enrico Arrigoni. "Correlation Phenomena in Solid State Physics: Quantum Systems out of Equilibrium". Lecture Notes. Graz University of Technology, 2016.

[17] Hans Niels Jahnke. *A History of Analysis.* Vol. 24. AMS and the London Mathematical Society, 2003.

[18] George L. Trigg. *Mathematical Tools for Physicists.* 1st ed. Wiley-VCH, 2005. ISBN: 9783527405480.

[19] Lehmann H. "Über Eigenschaften von Ausbreitungsfunktionen und Renormierungskonstanten quantisierter Felder". In: *Il Nuovo Cimento* 11 (1954). DOI: `https://doi.org/10.1007/BF02783624`.

[20] H. G. Evertz. "Fortgeschrittene Quantenmechanik". Lecture Notes. Graz University of Technology, 2004. URL: `https://itp.tugraz.at/LV/evertz/QM-2/qm2.pdf`.

[21] Freeman J. Dyson. "The S Matrix in Quantum Electrodynamics". In: *Physical Review* 75.11 (1949). DOI: `10.1103/PhysRev.75.1736`.

[22] N. N. Bogolyubov and D. V. Shirkov. *Introduction to the Theory of Quantized Fields.* Vol. 3. 1959, pp. 1–720.

[23] R.D. Mattuck. *A Guide to Feynman Diagrams in the Many-body Problem.* Dover Books on Physics Series. Dover Publications, 1992. ISBN: 9780486670478. URL: `https://books.google.at/books?id=pe-v8zfxE68C`.

[24] Takeo Matsubara. "A New Approach to Quantum-Statistical Mechanics". In: *Progress of Theoretical Physics* 14.4 (Oct. 1955), pp. 351–378. ISSN: 0033-068X. DOI: 10.1143/PTP.14.351. URL: https://academic.oup.com/ptp/article-lookup/doi/10.1143/PTP.14.351.

[25] J. Rammer and H. Smith. "Quantum field-theoretical methods in transport theory of metals". In: *Rev. Mod. Phys.* 58 (2 Apr. 1986), pp. 323–359. DOI: 10.1103/RevModPhys.58.323. URL: https://link.aps.org/doi/10.1103/RevModPhys.58.323.

[26] A G Hall. "Non-equilibrium Green functions: generalized Wick's theorem and diagrammatic perturbation with initial correlations". In: *Journal of Physics A: Mathematical and General* 8.2 (Feb. 1975), pp. 214–225. DOI: 10.1088/0305-4470/8/2/012.

[27] D. Sénéchal, D. Perez, and M. Pioro-Ladrière. "Spectral Weight of the Hubbard Model through Cluster Perturbation Theory". In: *Physical Review Letters* 84.3 (Jan. 2000), pp. 522–525. ISSN: 00319007. DOI: 10.1103/PhysRevLett.84.522. URL: https://link.aps.org/doi/10.1103/PhysRevLett.84.522.

[28] Matthias Balzer and Michael Potthoff. "Nonequilibrium cluster perturbation theory". In: *Physical Review B* 84.195132 (2011). DOI: 10.1103/PhysRevB.83.195132.

[29] Robert van Leeuwen, Nils Erik Dahlen, and Gianluca Stefanucci. "Introduction to the Keldysh Formalism and Applications to Time-Dependent Density-Functional theory". In: *arXiv:cond-mat* 0506130 (2005).

[30] Markus Aichhorn. "Ordering Phenomena in Strongly-Correlated Systems: Cluster Perturbation Theory Approaches". Dissertation. Technische Universitaet Graz, 2004.

[31] Yigal Meir and Ned S. Wingreen. "Landauer formula for the current through an interacting electron region". In: *Physical Review Letters* 68.16 (1992), pp. 2512–2515. ISSN: 00319007. DOI: 10.1103/PhysRevLett.68.2512.

[32] M. Büttiker. "Four-Terminal Phase-Coherent Conductance". In: *Phys. Rev. Lett.* 57 (14 Oct. 1986), pp. 1761–1764. DOI: 10.1103/PhysRevLett.57.1761. URL: https://link.aps.org/doi/10.1103/PhysRevLett.57.1761.

[33] Gernot Schaller. *Open Quantum Systems Far from Equilibrium*. Vol. 881. Springer Heidelberg, 2014.

[34] Gernot Schaller. "Non-Equilibirum Master Equations". Lecture Notes. TU Berlin, 2012.

[35] John Hubbard and Brian Hilton Flowers. "Electron correlations in narow energy bands". In: *Proceedings of the Royal Society of London* (1963). DOI: http://doi.org/10.1098/rspa.1963.0204.

[36] Martin Nuss et al. "Steady-state spectra, current, and stability diagram of a quantum dot: A nonequilibrium variational cluster approach". In: *Physical Review B* 86.24 (Dec. 2012), p. 245119. ISSN: 1098-0121. DOI: 10.1103/PhysRevB.86.245119. URL: https://link.aps.org/doi/10.1103/PhysRevB.86.245119.

[37] E. N. Economou. *Green's Functions in Quantum Physics*. Ed. by Berlin Springer. 3rd. 2010.

[38] Andreas Nyiri and Laszlo Baranyi. "Numerical Evaluation of a Generalized Cauchy Principal Value". In: *Miskolc Mathematical Notes* (2000), pp. 35–41. ISSN: 1787-2405.

[39] Juergen Audretsch. *Verschraenkte Systeme: Die Quantenmechanik auf neuen Wegen*. John Wiley and Sons, 2005. ISBN: 3527660569.

[40] Antonius Dorda et al. "Auxiliary master equation approach to nonequilibrium correlated impurities". In: *Physical Review B* 89.165105 (2014). DOI: 10.1103/PhysRevB.89.165105.